

THESIS FOR THE DEGREE OF DOCTOR OF PHILOSOPHY

DYNAMIC MODELING AND SIMULATION OF SAG  
MILL CIRCUITS WITH PEBBLE CRUSHING

HAIJIE LI



Department of Industrial and Materials Science  
CHALMERS UNIVERSITY OF TECHNOLOGY  
Gothenburg, Sweden 2024

**Dynamic Modeling and Simulation of SAG Mill Circuits with Pebble Crushing**

Haijie Li

ISBN 978-91-8103-092-1

**Copyright** © Haijie Li, 2024

Doctoral thesis at Chalmers University of Technology

New serial no. 5550

ISSN 0346-718X

**Published and Distributed by**

Department of Industrial and Materials Science

Division of Product Development

Chalmers University of Technology

SE-412 96 Gothenburg, Sweden

Telephone + 46 31-772 1000

**Cover:** A photo of a SAG mill and a Raptor 350 cone crusher are selected from FLSmidth product brochures, along with illustrations of simulation results taken from the author's papers.

**Printed in Sweden by**

Chalmers Digitaltryck

Gothenburg, Sweden 2024

# Abstract

Grinding is one of the most energy-consuming processes in the mining industry. As a critical part of the comminution process, autogenous grinding (AG) or semi-autogenous grinding (SAG) mills are often used for primary grinding. However, the breakage mechanism of a SAG mill is inefficient in grinding particles of a certain size, typically in the range of 25-55 mm, known as pebbles. Therefore, cone crushers are often used as pebble crushers and integrated into SAG mill circuits to break the critical-size particles that accumulate in the mill, which increases the performance of the primary grinding circuits.

Many studies have been carried out, mainly focusing on optimizing SAG mills and cone crushers, respectively. However, only a few have investigated the dynamic interactions between a SAG mill and its pebble crushers. The scope of this thesis is to examine the dynamic relationships and interdependencies between the SAG mill and the pebble crusher in a closed circuit. This knowledge and understanding of the process can help optimize grinding efficiency by selecting a suitable pebble crusher during the circuit design stage and by controlling the crusher during operation.

In this thesis, fundamental modeling methods and data-driven methods are presented for simulating the dynamics of the grinding process. The fundamental modeling method considers the underlying physics of the comminution process. A population balance framework is implemented for the mill with sub-models that estimate breakage and transportation. Dynamic models for cone crushers, conveyors, bins, and screens are also formulated with mass balance, material tracking, and size reduction.

Several data-driven methods are presented to find the nonlinear relations between some input variables and certain target outputs, such as the mill power, the mill pebble rate, and particle size estimation. Since the accuracy of such data-driven models depends not only on high-quality training data but also on the selection of appropriate signals as input features to the models, the understanding and knowledge of the process are essential.

The results from this work show that significant dynamic impacts can be induced by altering the pebble crusher operational settings. Thus, the performance of a SAG closed circuit can be improved with the optimized utilization of its recycle pebble crusher.

**Keywords:** SAG Mill, Cone Crusher, Modeling, Dynamic Simulation, Grinding, Crushing, Digital Twin, Data-driven Method, Machine Learning, Image Processing



# Acknowledgements

My journey began years ago when I received a call one afternoon from Dr. Mats Lindqvist. He offered me the opportunity to pursue research at Chalmers Rock Processing Systems (CRPS) and work at FLSmidth as an industrial Ph.D. student, funded by Denmark Innovation Fund. I am profoundly thankful to Mats for introducing me to the mining industry.

I would like to express my gratitude to the pioneers who came before me. It is on the foundation they built that I have been able to take further steps forward. They are the researchers I cited in my work, those who inspired and helped me along the way. My deepest thanks go to my supervisors, Prof. Magnus Evertsson, Docent Dr. Gauti Asbjörnsson, and Docent Dr. Erik Hulthén.

I would also like to thank those who have walked this journey with me—my colleagues, my peers, and those who have shared the scenery with me. I am grateful to my past and present colleagues in CRPS and R&D Mining at FLSmidth A/S, especially my managers, Steve Rowe, Jesper Gerdes Kyhnav, and Naveen Seelam, who have not only supported me but also guided me on my career path.

I am equally thankful to those who will come after me. Their citation of my research and further study will make my work and efforts truly meaningful.

Lastly, I am deeply thankful to my parents. Without their encouragement and unwavering support, I wouldn't have been able to travel thousands of miles from home to Denmark. Special thanks to my wife, Haomin, who has been by my side for the past 10 years.

Haijie Li

Copenhagen, Aug 2024



# List of Publications

## Appended papers:

- Paper A: Li, H., Evertsson, M., Lindqvist, M., Hulthén, E., & Asbjörnsson, G. (2018). Dynamic modeling and simulation of an AG/SAG mill with multi-component ore. *IMPC 2018 – 29th International Mineral Processing Congress*, Moscow, Russia.
- Paper B: Li, H., Evertsson, M., Lindqvist, M., Hulthén, E., & Asbjörnsson, G. (2018). *Dynamic modeling and simulation of a SAG mill-pebble crusher circuit by controlling crusher operational parameters*. *Minerals Engineering*, 127, 98-104.
- Paper C: Li, H., Evertsson, M., Lindqvist, M., Hulthén, E., Asbjörnsson, G., & Bonn, G. (2019). Dynamic modeling of a SAG mill – pebble crusher circuit by data-driven methods. *SAG Conference 2019*, Vancouver, Canada.
- Paper D: Li, H., Evertsson, M., Lindqvist, M., & Asbjörnsson, G. (2021). A data-driven method to isolate the effect of pebble recycling on SAG mill circuit. *Comminution 2021*, Cape Town, South Africa.
- Paper E: Li, H., Evertsson, M., Lindqvist, M., & Asbjörnsson, G. (2021). *Image process of rock size distribution using DexiNed-based neural network*. *Minerals*, 11(736).
- Paper F: Li, H., Evertsson, M., & Asbjörnsson, G. (2023). A Shapley value interpretation of a data-driven model for pebble rates in SAG mills. Extended abstract with poster presented at *SAG Conference 2023*, Vancouver, Canada.
- Paper G: Li, H., Asbjörnsson, G., Bhadani, K., & Evertsson, M. (2024). *Investigating dynamic behavior in SAG mill pebble recycling circuits: A simulation approach*. *Minerals*, 14(7), 716.

**Additional Publications:** The following research paper, while not directly contributing to the findings of this thesis, played a crucial role in deepening the author’s understanding of the research field. The results from this paper are discussed, but not utilized in addressing the research questions.

- Paper H: Lindqvist, M., & Li, H. (2021). *A cone crusher model with a coupled energy- and breakage dependency*. *Minerals Engineering*, 172, 107147.

# Work distribution:

- Paper A: Li and Evertsson initiated the idea, Li developed the model with support from Asbjörnsson, Li wrote the paper, Evertsson and Hulthén as reviewers.
- Paper B: Li and Lindqvist initiated the idea, Li developed the model with support from Evertsson and Asbjörnsson, Li wrote the paper, Evertsson and Hulthén as reviewers.
- Paper C: Li initiated the idea, Li implemented the code with a dataset from Bonn, Li wrote the paper, with Evertsson, Asbjörnsson, and Lindqvist as reviewers.
- Paper D: Li initiated the idea, Li wrote the paper, with Evertsson, Asbjörnsson, and Lindqvist as reviewers.
- Paper E: Li initiated the idea, Li implemented the code with a dataset from Asbjörnsson, Li wrote the paper, with Asbjörnsson and Lindqvist as reviewers.
- Paper F: Li initiated the idea, Li implemented the code with a dataset from KAZ Minerals, Li wrote the paper, with Evertsson and Asbjörnsson as reviewers.
- Paper G: Li initiated the idea and wrote the paper, Li developed the model with support from Asbjörnsson and Bhadani, Li wrote the paper, with Evertsson and Asbjörnsson as reviewers.



# Table of Contents

1	INTRODUCTION .....	1
1.1	Background and Problem Statement .....	1
1.2	Research Scope and Research Questions .....	3
1.3	Research Approach .....	4
2	LITERATURE REVIEW .....	7
2.1	Fundamental Models .....	7
2.1.1	SAG mill modeling .....	7
2.1.2	Cone crusher modeling .....	12
2.2	Data-driven Models .....	13
2.2.1	Process decomposition and sub-process .....	14
2.2.2	Introduction of generally used data-driven methods .....	15
2.2.3	Combination of Fundamental Models and Data-driven Models .....	16
3	METHOD .....	17
3.1	Fundamental Models .....	18
3.1.1	SAG mill .....	18
3.1.2	Simplified cone crusher model and other equipment .....	20
3.2	Data-driven Methods .....	21
3.2.1	SAG mill power .....	21
3.2.2	SAG mill pebble rate importance analysis .....	23
3.2.3	Rock size estimation from images .....	23
3.3	Data Mining and Data Analysis .....	24
4	RESULTS .....	27
4.1	Single SAG Mill Dynamic Modeling .....	27
4.2	Single Cone Crusher Modeling .....	29
4.3	SAG Mill with Pebble Crusher Circuit Dynamic Modeling .....	30
4.3.1	A single SAG-pebble crusher circuit .....	30
4.3.2	Responses of a dual SAG mill circuit with two cone crushers .....	32
4.4	Design of Experiment of SAG Mill Pebble Crushing circuit .....	34
4.5	SAG Mill Power Draw Prediction .....	38
4.6	SAG Mill Pebble Rate Prediction .....	41
4.7	The Impact of Recycling Load on a SAG Mill Circuit .....	46
4.8	Particle Size Distribution Estimation for Crushed Products .....	50
5	DISCUSSION .....	57
5.1	General Conclusions .....	57
5.2	Answering Research Questions .....	58

5.3 Future Work ..... 61

Appended papers:

- Paper A: Dynamic modeling and simulation of an AG/SAG mill with multi-component ore.
- Paper B: Dynamic modeling and simulation of a SAG mill-pebble crusher circuit by controlling crusher operational parameters.
- Paper C: Dynamic modeling of a SAG mill – pebble crusher circuit by data-driven methods.
- Paper D: A data-driven method to isolate the effect of pebble recycling on SAG mill circuit.
- Paper E: Image process of rock size distribution using DexiNed-based neural network.
- Paper F: A Shapley value interpretation of a data-driven model for pebble rates in SAG mills.
- Paper G: Investigating dynamic behavior in SAG mill pebble recycling circuits: A simulation approach.

# List of Abbreviations

AG	Autogenous mill
ANN	Artificial neural network
CNN	Convolutional neural network
CPA	Change point analysis
CRPS	Chalmers Rock Processing Systems
CSS	Closed side settings
DEM	Discrete element method
DoE	Design of experiment
FC	Fully connected layers
GBR	Gradient boosting regression
IAM	Integrated analysis method
JKMRC	The Julius Kruttschnitt Mineral Research Center
KNN	K-nearest neighbors
LSTM	Long short-term memory
PBM	Population balance method
PSD	Particle size distribution
RF	Random forest
RNN	Recurrent neural network
SAG	Semi-autogenous mill
SE	Specific energy



# List of Figures

Figure 1. Cumulative installed AG mill and SAG mill power sold until 2015 (Tozlu & Fresko, 2015).....	1
Figure 2. Example of a closed SAG mill circuit with pebble recycling: the feed has been pre-crushed due to the high competence of the material before being fed into the grinding circuit (Paper D). .....	2
Figure 3. Conveyor belt with pebbles between a SAG mill and its pebble crusher (left); Illustration of pebble size (right). .....	2
Figure 4. The applied problem-oriented research methodology based on Evertsson (Evertsson, 2000) and modified by Asbjörnsson (Asbjörnsson, 2015).....	5
Figure 5. Scheme of the drop weight test. ....	8
Figure 6. $t_{10} - t_n$ curve for the drop weight tests (King, 2001). Reconstructed plot from selected papers (Bourgeois, 1993; Narayanan & Whiten, 1983; Pauw & Maré, 1988).....	9
Figure 7. JK breakage rate function example of SAG mills (Kojovic et al., 2012). ....	10
Figure 8. Austin breakage rate function example where the total breakage rate $S$ is fitted by combining curve $S_1$ and a straight line $S_2$ (Austin & Cho, 2002).....	11
Figure 9. Simplified mill charge scheme modified from Morrell’s approach (Morrell, 1996b). .....	11
Figure 10. Schematic block diagram for a single crushing event of a cone crusher model framework. ....	12
Figure 11. A generic procedure for data-driven modeling and monitoring of plant-wide processes, modified from a framework proposed by Ge (Ge, 2017). ....	14
Figure 12. Schematic illustration of a hybrid fundamental-data model. The output of a physics-based model is used as a new feature in a data-based model, modified from Karpatne (Karpatne et al., 2017). ....	16
Figure 13. Overview of the thesis contents. ....	17
Figure 14. Schematic of data structure in the SAG mill simulation.....	18
Figure 15. Product PSD of different cone crusher settings. Data from Evertsson (Evertsson, 2000), tested on a Svedala Hydrocone cone crusher.....	21
Figure 16. The capacity of cone crushers with different settings. Data from Lindqvist (Lindqvist & Evertsson, 2004), tested on an FLS Raptor 900 cone crusher.....	21
Figure 17. Long Short-term Memory Cell structure. ....	22
Figure 18. A flowchart of the proposed processes of ore size distribution estimation (Paper E). .....	24
Figure 19. A generic procedure of isolating a certain variable (Paper D). ....	25
Figure 20. Dynamic response of the mill with a different feed rate (Paper A).....	27

Figure 21. The particle size distribution of different sections in the mill at $t = 1000$ minutes (Paper A). .....	27
Figure 22. Mill dynamics as a function of cycle number for a locked-cycle test using 1:1 QTZ/BIF mixture (Bueno et al., 2010) (Paper A). .....	28
Figure 23. Ratio of the soft/hard ore of mill product and load (Paper A). .....	29
Figure 24. Ratio of soft/hard ore size by size in the mill (Paper A). .....	29
Figure 25. Product PSD at corresponding min CSS, the Bond Work Index is 12, 16, 20 kWh/t (Paper H). .....	29
Figure 26. Product PSD operating at different CSS (Paper H). .....	29
Figure 27. Flowsheet of the simulation with single SAG mill and single pebble crusher (Paper B). .....	30
Figure 28. Simulation results from the single SAG mill grinding circuit. Feeding starts at $t = 100$ minutes (Paper B). .....	31
Figure 29. PSD in SAG mill, simulation time at 150 min (Paper B). .....	32
Figure 30. PSD in SAG mill, simulation time at 1500 min (Paper B). .....	32
Figure 31. Flowsheet of the simulation with dual SAG mills, screenshot from Simulink (Paper B). .....	33
Figure 32. Simulation results from simulating with dual SAG mills (Paper B). .....	34
Figure 33. Flowsheet of a typical SAG mill-pebble crusher circuit with options adding pre-crushers, stockpiles and other circuit configurations. These different layouts will be simulated using a DoE approach (Paper G). .....	35
Figure 34. Simulation results from Run 1 to Run 4 include the circuit with stockpile and fine crusher settings. Figure (a) shows the throughput, fresh feed rate, and recycle rate of each SAG mill. Figure (b) shows the pebble crusher utilization rate. Figure (c) shows the pebble rate and crusher bin level (Paper G). .....	36
Figure 35. Normal plots to assess the significance of effects in the DoE results. (a) is for fresh feed rate, (b) is for pebble rate, (c) and (d) are the crusher capacity utilization. Blue line has slope equal to Lenth's PSE, red line slope is 1 (Paper G). .....	38
Figure 36. SAG mill power prediction with weighted results from individual predictors (Paper C). .....	39
Figure 37. Sketch of the forecasting model structure with CNN layers and LSTM layers (Paper C). .....	40
Figure 38. 2-minute forecasting model for SAG mill power with 20 minutes of historical data (Paper C). .....	41
Figure 39. Vibration sensor measurement and SAG mill power from period 1 (Paper F). .....	42
Figure 40. Vibration signals plot with SAG mill power draw. The signals are clustered based on Gaussian mixture models (Paper F). .....	43

Figure 41. SAG mill power time-series plots. Data points are labeled based on vibration signal clusters (Paper F).....	43
Figure 42. A soft sensor of the SAG mill liner wear. Vibration clusters are added to remove the outliers and to generate a smoother liner wear estimation. The scatters in orange color show data with cluster 0 and cluster 1, see Figure 41 (Paper F).....	44
Figure 43. The pebble rate prediction: a) A time series plot of measured pebble rate and predicted pebble rate. b) Scatter plot of predictions against measured values. The blue dot is from the original features; the orange cross is with added features (vibration clusters and liner wear soft sensor) (Paper F). .....	45
Figure 44. The Shapley Value of all features of the SAG mill pebble rate prediction (Paper F). .....	46
Figure 45. Kernel density estimation plot of the pebble crusher power and pebble specific energy (Paper D). .....	47
Figure 46. Clusters of recycling load based on crusher power and pebble specific energy (Paper D). .....	47
Figure 47. Change points of fresh feed rate. It is categorized into three classes based on their average value in each period (Paper D).....	47
Figure 48. Comparison of SAG mill parameters under different cone crusher clusters (Paper D).....	48
Figure 49. Comparison of operational data under different SAG mill feed rate clusters (Paper D).....	49
Figure 50. The correlations between crusher clusters and SAG mill fresh feed rate clusters (Paper D). .....	50
Figure 51. An example of raw image and processed results: (a) the raw image; (b) the binary image of detected edge; (c) all contours found; (d) fine region; (e) connected rock region; (f) single rock region (Paper E). .....	51
Figure 52. An example of the connected neighboring rocks and the contour map of the extracted images with the new threshold value (Paper E).....	52
Figure 53. The processed results: (a1,b1,c1,d1,e1) raw images of lab samples; (a2,b2,c2,d2,e2) edge maps of input images; (a3,b3,c3,d3,e3) contour maps with three filters results, where the light green contour is the fine region, the white contour is the connected rock region and the blue is single rock region (Paper E). .....	53
Figure 54. The results of the estimated mass distribution compared with lab sampling: (a) frequency of the size distribution; (b) cumulative size distribution; (c) R <sup>2</sup> of the estimated results (Paper E). .....	55
Figure 55. Illustration of the relationships between the appended papers and research questions. The size of the markers indicates the strength of the relationships.....	58





# 1 INTRODUCTION

*The aim of this chapter is to:*

- *Introduce the background and hypothesis of the research project.*
- *Introduce the research scope and research questions.*
- *Give a summary of the thesis contents.*

## 1.1 Background and Problem Statement

The SAG mill was invented in the late 1950s and quickly became dominant in the primary grinding process (Napier-Munn et al., 1996). The comminution process is one of the most energy-intensive processes in the minerals industry. Studies show that the comminution process consumes approximately 2% of the annual global electricity consumption (Fuerstenau & Han, 2003). Haque (Haque, 1999) also reports that the energy consumption of SAG mills (including operating power and the energy used during the mill components production procedures) accounts for 50% of the minerals industry, and the efficiency of grinding equipment can be as low as 1%. In 2015, Jones and Fresko conducted a thorough survey among the AG mill and SAG mill main manufacturers. The total installed power has been sold until 2015 can be seen in Figure 1. The chart presents that the demands of the SAG mills has been significantly increased since the beginning of the 21 century. Some experts also expressed their concerns about the future of autogenous and semi-autogenous mills. In a conversation between Prof. Barry Wills and Prof. Alban Lynch (posted by MEI blog), the latter says that “the SAG energy efficiency is poor.” Similarly, O’Bryan points out in an interview (O’Bryan, 2014) that “SAG mills have to be bigger to meet these demands. Some are up to 12.1-12.8 m in diameter in order to handle the higher tonnages, and the size of these mills makes them harder to install and operate efficiently”. Therefore, efforts have been devoted during the past decades to increase the grinding process efficiency.

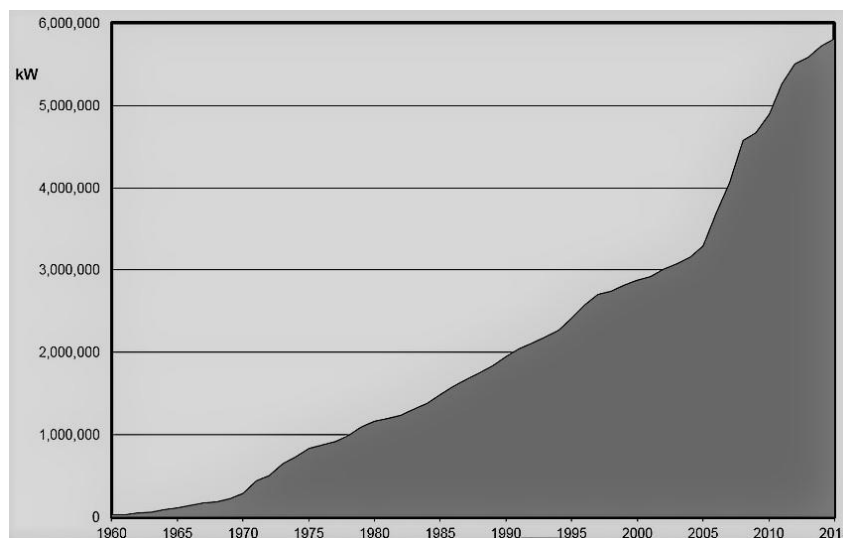


Figure 1. Cumulative installed AG mill and SAG mill power sold until 2015 (Tozlu & Fresko, 2015).

The word “autogenous” in AG mills indicates the grinding media is formed exclusively by ore particles. In a SAG mill, external grinding balls are added in the chamber to aid in the grinding process. Napier-Munn (Napier-Munn et al., 1996) classified the breakage mechanisms occurring within SAG mills into three categories: high energy related impact breakage, low energy related abrasion, and attrition. Due to the SAG mill inherent breakage mechanism, particles of a size in the range of 25-55 mm (so-called critical size fraction) are not easily broken thoroughly and are likely to accumulate in the mill charge (Yu, 2017). The buildup of critical particles in a mill consumes a remarkable amount of power and leads to a lower mill throughput. Therefore, these pebble-sized particles need to be discharged from the mill and then addressed by an external crusher, usually a cone crusher (Johnson et al., 1994). A simplified SAG-pebble circuit flowsheet can be seen in Figure 2. And in Figure 3, a conveyor belt with pebbles and its sampled photo are illustrated. One can see the size and shapes of pebbles by comparing them to the author’s hand.

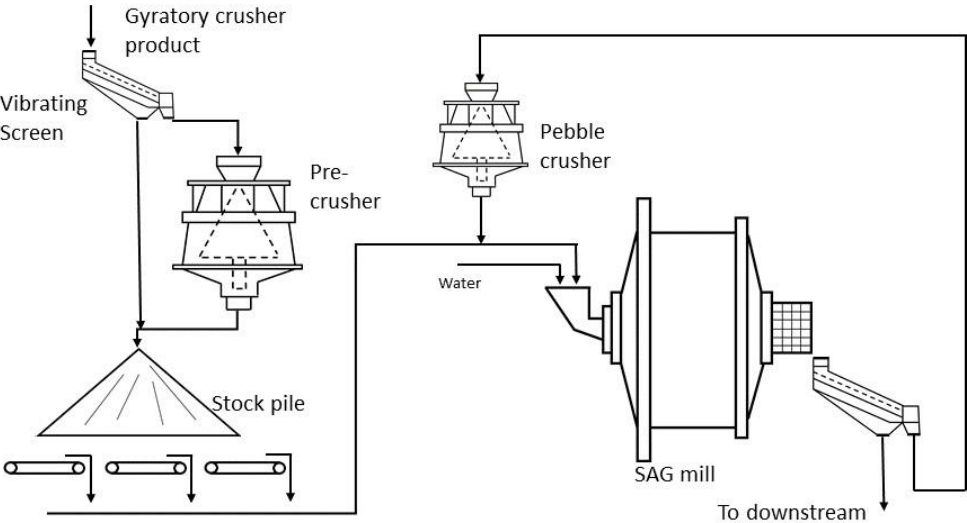


Figure 2. Example of a closed SAG mill circuit with pebble recycling: the feed has been pre-crushed due to the high competence of the material before being fed into the grinding circuit (Paper D).

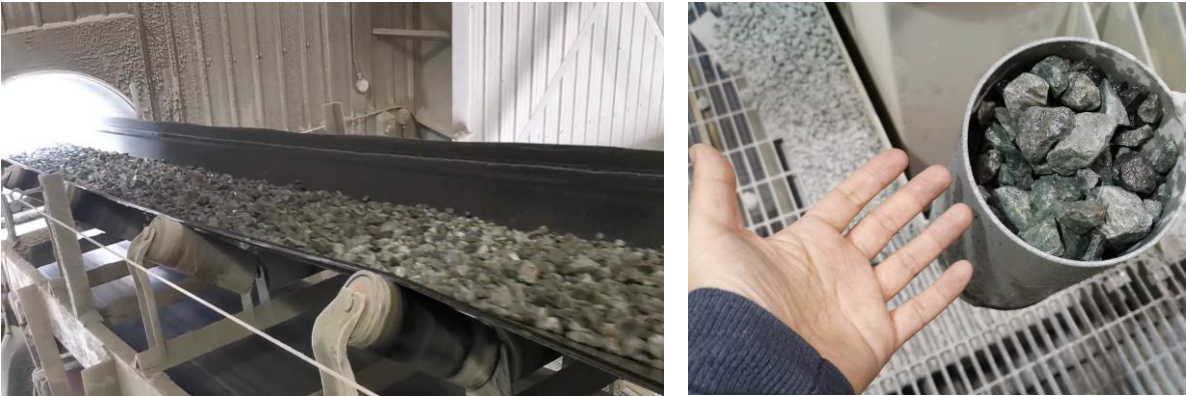


Figure 3. Conveyor belt with pebbles between a SAG mill and its pebble crusher (left); Illustration of pebble size (right).

To gain a better understanding of the comminution process, and for the purpose of control and optimization, many approaches have been developed for the modeling of SAG mills. These methods include empirical black-box modeling (Morrell, 1996a), fundamental dynamic

modeling (Valery & Morrell, 1995; Kojovic et al., 2012; Yu et al., 2014), discrete element method (Carvalho, 2013; Morrison & Cleary, 2004), and data-driven methods (Hoseinian et al., 2017; Xing-yu et al., 2017). Similarly, many studies on modeling cone crushers have been conducted, including a fundamental breakage cone crusher model proposed by Evertsson (Evertsson, 2000), cone crusher wear dynamics modeling by Lindqvist (Lindqvist & Evertsson, 2006), active cone crusher speed control algorithm by Hulthén (Hulthén, 2010), and DEM breakage modeling method (Delaney et al., 2015; Quist & Evertsson, 2016). Based on these cone crusher models, as well as models for other equipment such as bins, screens, and conveyor belts, the dynamics of crusher plants and their optimizations are systematically examined and discussed (Asbjörnsson, 2015; Bhadani, 2022).

However, these models mainly have focused on the optimization of mills and cone crushers respectively, few have considered the connections of these two machines and investigated them as a whole system. The power draw of a big SAG mill can be up to 28 MW, while its pebble crusher power draw is usually only 300 to 1000 kW. It needs to be mentioned that the recycling load occupies around 20% of the total SAG mill throughput and up to 50% in an AG mill circuit (data based on the author's observations from FLSmidth customer plants). Moreover, Evertsson and Powell reported a generally poor utilization of pebble crushers in many grinding circuits (Powell et al., 2019).

The hypothesis of this research can thereby be summarized as follows: In addition to the individual optimizations of SAG mills and cone crushers, the performance of the grinding circuit can be improved through the selection of the pebble crusher during the circuit design phase and by actively controlling the cone crusher during operation.

## 1.2 Research Scope and Research Questions

The overall objective of this thesis is to investigate the dynamic interactions between a SAG mill and its pebble crusher to enhance circuit efficiency by increasing the total throughput or reducing specific energy consumption. Approaches are proposed to develop high-fidelity dynamic models of the SAG mill, the cone crusher, and other units in the grinding circuit. Furthermore, validations with industrial data are carried out for future circuit design and optimization.

The objectives of this work can be formulated by the following research questions:

- RQ 1: What are the dynamic interactions between the SAG mill and the pebble crusher in a grinding process?

*It has been validated that using a pebble crusher can enhance the performance of a SAG mill grinding circuit by reducing the residence time, decreasing particle build-up in the mill chamber, and lowering overall circuit energy consumption. However, limited research has been done on investigating the circuit response during dynamic fluctuations. The operations in a grinding circuit are not always steady or ideal.*

- RQ 2: What approach can be used to model these interactions and other internal dynamics for SAG mills and pebble crushers?

*Fundamental models describe the working principles of these machines based on physical laws, though some fitting parameters are adopted to simplify certain processes. Data-driven models show advantages in finding non-linear relations*

*between complex operating signals and desired outputs, however lack of the interpretations of why and how the black-box model works.*

RQ 3: How can these approaches be adapted and implemented in industrial applications?

*Different purposes require different demands, such as flowsheet design, soft sensing, energy consumption prediction or data analytics from annual historical data.*

RQ 4: How can operational signals be used to identify different units' working conditions to improve the modeling accuracy?

*During operations, neither the operator nor the control system can keep the machines running at an optimal performance state. Such underperformance could be caused by wear, overload, or bypasses due to maintenance. A generic model is designed to describe the steady-state operations, however it struggles to accurately represent the machines when they are operating under poor conditions.*

RQ 5: What additional information needs to be collected on top of the current sensing system to help enhance the process modeling and controlling?

*Condition monitoring in the minerals processing ensures operational supervision, fault detection, and maintenance scheduling. Nevertheless, not all critical information can be easily collected. Some data collection still requires an extensive workforce and sometimes necessitates sacrificing process operating time, such as belt-cut surveys and liner wear inspections inside the mill.*

### 1.3 Research Approach

The research methodology used in this thesis has been proposed and used by the Chalmers Rock Processing Systems (CRPS) research group in several research projects over the last three decades. The group is part of the Division of Product Development at Chalmers University of Technology. The proposed problem-oriented research approach was initially proposed by Evertsson (Evertsson, 2000) for developing new knowledge focusing on the problem itself. Asbjörnsson (Asbjörnsson, 2015) adopted this problem-oriented research approach and integrated it into a broader scope to include system development. The description of the approach is illustrated in Figure 4.

Projects carried out at CRPS are initiated and formulated from an identified industrial problem or knowledge gap with industrial relevance. After the problem formulation, systematic investigations are conducted, including literature studies, initial experiments, interviews, and industrial data analysis. Following the initial study, the next task is to select a suitable research method, as shown in Figure 4, the system-building phase. This problem-oriented research focuses on solving the problem based on the nature of the problem itself. Therefore, different methods can be compared and verified with respect to modeling fidelity. This iterative process continues until the chosen methods show adequate performance in system modeling accuracy and suitability for various future applications. The final step after system building is validation, where case studies are applied to further evaluate the modeling methods. An early implementation during the research phase, as mentioned by Hulthén (Hulthén, 2010), provides additional insights into the examined system. Moreover, new problems could arise during the implementation step before the final industrial-scale application.

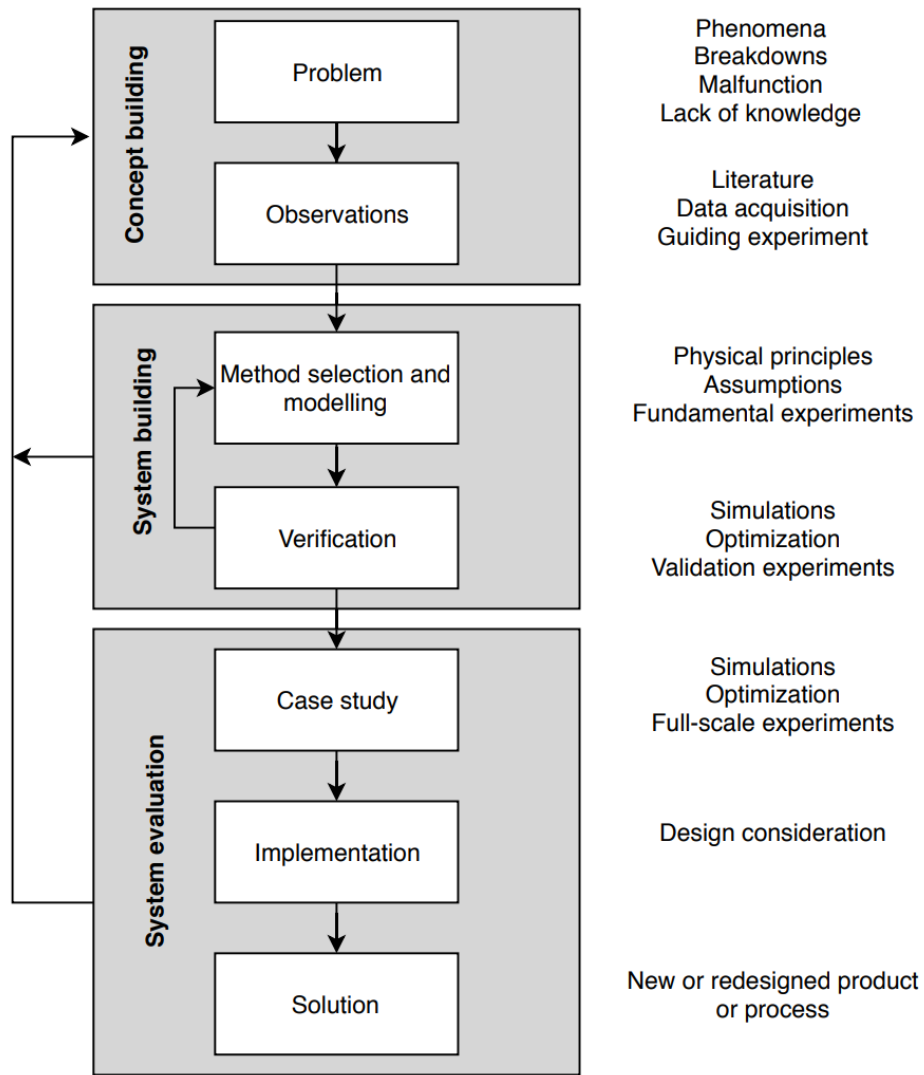


Figure 4. The applied problem-oriented research methodology based on Evertsson (Evertsson, 2000) and modified by Asbjörnsson (Asbjörnsson, 2015).



# 2 LITERATURE REVIEW

*The aim of this chapter is to:*

- *Introduce research that has been focused on SAG mill dynamic modeling and cone crusher modeling.*
- *Provide recent research on data-driven methods in the minerals industry.*

## 2.1 Fundamental Models

Morrell divided SAG mill modeling methods into two groups: black-box models and mechanistic models (Napier-Munn et al., 1996). The black-box models do not typically represent the fundamental physics of the comminution process. Instead, this type of modeling technique is mainly derived from statistical analysis based on industrial data. The advantages of black-box models include simplicity, low computational requirements, and good predictive accuracy for specific devices (Yu, 2017). However, the drawbacks are that they are only useful within a defined boundary, depend on the quality of trained data, and offer limited generality across different plants.

Fundamental models, on the other hand, incorporate the underlying physics of the comminution process. These models consider ore breakage behavior and the interactions between particles and other elements within a mill (Napier-Munn et al., 1996). The advantage of fundamental models compared to black-box data-driven models is their broader applicability, such as advanced control and optimization for new devices. In the comminution field (including crushing, screening, grinding, and classification), fundamental models are often referred to as mechanistic models.

### 2.1.1 SAG mill modeling

Morrell proposed a simplified structure for SAG mills, in which three main components are used to describe the grinding dynamics (Morrell, 1992):

- Collision frequency (breakage rate)
- Ore size distribution after collision (appearance distribution function)
- Particle transport out of the mill

For a steady-state situation with the perfect mixing mass balance model, the grinding process within a mill can be summarized as follows as proposed by Whiten (Whiten, 1974):

$$0 = f_i - p_i + \sum_{j=1}^i r_j s_j a_{ij} - r_i s_i \quad (2.1)$$

$$p_i = d_i s_i \quad (2.2)$$

Where  $f_i$  is feed rate of particles of size  $i$ ;  $p_i$  is product rate of particles of size  $i$ ;  $r_i$  is breakage rate of particles of size  $i$ ;  $s_i$  is mill contents of particles of size  $i$ ;  $a_{ij}$  is appearance function, size class  $i$  breaks from size class  $j$ ;  $d_i$  is discharge rate of size class  $i$ .

Based on the steady-state population balance method (PBM) as seen in Equation (2.1) and Equation (2.2), Valery and Morrel (Valery & Morrell, 1995) proposed a dynamic mill model

that calculates dynamic responses in terms of mill charge level, slurry level, mill power draw, feed ore size, and water addition:

$$\frac{ds_i(t)}{dt} = f_i - p_i + \sum_{j=1}^{i-1} r_j s_j a_{ij} - (r_i s_i - r_i s_i a_{ij}) \quad (2.3)$$

$$p_i = d_i s_i \quad (2.4)$$

Where  $s_i(t)$  is the mass of particles in the mill of size  $i$  at time  $t$ .

The particle breakage behavior may be defined as a solid particle that under a certain input energy thus causes mass loss of the original particle, and leads to generate daughter fragments (Carvalho, 2013).

To study the main particle breakage characteristics namely, size and energy level dependency, Narayanan (Narayanan, 1987) introduced the drop weight test on single particles, as illustrated in Figure 5. In this test, a steel ball is dropped from a known height onto a single particle placed on a hard surface. The impact energy that the particle receives can be calculated from the mass and height of the steel ball. By varying the drop height, multiple tests and different impact energies can be applied to this single particle. The fragments from the original particle can be then collected to analyze the breakage behavior under a given energy.

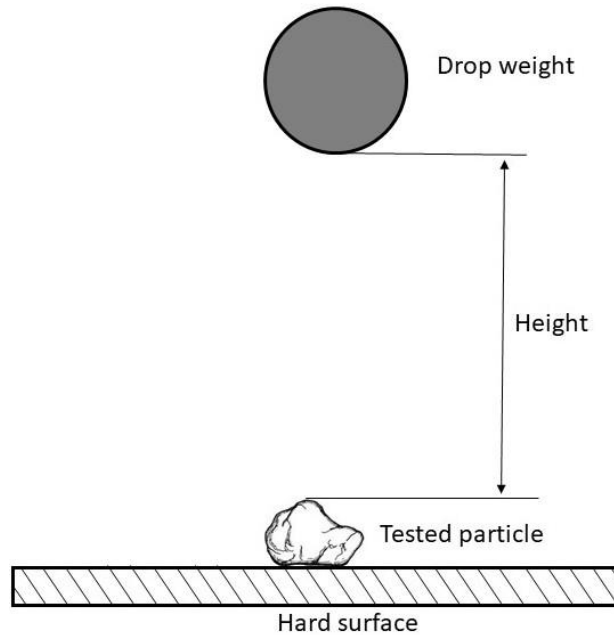


Figure 5. Scheme of the drop weight test.

The results of single particle drop weight tests have shown that the breakage characteristics are primarily determined by the energy applied to the particle. The greater the energy of the impact, the finer the fragments generated. This occurs due to the successive breakage and rebreakage of the daughter fragments until all applied energy is dissipated (King, 2001).

The breakage product size distribution can be described using  $t_n$  curves. This  $t_n$  parameter is the percentage passing an aperture of  $1/n$  of the original ore particle size, such as  $t_2$ ,  $t_4$ ,  $t_{10}$ ,  $t_{25}$ ,  $t_{50}$  and  $t_{75}$ . Among these representative parameters,  $t_{10}$  is generally selected as the reference to characterize the breakage size distribution. King (King, 2001) combined the test



results from several researchers (Bourgeois, 1993; Narayanan & Whiten, 1983; Pauw & Maré, 1988) and presented the  $t_{10} - t_n$  family curve in Figure 6. In these studies, a wide range of materials with different properties were tested, and their breakage curves showed great similarity.  $t_{10}$  is mainly determined by the energy the particle receives during the impact test, thus the relations between  $t_{10}$  and the impact energy can be fitted to a format as shown in Equation (2.5),

$$t_{10} = A[1 - e^{-bE_{cs}}] \quad (2.5)$$

where,  $A$  and  $b$  are the ore breakage parameters determined from drop weight tests,  $E_{cs}$  is the specific comminution energy. A low value of  $A \cdot b$  suggests that the ore requires more energy to breakage.

If  $E_{cs}$ , the ore parameters  $A$  and  $b$  are given, then the corresponding  $t_{10}$  and the entire appearance function can be obtained from Figure 6. This provides great convenience and standardization in building a breakage model.

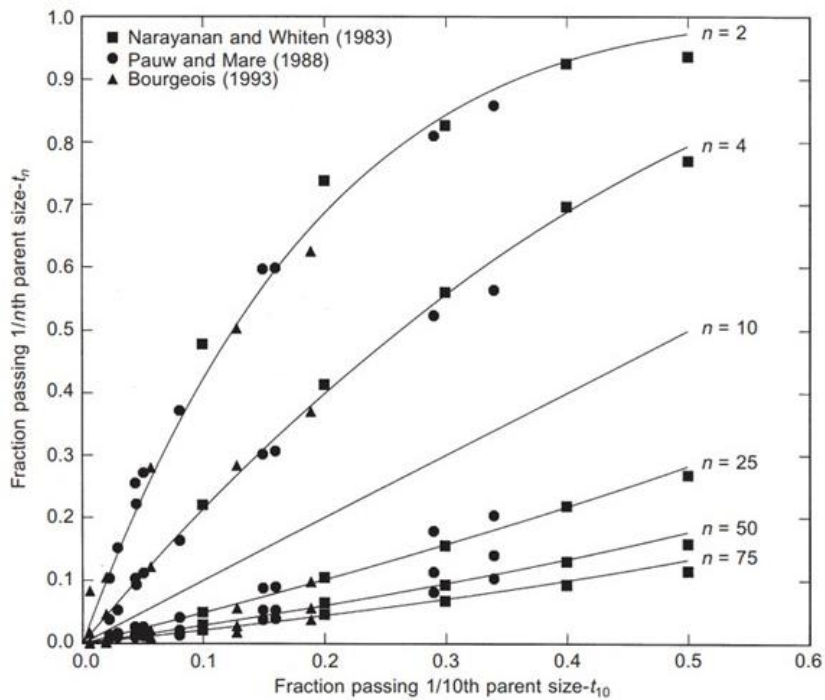


Figure 6.  $t_{10} - t_n$  curve for the drop weight tests (King, 2001). Reconstructed plot from selected papers (Bourgeois, 1993; Narayanan & Whiten, 1983; Pauw & Maré, 1988).

Building on the JK tumbling model, Yu (Yu, 2017) developed an integrated, mechanistic dynamic mill model based on the population balance framework. This model incorporates a full breakage function along with material characteristic-dependent appearance function, slurry transport function, and discharge function.

In this integrated framework, the appearance function is derived from an updated JKMRC appearance function (Kojovic et al., 2012), which involves the size-dependent parameters as shown below:

$$t_{10} = M[1 - e^{-F_{mat} \cdot X \cdot E_{cs}}] \quad (2.6)$$

$$A \cdot b = 3600 \cdot M \cdot F_{mat} \cdot X \quad (2.7)$$

where  $M$  is the maximum possible value of  $t_{10}$  in impact,  $F_{mat}$  is material property relates to the ore-specific constants,  $X$  is the average particle size. The parameters in the appearance equations are determined by the drop weight test.

The breakage rate, also sometimes called the selection function, is defined as the fraction of particles selected to be broken per unit of time. In the JK tumbling mill model, the breakage rate function is back-calculated (Kojovic et al., 2012) using a simplified population balance method equation, which can be obtained under the assumption of perfect steady-state mixing:

$$f - R \cdot s + A \cdot R \cdot s - D \cdot s = 0 \quad (2.8)$$

where  $f$  is feed rate;  $R$  is breakage rate or selection function;  $s$  is mill content;  $D$  is discharge rate;  $A$  is appearance function. The selection function  $R$  then can be back calculated with a given feed and product particle size distribution and the appearance function. In this JK selection function format as seen in Figure 7, five spline knots at 0.25 mm, 4 mm, 16 mm, 44 mm and 128 mm, are generally used to fit the cubic curve.

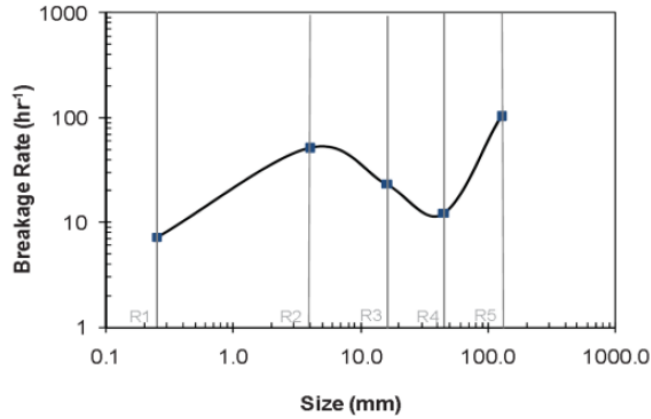


Figure 7. JK breakage rate function example of SAG mills (Kojovic et al., 2012).

As an alternative method for describing the breakage rate, Austin and Cho (Austin & Cho, 2002) used two fitting curves to capture the breakage characteristics in a fully mixed mill model. An example of the Austin breakage rate function can be seen in Figure 8. The equations chosen for the specific breakage rate are expressed as:

$$S_{1i} = A_1 \left( \frac{x_i}{x_0} \right)^{\alpha_1} \left[ \frac{1}{1 + \left( \frac{x_i}{\mu x_0} \right)^A} \right] \quad (2.9)$$

$$S_{2i} = A_2 \left( \frac{x_i}{x_0} \right)^{\alpha_2} \quad (2.10)$$

$$S_i = S_1 + S_2 \quad (2.11)$$

where  $S_i$  is the selection function of the size interval indexed by  $i$ ,  $x_i$  is the upper size of the size interval indexed by  $i$ ,  $x_0$  is a standard size (usually 1 mm).  $A_1$ ,  $\alpha_1$ ,  $\mu$  and  $\Lambda$  is for the nipping breakage of smaller particles by larger grinding media, while  $A_2$ ,  $\alpha_2$  is for the breakage of large lumps by collision with media and lumps of similar size (self-breakage). The units of  $A_1$  and  $A_2$  are  $time^{-1}$ . The parameters  $\alpha_1$ ,  $\alpha_2$ ,  $\mu$ ,  $\Lambda$  are dimensionless.

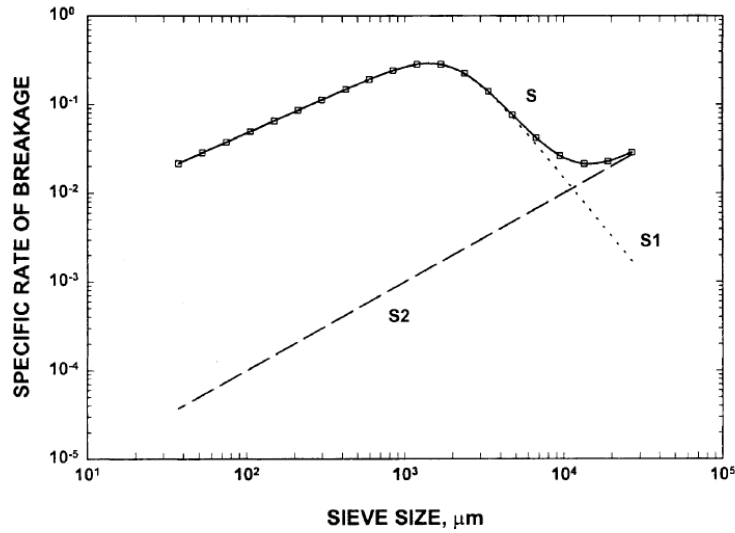


Figure 8. Austin breakage rate function example where the total breakage rate  $S$  is fitted by combining curve  $S_1$  and a straight line  $S_2$  (Austin & Cho, 2002).

The mill power estimation is of great importance in the design of comminution circuits. Some studies estimate SAG mill power based on the mill geometry and the charge profile in the chamber. Morrell (Morrell, 1996b) proposed a theoretical power estimation approach for all types of tumbling mills. This model considers the motion of the grinding charge and the amount of potential and kinetic energy transferred from the mill shell to the particles inside the mill. A simplified mill charge scheme is shown in Figure 9.

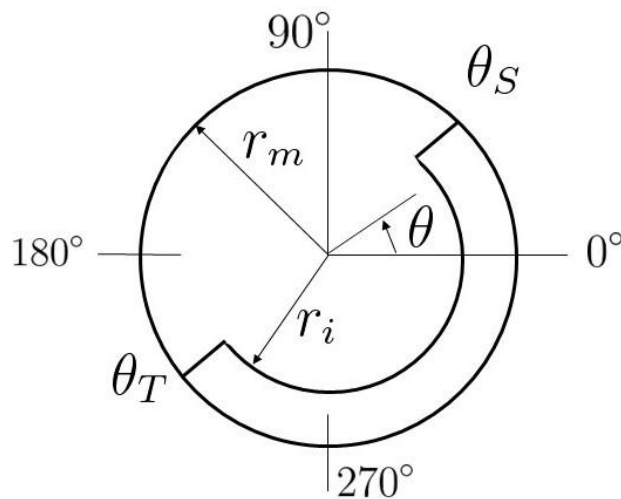


Figure 9. Simplified mill charge scheme modified from Morrell's approach (Morrell, 1996b).

The mill is divided into cylindrical and conical sections to capture more accurate geometric information. The power draw is calculated in Equation (2.12) for cylinder part and cone part in Equation (2.13):

$$P_{cylinder} = \int_{r_i}^{r_m} V_r L r g \rho_c (\sin \theta_s - \sin \theta_t) + \rho_p (\sin \theta_s - \sin \theta_{tp}) dr \quad (2.12)$$

$$P_{cone} = \int_0^{L_i} \int_{r_i}^{r_{cone}} V_r L r g \rho_c (\sin \theta_s - \sin \theta_t) + \rho_p (\sin \theta_s - \sin \theta_{tp}) dr dL_c \quad (2.13)$$

Where  $r_m$  is the radius of mill inside the liners;  $r_{cone}$  is the radius of the conical section at a distance  $L_c$  from the cylindrical section;  $V_r$  is the tangential velocity of a particle at radial distance  $r$ ;  $L$  is the length of the cylindrical section of the mill inside liners;  $L_i$  is the length of charge surface within cone ends;  $\theta_s$  is the shoulder angle;  $\theta_t$  is the toe angle;  $\theta_{tp}$  is the angular displacement of the slurry toe position;  $\rho_p$  is the pulp density and  $\rho_c$  is the density of the total charge, including balls and rocks.

Morrell (Morrell, 1996a) also proposed an simplified empirical power model where fitting parameters were adopted:

$$P_{total} = N_{load} power + (KD^{2.5} L_e \rho_c \alpha \delta) \quad (2.14)$$

$$P_{idle} = 1.68 D^{2.05} [\phi (0.667 L_d + L)]^{0.82} \quad (2.15)$$

Where  $D$  is the diameter of the cylindrical section of the mill inside the liners;  $K$  is the lumped parameter used in the calibration of the model.  $L$  is the length of the cylindrical section of the mill inside the liners;  $L_d$  is the length of cone-end;  $L_e$  is the effective grinding length;  $\alpha$  is an empirical parameter;  $\phi$  is the fraction of critical speed;  $\rho_c$  is the density of total charge.

### 2.1.2 Cone crusher modeling

Cone crushers are widely used in aggregate production and in the mining industry. Evertsson (Evertsson, 2000) proposed a cone crusher model where the laws of mechanics and rock breakage characteristics are concerned. The framework is illustrated in Figure 10.

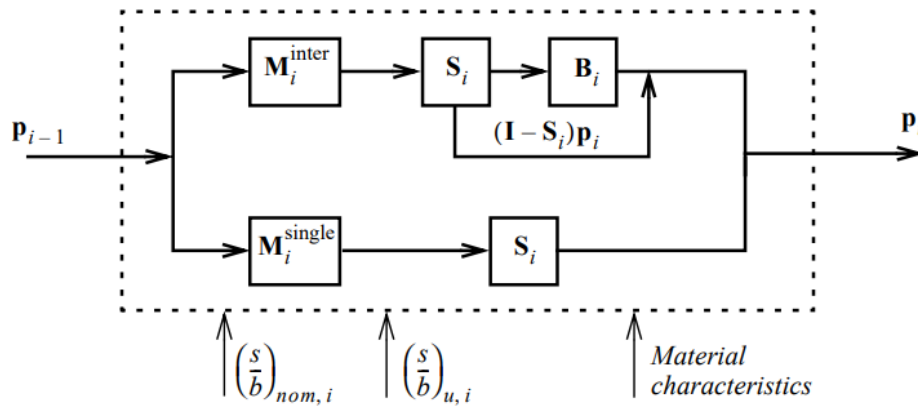


Figure 10. Schematic block diagram for a single crushing event of a cone crusher model framework.

The corresponding mathematical expressions for single particle and interparticle breakage is given in Equation (2.16) and (2.17):

$$\mathbf{P}_i = \left[ [\mathbf{B}_i^{inter} \mathbf{S}_i + (\mathbf{I} - \mathbf{S}_i)] \mathbf{M}_i^{inter} + \mathbf{B}_i^{single} \mathbf{M}_i^{single} \right] \mathbf{P}_{i-1} \quad (2.16)$$

$$\mathbf{M}_i^{inter} + \mathbf{M}_i^{single} = \mathbf{I} \quad (2.17)$$

In Equation (2.16),  $\mathbf{P}_i$  is the product size distribution from crushing zone  $i$  and  $\mathbf{P}_{i-1}$  represents the product from the previous crushing zone;  $\mathbf{B}_i$  is the breakage matrix and  $\mathbf{S}_i$  is the selection matrix; the  $\mathbf{M}_i$  matrix represents the proportion between single particle and interparticle breakage in a crushing zone and the sum of them should be an identity matrix  $\mathbf{I}$ .

Evertsson also introduced the cone crusher capacity calculation by integrating the mass-flow field over a horizontal cross-section of the crushing chamber. The mass flow is divided into the downward direction and the upward direction in Equation (2.18) and (2.19):

$$Q_{down} = \int_0^{\alpha_c} \int_{R_i(\alpha)}^{R_0} \rho v(\alpha) r dr d\alpha \quad (2.18)$$

$$Q_{up} = \frac{1}{2} \int_{\alpha_c}^{2\pi} \int_{R_i(\alpha)}^{R_0} \rho v(\alpha) r dr d\alpha \quad (2.19)$$

The overall capacity is calculated, as shown below:

$$Q = \eta_v (Q_{down} - Q_{up}) \quad (2.20)$$

Where  $R_i$  is the mantle radius;  $R_0$  is the concave radius;  $\alpha$  is the angle;  $v$  is the velocity vector;  $\rho$  is the bulk density of the material;  $\eta_v$  is a volumetric filling ratio.

However, as mentioned by Asbjörnsson (Asbjörnsson, 2015), the Evertsson crusher model is computationally heavy and needs a considerable amount of calculation time as the proposed model requires more detailed information, such as chamber geometry and breakage behavior.

## 2.2 Data-driven Models

As an alternative to the physics-based fundamental methods, and with the increasing use of new measurement technologies and distributed control systems, data collection and analysis in industrial processes are becoming increasingly important (Ge et al., 2013). In minerals engineering, machine learning and data-driven techniques have attracted the attention of many researchers in recent years (Ding et al., 2017; Tang et al., 2010). Data-driven models can be used to develop soft sensors for mill load (Tang et al., 2012); plant monitoring and fault diagnosis (Horn et al., 2017); mill dynamic modeling (Hoseinian et al., 2017), and flotation froth analysis (Xing-yu et al., 2017). McCoy conducted a literature review of machine learning applications in minerals processing (McCoy & Auret, 2019) over the past few decades. He suggested that a combination of the following factors is essential for the mineral processing engineers of tomorrow:

- Large quantities of diverse, high-quality data
- Mineral processing expertise
- In-depth knowledge and extensive experience in data analysis

- Computational thinking

Ge (Ge, 2017) proposed a general framework for data-driven modeling of plant-wide processes, which includes subsections such as process decomposition, data preprocessing, feature and sample selection, model training, and real-time online process monitoring. Figure 11 illustrates the flowchart of the data-driven modeling structure.

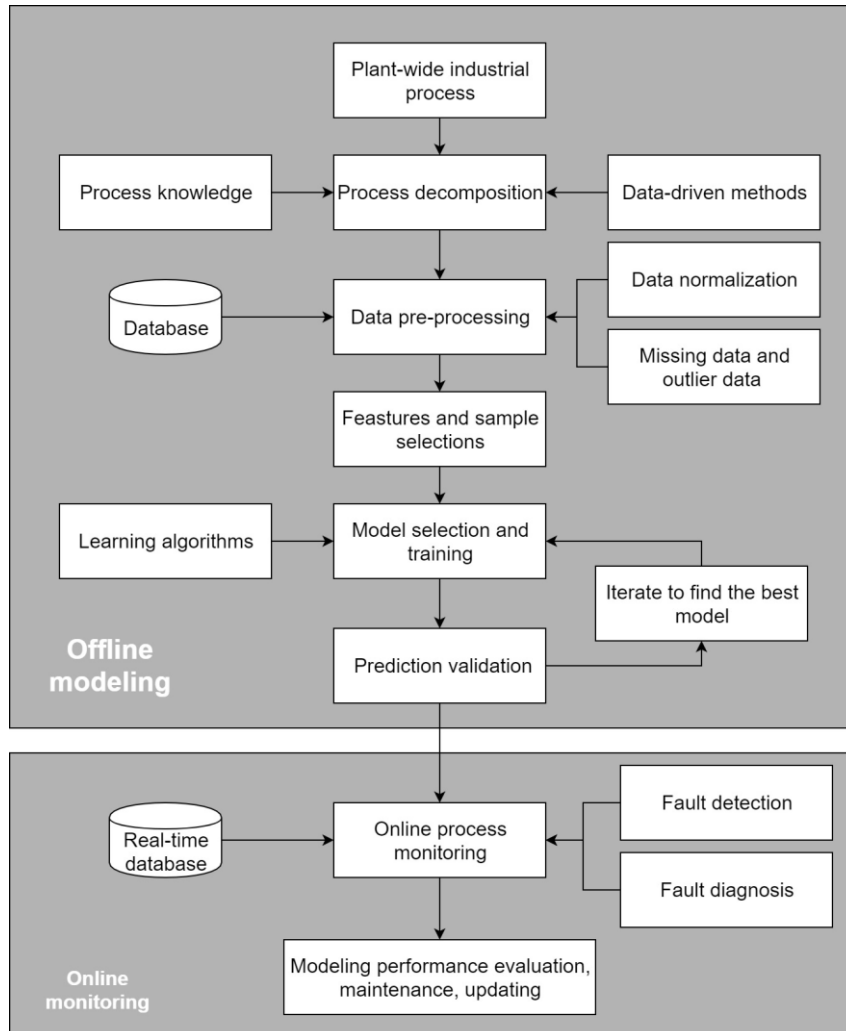


Figure 11. A generic procedure for data-driven modeling and monitoring of plant-wide processes, modified from a framework proposed by Ge (Ge, 2017).

### 2.2.1 Process decomposition and sub-process

Process decomposition is typically the first step in handling large-scale, plant-wide process simulations. This strategy offers several advantages. First, dividing a complex system into multiple distributed blocks can reduce computational costs. Second, a multi-block framework is more flexible to maintain and update. Third, it enhances fault tolerance.

Data preprocessing is an essential step in data-driven modeling and the data mining process. Industrial data often contains errors, as well as incomplete or inconsistent information. Data preprocessing can mitigate these issues and reformat raw data into a logical structure. The general methods used in data preprocessing include interpolation, data dimension reduction, normalization and standardization, and data feature selection and creation.

Feature and model selection follows data preprocessing, where appropriate machine learning algorithms and data model structures are considered. It is important to note that model selection is highly dependent on the data characteristics and the relationships among process operational variables (Ge, 2017). For example, non-Gaussian data modeling methods should be applied to variables with non-Gaussian distributions; a nonlinear algorithm, such as artificial neural networks, should be used if there are nonlinear relationships between variables and the desired predictions; and a dynamical learning method should be employed for time-series problems (Choi et al., 2008).

The next step before online utilization is model validation and performance evaluation. Several well-defined methods are available for this process, such as cross-validation, model stability analysis, and sensitivity analysis (Bishop, 2006).

## 2.2.2 Introduction of generally used data-driven methods

Generally, data-driven methods can be categorized into four groups: supervised learning, unsupervised learning, semi-supervised learning, and reinforcement learning. In industry applications, supervised and unsupervised learning are most commonly adopted, accounting for more than 80% of usage (Sun, 2021; Ge et al., 2017). Brief reviews of several representative learning methods are described as follows.

The decision tree is a popular algorithm for supervised learning problems (Hastie et al., 2005). The main idea is to build a binary tree that splits its space into two regions. Each branch then continues to split into two more regions, and this process repeats until a stopping criterion is met. However, decision trees are prone to overfitting, especially when the tree is deep.

Random Forests (RF) algorithm was developed by Breiman (Breiman, 2001). An RF is a collection of decision trees whose results are aggregated into a single output. The overfitting problem is mitigated by its voting mechanism. RF also improves forecasting accuracy by averaging the predictions of many noisy but unbiased trees (Zhang & Haghani, 2015).

Gradient Boosting Regression (GBR) is similar to RF in that both are ensemble learning methods that predict by combining the outputs of individual trees. The major difference between GBR and RF is that in GBR, the probability of selecting an individual sample is not equal, whereas in RF, the samples are selected uniformly (Zhang & Haghani, 2015). This random selection helps to make the method more robust than decision trees and less likely to overfit on the training data.

An effective classification and regression method is the K-Nearest Neighbors (KNN) model (Witten et al., 2002). KNN is one of the oldest and simplest algorithms used in data mining and machine learning. A typical KNN uses Euclidean distances to measure the dissimilarities of input vectors (Weinberger et al., 2006). The decision of a class label for an input pattern is based on the class labels of its closest neighboring vectors.

An Artificial Neural Network (ANN) is a flexible and robust mathematical architecture capable of identifying complex non-linear relationships between input and output signals. Inspired by biological nerve systems, the processing nodes in an ANN, called neurons, are arranged in a computational network (Lippmann, 1987). These neurons are connected in parallel through activation functions and weights. Once the network is trained, it can be used to calculate the output for any arbitrary set of input data, as long as the input data falls within the space defined by the training data sets.

### 2.2.3 Combination of Fundamental Models and Data-driven Models

It should be noted that data-driven methods have a major limitation: they are agnostic to underlying physical principles. Black-box data-driven models are often highly dependent on the labeled data with which they are trained. While the model's predictions may appear deceptively accurate on both training and test datasets, they may not generalize well beyond the available labeled data (Karpatne et al., 2017; Karpatne et al., 2022). Additionally, a primary concern with black-box models is their lack of scientific consistency with respect to the laws of physics. Even though their predictions may sometimes be more accurate, data-driven models cannot provide mechanistic insights into the physical processes they represent.

To combine the advantages of data-driven models and fundamental models, Karpatne (Karpatne et al., 2017; Karpatne et al., 2022) introduced a framework that integrates physics knowledge into neural networks. Figure 12 illustrates one method that incorporates physical models into data-driven models. In this approach, the output of the physics-based model is treated as a new feature in the data-driven model, alongside the original dataset. Additionally, the use of physics-based loss functions in the learning objective to ensure that the model's predictions not only have fewer errors but are also consistent with known physical laws.

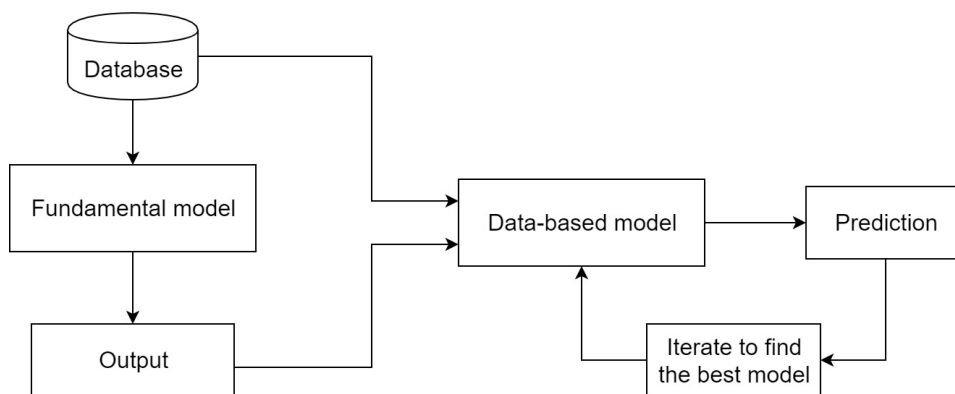


Figure 12. Schematic illustration of a hybrid fundamental-data model. The output of a physics-based model is used as a new feature in a data-based model, modified from Karpatne (Karpatne et al., 2017).

This kind of hybrid-physics-data structure is studied and applied in many engineering systems. For example, Jia proposed a physics guided recurrent neural network to simulate a lake temperature profiles (Jia et al., 2019), Long applied convolutional Long short-term memory (LSTM) as the backbone to predict the external forces on a dynamic system (Long et al., 2018), and Zhang showed improved performance on simulating a power grid via physics-deep unrolled neural networks (Zhang et al., 2018). Recently investigators have examined the effects of physics understandings on pure data-driven methods. The hybrid-physics-data framework shows better generalizability, and more importantly, it introduces physically meaningful results in comparison to black-box data methods (Karpatne et al., 2017).



# 3 METHOD

The aim of this chapter is to:

- Introduce the research methodology used in this thesis.
- Describe the adopted fundamental models of SAG mills and cone crushers.
- Describe the data-driven algorithms for SAG mill power and pebble rate prediction.
- Propose a framework for data analysis.

A typical grinding circuit generally consists of one or several SAG mills and pebble crushers, as well as conveying systems, screens, and storage units. This study focuses not only on the modeling of SAG mills and cone crushers but also on the interactions between these units. For example, in some grinding processes with multiple pebble crushers, the crushers are often switched on and off or bypassed for certain maintenance and cost-saving reasons. The impact of these operations on the entire grinding system is one of the main areas of study in this research.

To better address the research questions raised in the previous sections and to inspire further related research, the methods covered in this thesis can be divided into three categories: fundamental methods, data-driven methods, and data analytics. The topics and papers corresponding to these methods are shown in Figure 13. More detailed modeling methods can be found in the corresponding articles.

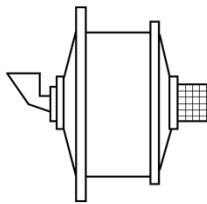
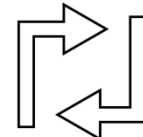
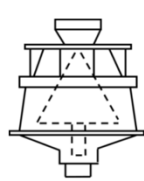

Units	Methods	Topics	Papers
 <p>AG/SAG mill</p>	<div style="border: 1px solid black; padding: 2px; margin-bottom: 5px;">Fundamental methods</div> <div style="border: 1px solid black; padding: 2px; background-color: #cccccc; margin-bottom: 5px;">Data-driven methods</div>	<ul style="list-style-type: none"> <li>• Mass flow</li> <li>• Product size</li> <li>• In mill dynamics</li> </ul>	<p>Paper A</p> <p>Paper B</p>
 <p>Recycling impacts</p>	<div style="border: 1px solid black; padding: 2px; margin-bottom: 5px;">Fundamental methods</div> <div style="border: 1px solid black; padding: 2px; background-color: #cccccc; margin-bottom: 5px;">Data analytics</div>	<ul style="list-style-type: none"> <li>• Mass flow</li> <li>• Product size</li> <li>• Selected key variables</li> </ul>	<p>Paper B</p> <p>Paper D</p> <p>Paper G</p>
 <p>Pebble (cone) crusher</p>	<div style="border: 1px solid black; padding: 2px; margin-bottom: 5px;">Fundamental methods</div> <div style="border: 1px solid black; padding: 2px; background-color: #cccccc; margin-bottom: 5px;">Data analytics</div>	<ul style="list-style-type: none"> <li>• Product size</li> <li>• Operating conditions</li> </ul>	<p>Paper B</p> <p>Paper D</p>
 <p>Feed / product size</p>	<div style="border: 1px solid black; padding: 2px; background-color: #cccccc; margin-bottom: 5px;">Data-driven methods</div>	<ul style="list-style-type: none"> <li>• Rock size distribution estimation</li> </ul>	<p>Paper E</p>

Figure 13. Overview of the thesis contents.

### 3.1 Fundamental Models

The fundamental model is one of the most classical approaches for studying the comminution process, such as the Magnus cone crusher model (Evertsson, 2000), the Morrell (Morrell, 1992, 1996b), Austin (Austin & Cho, 2002) and Yu (Yu, 2017) tumbling mill models. These methods take into account the crushing/grinding process of the particles and consider factors such as energy consumption, breakage rate, particle movement, and the coupling of these sub-processes. Physics-based models have the advantage over data-driven models in that they offer a broader simulation range, whereas data-driven model applications are limited by the boundaries of the training data.

#### 3.1.1 SAG mill

In both Paper A and Paper B, the proposed dynamic model of a SAG mill includes several interlinked sub-process modules, and each of these modules can be updated individually. As shown in Figure 14 adapted from Paper A, the mill is divided into  $n$  sections, where  $m$  is the section number, and  $q$  is the mass of transported material. All sections have the same length, and each section contains a dataset of particle information at each simulation time step, such as particle size, mass, energy gain, and breakage rate. The dataset is calculated and updated continuously. Each particle is ground into new particles according to the breakage rate and appearance function, and then the probability of moving to the next section is estimated based on the mass transfer coefficient and the slurry flow rate.

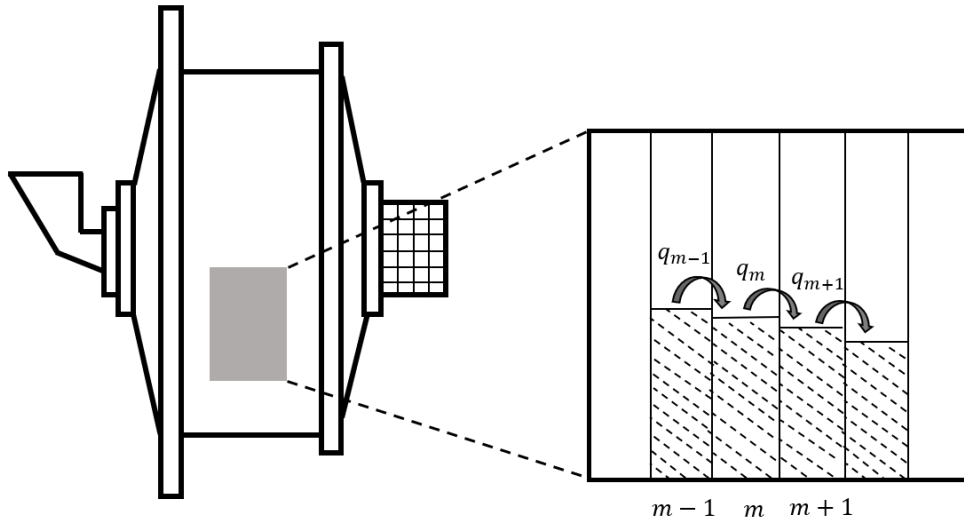


Figure 14. Schematic of data structure in the SAG mill simulation.

Austin introduced a simple algebraic equation set that describes a time-independent breakage model and treats the mill as a series of fully mixed reactors (Austin & Cho, 2002), as in Equation (3.1).

$$Sel_i = A_1 \left( \frac{x_i}{x_0} \right)^{\alpha_1} \left[ \frac{1}{1 + \left( \frac{x_i}{\mu x_0} \right)^\Lambda} \right] + A_2 \left( \frac{x_i}{x_0} \right)^{\alpha_2} \quad (3.1)$$

where  $Sel_i$  is the selection function of the size interval indexed by  $i$ ,  $x_i$  is the upper size of the size interval indexed by  $i$ ,  $x_0$  is a standard size (usually 1 mm).  $A_1$ ,  $\alpha_1$ ,  $\mu$  and  $\Lambda$  is for the nipping breakage of smaller particles by larger grinding media, while  $A_2$ ,  $\alpha_2$  is for the breakage of large lumps by collision with media and lumps of similar size (self-breakage). The units of  $A_1$  and  $A_2$  are  $time^{-1}$ . The parameters  $\alpha_1$ ,  $\alpha_2$ ,  $\mu$ ,  $\Lambda$  are dimensionless.

The energy applied in each section can be estimated as:

$$E_i^m = \frac{E_{tot}}{n \cdot \left( \sum_{i=1}^j m_i + m_{ball} \right)} \quad (3.2)$$

In Equation (3.2), there are  $n$  equally long sections and  $E_i^m$  is the mean energy for particle size class  $i$  in section  $m$ .  $m_i$  is particle mass of size class  $i$  and  $m_{ball}$  is the steel ball mass, and  $E_{tot}$  is the total net energy applied on the mill charge.

In work from Paper A and Paper B, the standard Broadbent-Calcott model (Whiten, 1974) for the appearance function is applied instead of the JKMRC  $t_{10}$  model. The standard appearance function covers a broader size range and is independent of ore type. This standard appearance function is used to validate the proposed hypotheses in a general manner. In contrast, the JKMRC model and laboratory tests are conducted on the actual ore, providing more accurate information for a specific plant.

The transport function plays a crucial role in dynamic mill modeling, influencing particle size distribution, mill load, throughput, residence time, and other parameters (Yu et al., 2014). In this work, the mill is modeled as a series of interconnected sections, where particles in each section are considered to be perfectly mixed. The diffusion relationships for each ore size class are described in Equation (3.3).

$$q_i = -D_i \cdot \frac{d\rho_i}{dx} \quad (3.3)$$

Where  $i$  indicates the  $i$  th size class of particles,  $q$  is the mass flux through the controlled area,  $D_i$  is the mass transfer coefficient and  $d\rho/dx$  is slurry density changing along the mill sections. The transfer coefficient needs to be tested and updated from pilot or plant data.

The discharge function for each particle size class in SAG mills can be expressed as the maximum discharge rate ( $D_{max}$ ) times the classification function, see Equation (3.4). The classification function is characterized into three zones (Kojovic et al., 2012) using the size of slurry (particles smaller than this size behaves like liquid), size of grate aperture, and pebble port size.

$$d_i = D_{max} \cdot c_i \quad (3.4)$$

Where  $d_i$  is the discharge rate of size class  $i$ ,  $c_i$  is the classification function for size class  $i$ .

Valery and Morrell (Napier-Munn et al., 1996) developed a conceptual dynamic model for SAG mills to provide an accurate dynamic response such as power draw, mill charge level, product size distribution feed hardness, etc. In Paper A and Paper B, the dynamic equations are

updated based on Valery and Morrell's equation, see Equation (2.3), the particle population model for each section in a mill is described in Equation (3.5). In this dynamic equation, the material change in each section is calculated individually:

$$\frac{ds_i(t)}{dt} = q_i^{in} - q_i^{out} + \sum_{j=1}^i r_j s_j a_{ij} - r_i s_i \quad (3.5)$$

Where  $s_i$  is section content of size class  $i$  at time  $t$ ,  $q_i^{in}$  is particles transported from the previous section of size class  $i$ ,  $q_i^{out}$  is particles transported to the next section of size class  $i$ ,  $r_i$  is particles breakage rate of size class  $i$ ,  $a_{ij}$  is appearance function, size class  $i$  break from size class  $j$ . At the first section,  $q_i^{in}$  is feed particles of size class  $i$ , and at the last section,  $q_i^{out}$  is discharged particles of size class  $i$ .

The dynamic framework presented in Paper A and Paper B models a mill as a series of perfectly mixed sections, incorporating a breakage/appearance function and a mass transfer function. The method applies basic calculation rules and avoids utilizing too many empirical relations. At each simulated time step, the fresh feed, product, and mill operating parameters are considered. The status of all particles is calculated in terms of breakage probability, motion behavior, position in the mill, discharge likelihood, and other factors. If the system reaches stable operation within a certain period, it is considered to be in a steady state. This model is designed to be based on real plant data and to back-calculate the sub-process functions previously used, which in turn leads to broader applications and more accurate predictions.

### 3.1.2 Simplified cone crusher model and other equipment

In Paper B, the dynamic behavior of the entire system, including the SAG mill and cone crusher operating in a closed circuit, is examined. Therefore, in addition to the SAG mill model, the dynamic simulation of cone crushers, conveyors, bins, and screens is also included. Asbjörnsson (Asbjörnsson, 2015) studied the dynamic behavior of crushing plants and discussed the machinery bottlenecks that affect throughput. Here, dynamic models similar to those presented by Asbjörnsson are used to model conveyors and screens. A time delay is incorporated into the conveyor model based on its length and speed, as shown in Equation (3.6). Additionally, the screens are modeled with a constant time delay, which depends on the screen size. The large surge bin for material storage is assumed to be perfectly mixed, and the level in the bin is a function of mass flow and the bin dimensions.

$$\chi(t) = u(t - t_{delay}) \quad (3.6)$$

A small bin is modeled for the cone crusher chamber, where the particles are assumed to be perfectly mixed. The product particle size distribution of the cone crusher is shown in Figure 15 from Paper B. The eccentric speed settings in Figure 15 are 280, 360, and 440 rpm. It can be seen from the plot that the closed side setting (CSS) and eccentric speed of a cone crusher can significantly affect the final PSD. A change in the CSS shifts the product PSD horizontally, while variations in eccentric speed pivot the curve around a specific point (Hulthén, 2010). Furthermore, the crusher capacity is also a function of CSS and eccentric speed, as shown in Figure 16 from Paper B. With a given CSS, the capacity decreases as the eccentric speed increases.

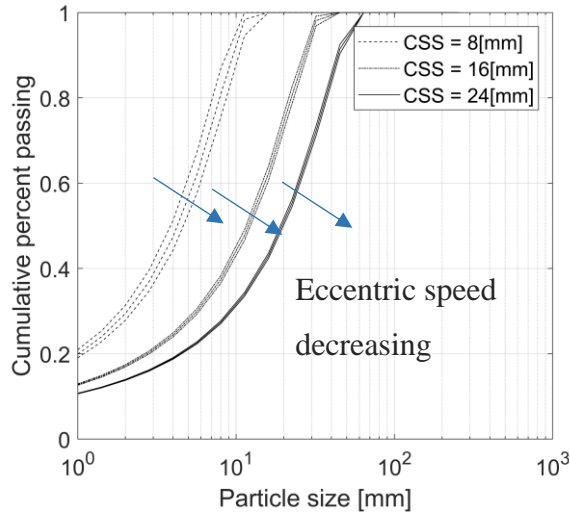


Figure 15. Product PSD of different cone crusher settings. Data from Evertsson (Evertsson, 2000), tested on a Svedala Hydrocone cone crusher.

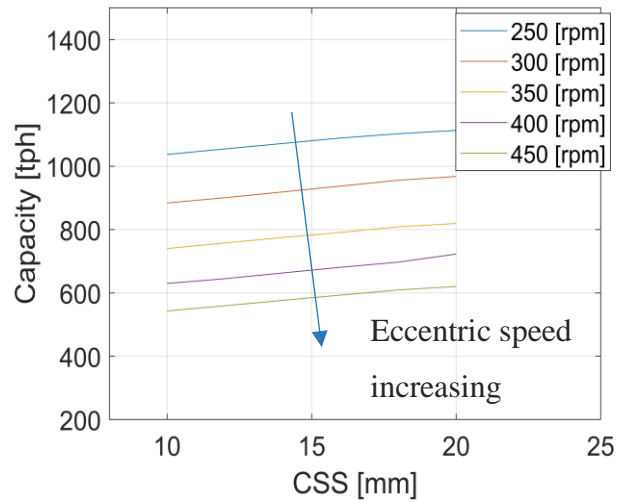


Figure 16. The capacity of cone crushers with different settings. Data from Lindqvist (Lindqvist & Evertsson, 2004), tested on an FLS Raptor 900 cone crusher.

## 3.2 Data-driven Methods

In this thesis, several data-driven models are applied to estimate the energy consumption and pebble rate of the SAG mill. Thanks to advancements in sensor technology over recent decades, control systems can now acquire large amounts of real-time operating data. In cases involving complex mechanisms, difficulties in building physical models, and dynamic disturbances, a well-selected data-driven algorithm can yield promising prediction results when trained on a pre-processed dataset.

### 3.2.1 SAG mill power

Two data-driven methods are presented in Paper C, where a SAG power prediction and a two-minute power forecast are performed. The forecasting model utilizes modified Recurrent Neural Networks (RNN). RNNs are developed to recognize patterns in sequences of data, such as text, spoken words, numerical time series data, and stock market trends. However, standard RNNs often fail to learn long time lags between relevant input events and target output signals (Gers et al., 1999). To address this limitation, a special type of recurrent neural network called Long Short-Term Memory (LSTM) was developed by German researchers Hochreiter and Schmidhuber (Hochreiter & Schmidhuber, 1997). LSTM was designed to overcome the problems of vanishing gradient and store information for long periods to solve complex long-time lag issues (Marino et al., 2016). Figure 17 illustrates a single LSTM cell.

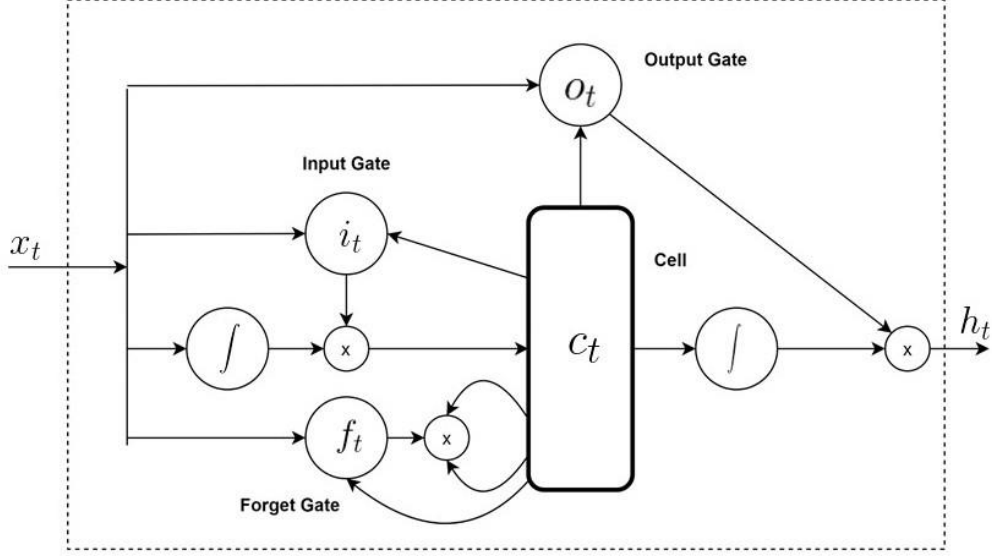


Figure 17. Long Short-term Memory Cell structure.

The key equations of an LSTM network are shown through Equation (3.7) (Graves et al., 2013):

$$\begin{aligned}
 i_t &= \text{sigm}(W_{xi}x_t + W_{hi}h_{t-1} + W_{ci}c_{t-1} + b_i) \\
 f_t &= \text{sigm}(W_{xf}x_t + W_{hf}h_{t-1} + W_{cf}c_{t-1} + b_f) \\
 c_t &= \text{tanh}(W_{xc}x_t + W_{hc}h_{t-1} + b_c) \\
 o_t &= \text{sigm}(W_{xo}x_t + W_{ho}h_{t-1} + W_{co}c_t + b_o) \\
 h_t &= o_t \tanh(c_t)
 \end{aligned} \tag{3.7}$$

In the equations,  $i_t$  denotes the input gate,  $f_t$  denotes the forget gate and  $o_t$  is the output gate.  $x_t$  is the input signal at time step  $t$  and  $h_t$  is the cell output.  $W$  is the weight matrix,  $\text{sigm}$  is the logistic sigmoid function and  $\text{tanh}$  is the hyperbolic tangent function.

Two different data-driven models are introduced for different purposes. The first method is trained on data points at a specific time step to estimate the SAG power draw at that same time step. This data-driven model is commonly used for complex non-linear input-output relationships. Four algorithms were adopted, ranging from the basic statistical method KNN to the more advanced ensemble methods RF and GBR. A combination of these four methods, weighted by their errors, was then performed, see Equation (3.8) and (3.9). Generally, the integrated result shows better accuracy than the individual results.

$$w_i \leftarrow \frac{1}{\text{MSE}(P_i)} \tag{3.8}$$

$$E = W \cdot X \tag{3.9}$$

Where  $w_i$  is the weight,  $W$  is the weight vector, and  $E$  is the combined predictor.

The second method in Paper C is a forecasting model that utilizes historical and current data points to predict the SAG power draw. The algorithm's structure in this method is a combination

of Convolutional Neural Networks (CNN) and LSTM. This prediction model aligns more closely with our expectations of the SAG dynamic model and shows greater potential for application, particularly in advanced process control.

The sliding window technique is employed to reframe the original dataset for the forecasting model, where a fixed-length window slides along the dataset and captures the data within it as the training/testing input. Although the same raw dataset is used, the size of the time-series forecasting model's data increases dramatically, requiring greater computational power.

### 3.2.2 SAG mill pebble rate importance analysis

As pointed out in the previous sections, one of the drawbacks of data-driven models, as a class of black-box models, is their difficulty in interpretation. While the accuracy of model predictions is certainly a crucial factor, gaining insight into the underlying physical phenomena is essential for the development of reliable process models. (Aldrich, 2020).

The importance analysis used in Paper F for the pebble rate prediction is based on the Shapley Value. The Shapley value is a classic method in game theory that to estimate the contributions generated by all players (Jia et al., 2019), as seen in Equation (3.10).

$$s_i = \sum_{S \subseteq N \setminus \{i\}} \frac{1}{N \binom{N-1}{|S|}} [U(S \cup \{i\}) - U(S)] \quad (3.10)$$

Where  $U$  is a utility function,  $i$  indicates the  $i$  th player or  $i$  th feature used in the prediction model.

### 3.2.3 Rock size estimation from images

In a comminution circuit, it is desirable to have an accurate knowledge of the particle size in various process steps. Nowadays, most mineral and crushing plants detect material size by manual screening, which involves enormous human labor resources. Therefore, image analysis offers an opportunity to measure the size of rock particles more efficiently.

The proposed method can be divided into four main steps, see Figure 18. First, the raw input images are preprocessed using gray scaling and contrast-limited adaptive histogram equalization (CLAHE). The preprocessed images have higher contrast, sharper edges, and more even lighting conditions. Next, a CNN-based network is applied to predict the thin edge maps. The edge maps then undergo binarization and morphological transformations. In this step, the particle contours are classified into fine particles, adjacent rocks, and individual rocks. Each adjacent rock contour is further separated into smaller segmentation areas. Finally, the pixel areas of rock fragments are collected and calculated to generate the particle size distribution for the given image.

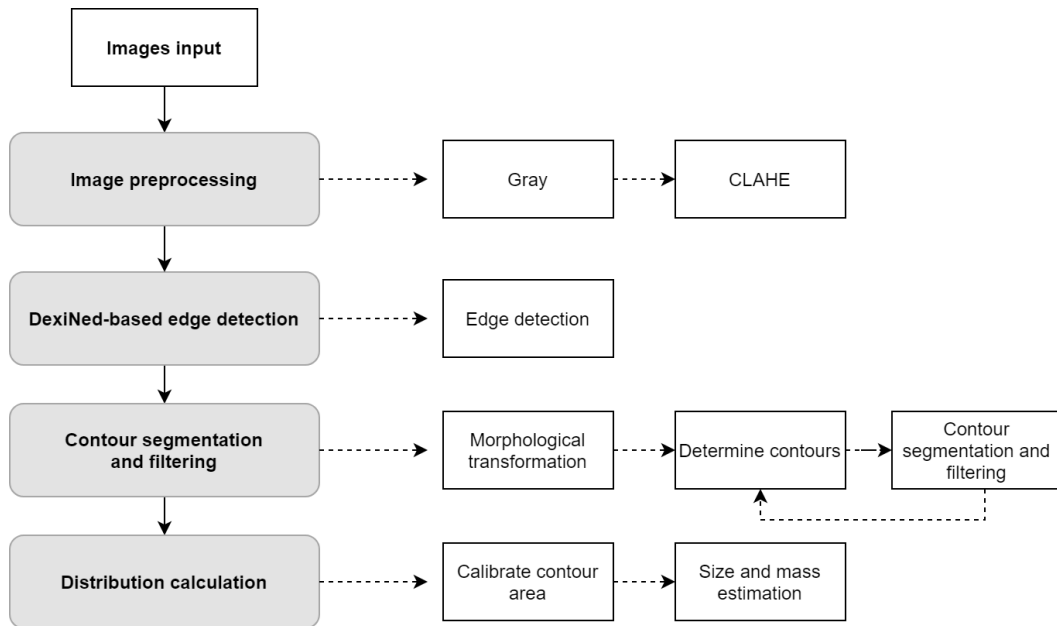


Figure 18. A flowchart of the proposed processes of ore size distribution estimation (Paper E).

### 3.3 Data Mining and Data Analysis

A framework for data analysis that can isolate the impact of a specific variable on the target is introduced in Paper D. This method enables the extraction of information by investigating historical data, allowing for the evaluation of various operating settings on processing performance. Suriadi introduced an Integrated Analysis Method (IAM) that combines and studies both rock properties and operational data (Suriadi et al., 2018). With this framework, a wide range of analysis tools can be included and implemented. Modified from IAM, the procedure for isolating certain variables is illustrated in Figure 19. The steps for conducting an analysis are listed below:

- **Preprocessing:** The original dataset should be preprocessed to remove outliers, missing data, and noise.
- **Clustering Analysis:** Data patterns are examined through clustering analysis, which can identify different clusters within the dataset, corresponding to various operating modes of the process. Clustering methods are designed to discover groups among  $n$  individuals described by  $Q$  variables (Maugis et al., 2009). Generally, clustering methods fall into two main categories. The first category measures the distances between data points, as seen in methods like K-means and hierarchical clustering. The second category involves fitting data points to a model for clusters, such as Gaussian mixture distributions.
- **Selection and Clustering of Key Variables:** Key variables are selected and clustered into new labels. Once the clusters are determined, new columns of labels can be added to the dataset based on these clustered groups. In this case, the critical variable studied is the pebble crusher utilization, determined by crusher power and pebble specific energy. The target variable is the fresh feed rate to the SAG circuit.
- **Mapping Clustering Variables to Target Performance Variables:** The next step is to establish a relationship between the clustering variables (e.g., crusher utilization) and the target performance variables (e.g., fresh feed rate). It is important in this step



to visualize statistical differences, such as demonstrating that one cluster has a higher tonnage or that certain variables are more sensitive to rock feed size.

Eventually, conclusions can be drawn on essential operating conditions correlated to the target process performances.

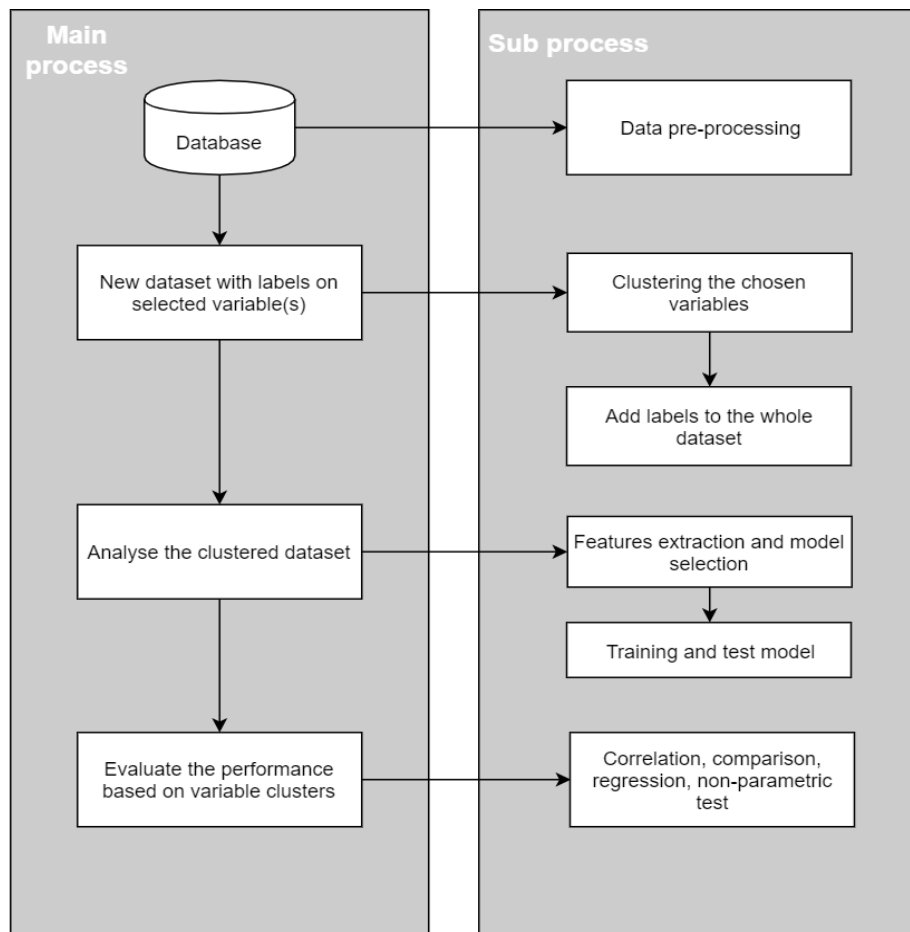


Figure 19. A generic procedure of isolating a certain variable (Paper D).



# 4 RESULTS

The aim of this chapter is to:

- Present the results in a summarized form.

## 4.1 Single SAG Mill Dynamic Modeling

In Paper A and Paper B, dynamic models for SAG mills are presented. These models have a similar structure and share fundamental concepts. The mill model is divided into discrete sub-processes that represent the physical interactions occurring within the mill. Particle breakage, transportation, and discharge behavior are calculated and updated over time in the simulation.

The single mill dynamic model is evaluated and compared with Yu's work (Yu et al., 2014). A similar feed rate to the mill is used to validate the dynamic response. As shown in Figure 20, the mill is initially empty, and a constant feed rate is applied, starting at 0 and increasing to 600 tph at  $t=100$  minutes. The feed rate then decreases to 480 tph at  $t=400$  minutes, and subsequently increases again to 780 tph at  $t=700$  minutes. The flow rate of the mill product changes accordingly in response to these feed rate adjustments.

The mill begins to discharge material at time  $t=120$  minutes, and it takes about 1.5 hours for the mill to reach a steady state. The time delay between the mill feed and the product can be explained by two main factors. First, the material in the mill needs to be ground and transported to the other end before it can be discharged. Second, due to the design of the grate, the ore in the mill must reach a sufficient volume to flow through the apertures and be discharged. Figure 21 shows the product PSD of each section. The mill is divided into four sections, and the particles are progressively ground as predicted as they move along the milling chamber.

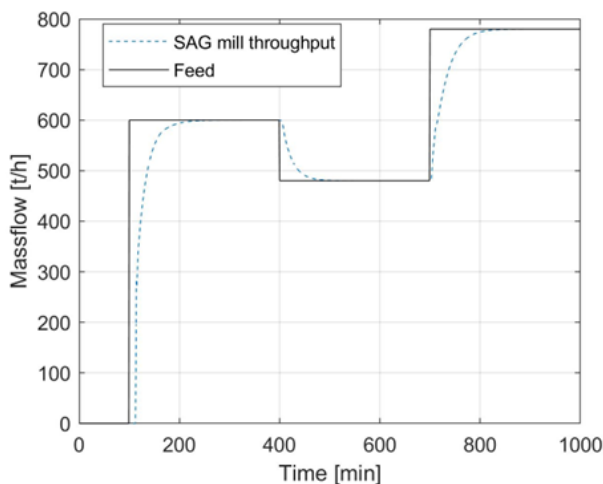


Figure 20. Dynamic response of the mill with a different feed rate (Paper A).

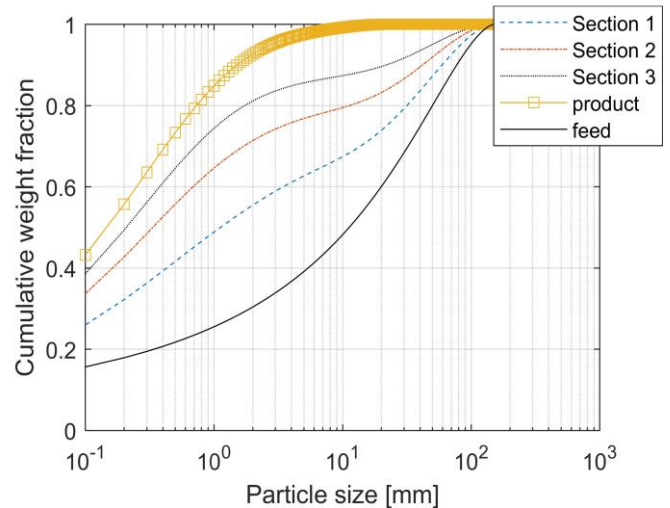


Figure 21. The particle size distribution of different sections in the mill at  $t = 1000$  minutes (Paper A).

In Paper A, a case study of feeding multi-component ore to the dynamic SAG mill model is presented. This example illustrates how the proposed model can provide reasonable predictions

for multi-component grinding. In this case, two ores of different hardness are considered. The hard component may act as grinding media to break the soft component, so the breakage rate will change according to the proportion of hard material. However, in this study, it is assumed that the breakage rate will not change with the load PSD, nor will it be affected by the hard ore ratio. The size-independent appearance function used here is based on JKMRC standard appearance function data, where  $t_{10} = 10\%$  for the hard ore, and  $t_{10} = 30\%$  for the soft ore. Both the breakage rate and the appearance function will need to be updated and validated with plant data for further applications.

Figure 22 presents the result from the the SAG locked-cycle tumbling test (Bueno et al., 2010). The SAG locked-cycle test was developed to simulate the steady-state continuous operation of an open circuit SAG mill. When the mill reaches steady-state, the test is paused, and the recycled load as well as the product are collected and analyzed by size. While this test provides valuable insights into the effects of ore blending, it is quite time-consuming and requires substantial effort. The results in Figure 22 show that the amount of hard ore (BIF) in the mill builds up as the cycle number increases. It takes approximately 18 cycles to reach steady-state, with each cycle lasting around 20 minutes (Bueno et al., 2010).

The simulation results are in good agreement with the experimental results in terms of the dynamic response and the ore blending interaction, as illustrated in Figure 23, from  $t = 100$  to  $t = 450$  minutes. Similar results can also be found in Kapur and Fuerstenau’s publications (Kapur & Fuerstenau, 1989). Shortly after the feeding stops, the volume of soft material drops dramatically, as shown in Figure 23. After  $t = 600$  minutes, all the soft ores have been ground and discharged. The material in the mill must reach a certain volume before it can be discharged, a portion of the volume referred to as dead slurry holdup. Thus, when all the soft material is discharged, the proportion of hard material will reach 100%. Figure 24 presents the details of the soft and hard material ratio.

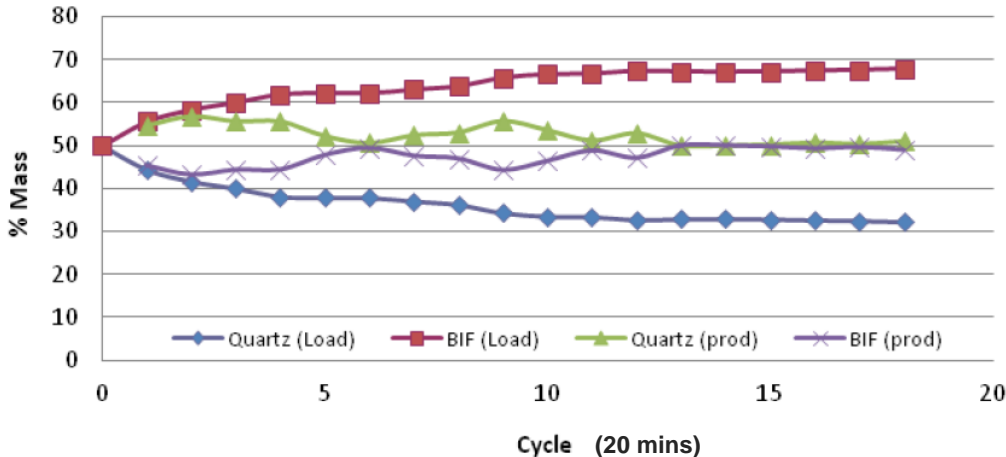


Figure 22. Mill dynamics as a function of cycle number for a locked-cycle test using 1:1 QTZ/BIF mixture (Bueno et al., 2010) (Paper A).

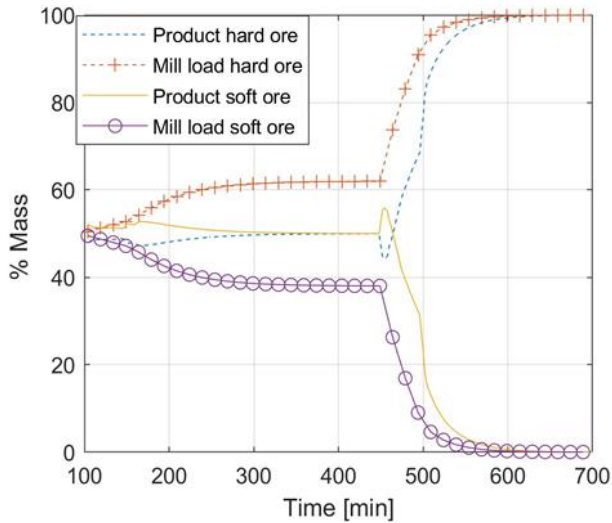


Figure 23. Ratio of the soft/hard ore of mill product and load (Paper A).

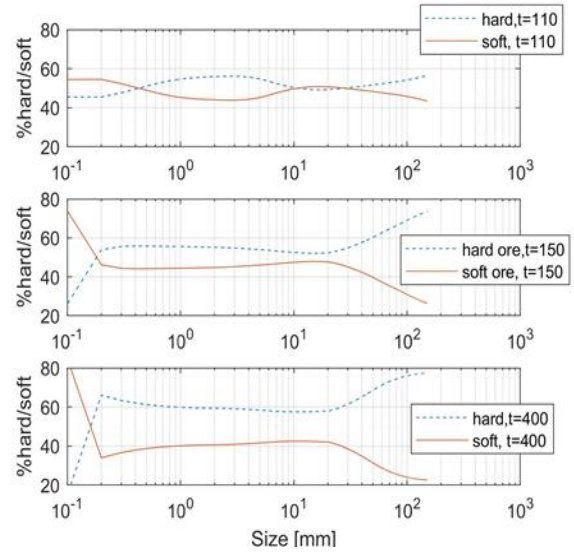


Figure 24. Ratio of soft/hard ore size by size in the mill (Paper A).

## 4.2 Single Cone Crusher Modeling

The application examples of the cone crusher model developed by Lindqvist and Li can be found in Paper H. Here, the simulation results of crushing rocks with different bond work index are presented in Figure 25. As expected, the minimum CSS corresponding to the crushing of harder rocks is bigger in comparison to the crushing of softer rocks. The min CSS are 21, 31 and 40 mm for the Bond Work Index 12, 16 and 20 kWh/t.

The results of simulating the crusher at a different CSS are presented in Figure 26. If the cone crusher operating at a larger CSS, a coarser steeper product curve is generated with a lower power draw and larger tonnage.

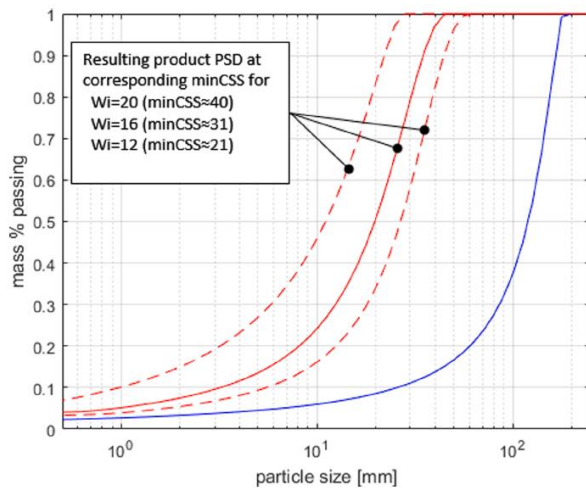


Figure 25. Product PSD at corresponding min CSS, the Bond Work Index is 12, 16, 20 kWh/t (Paper H).

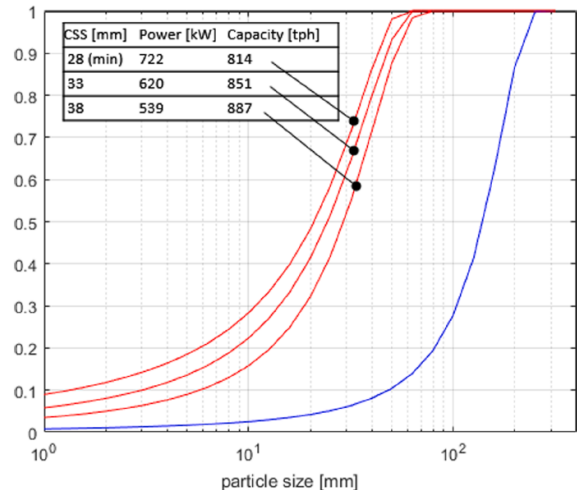


Figure 26. Product PSD operating at different CSS (Paper H).

### 4.3 SAG Mill with Pebble Crusher Circuit Dynamic Modeling

The dynamic modeling of the grinding circuit is discussed throughout Paper B. Dynamic fundamental models are implemented and combined for SAG mills, cone crushers, screens, and conveyor belts. Two numerical examples are demonstrated in the paper. The first simulation involves a typical SAG-cone crusher circuit and tests the dynamic response of the SAG model, including feed size data, flow rate, in-mill transportation, in-mill particle size distribution, and interactions with a cone crusher and a screen. The second scenario considers a more complex situation where two identical SAG mills and two cone crushers are included. In this case, the recycling load exceeds what one cone crusher can handle, so the second cone crusher is switched on and off to prevent the surge bin from overflowing.

#### 4.3.1 A single SAG-pebble crusher circuit

A simulation of a typical SAG-pebble crusher circuit is conducted to validate the hypothesis and to illustrate the capability of the dynamic model. The process is simulated using Matlab/Simulink, as shown in Figure 27 from Paper B. Initially, this plant has zero fresh feed. Fresh feed to the plant begins at  $t=100$  minutes with a flow rate of 480 tph, continuing until  $t=800$  minutes, after which the flow rate drops to 340 tph.

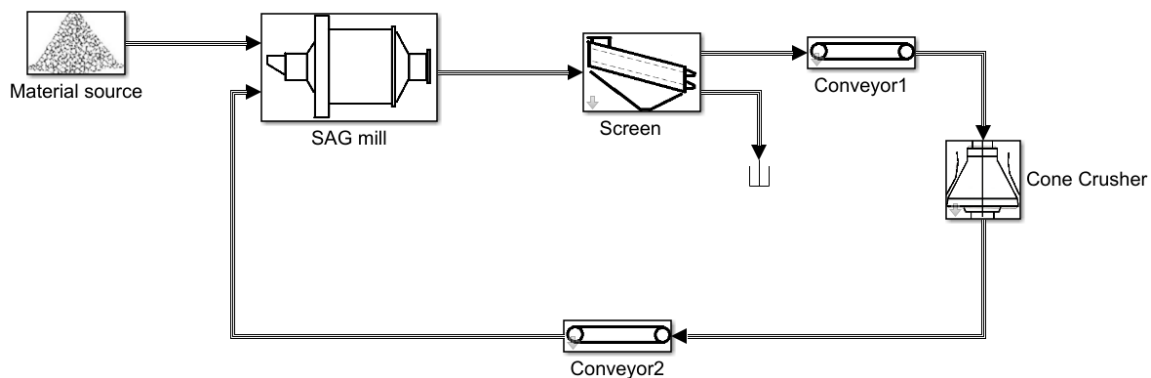


Figure 27. Flowsheet of the simulation with single SAG mill and single pebble crusher (Paper B).

Figure 28 shows the feed rate to the plant with 5% noise and its dynamic responses to various settings of the cone crusher. The time delay in the SAG product, as shown in the top plot, is due to the dead slurry pool and particle transport within the chamber. In the second plot of Figure 28, it can be observed that the recycling loads range from about 15% to 20% of the feed rate. Among these, the 'no cone crusher' scenario exhibits the highest recycling load, while the setting with 'CSS=10 mm, eccentric speed=400 rpm' results in the lowest recycling load. The third plot displays the plant throughput, showing a slightly different response time to reach steady-state conditions.

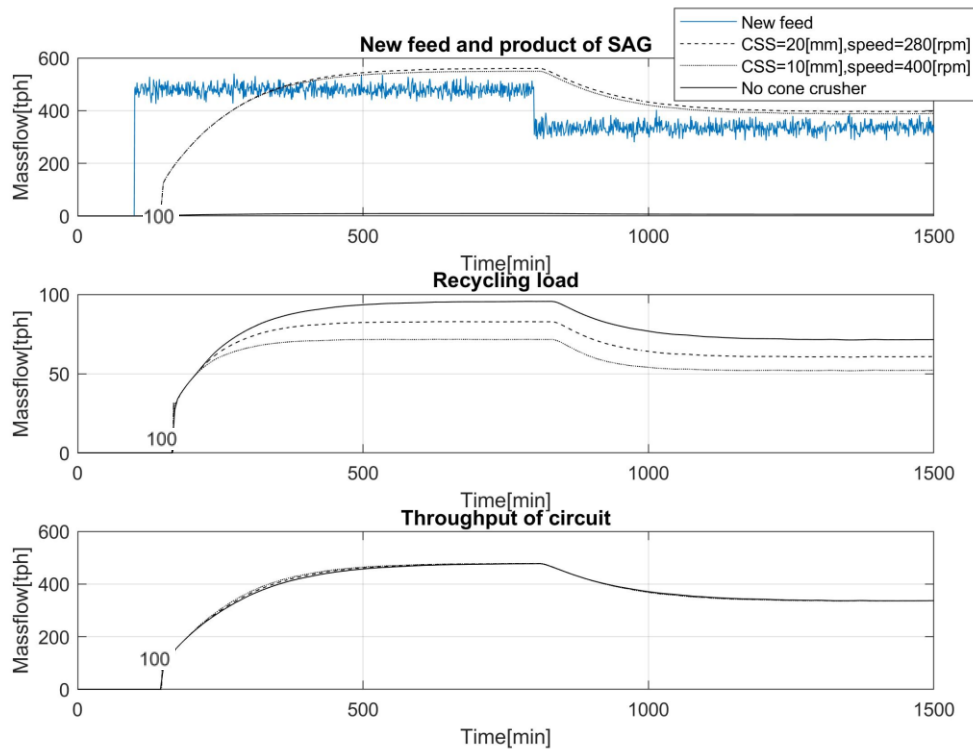


Figure 28. Simulation results from the single SAG mill grinding circuit. Feeding starts at  $t = 100$  minutes (Paper B).

Figure 29 and Figure 30 show the particle size distributions inside the SAG mill at different time steps with cone crusher settings  $CSS=20$  mm and eccentric speed=280 rpm. In this simulation, the SAG mill is divided into 10 sections. Figure 29 shows the PSD in section 1, 4, 7, as well as feed and product. The particles in the mill are progressively ground, and as expected, the PSD becomes finer as the material moves along the mill. At the non-steady state,  $t=150$  minutes, the particles in the chamber are coarser than at steady-state at  $t=1500$  minutes, as shown in Figure 30. This phenomenon is due to the dynamic response of the SAG mill and plant. Initially, the ore required more time to be ground. Additionally, the recycling load was relatively small at the beginning, so fewer fine particles were recycled to the SAG mill. The PSD continued to become finer until the steady state was reached. On the other hand, if we closely compare PSD at  $t=820$  and  $t=1500$ , the PSD at  $t=820$  is a little bit finer. This is because the new feed to the SAG dropped, but the recycling load was still high.

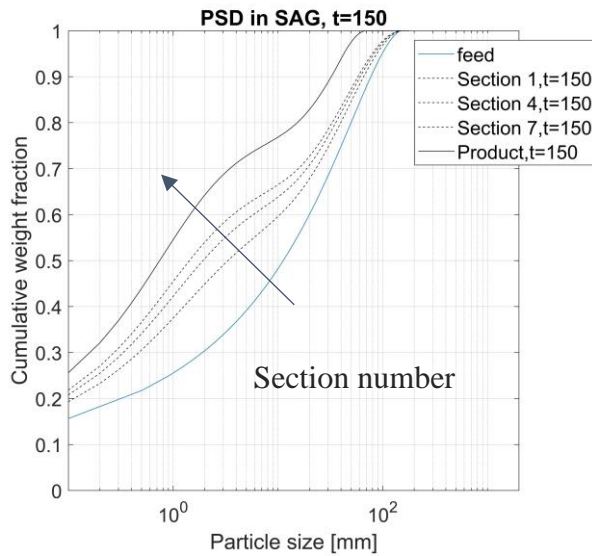


Figure 29. PSD in SAG mill, simulation time at 150 min (Paper B).

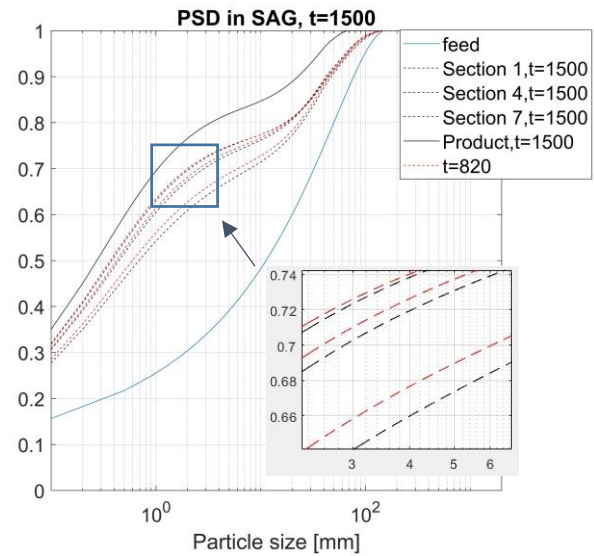


Figure 30. PSD in SAG mill, simulation time at 1500 min (Paper B).

#### 4.3.2 Responses of a dual SAG mill circuit with double cone crushers

In a second scenario, a more complex circuit is modeled. The circuit, shown in Figure 31, includes two identical SAG mills operating in parallel, two pebble crushers positioned after the screens, and a surge bin for the pebbles. In this scenario, a single cone crusher is insufficient to handle all the recycling products. Consequently, a second cone crusher needs to be intermittently switched on and off to keep the surge bin level below 100%. The purpose of this simulation is to study how the settings of the cone crushers influence the circuit dynamics.

The assumptions for this scenario are listed below.

- The capacity of all components remains constant, regardless of wear.
- Cone Crusher 1 always operates at 100% capacity. When the level in the bin reaches 300 tonnes, the second cone crusher is switched on, also running at 100% capacity.
- Bin 1 and Bin 2 function as perfect mixing surge bins. Bin 1 has a full load capacity of 300 tonnes, while Bin 2's storage capacity is negligible, so it acts as a perfect mixer.
- Ideal screens and splitters are used to separate the stream, ensuring that the recycling load is equal for both mills.



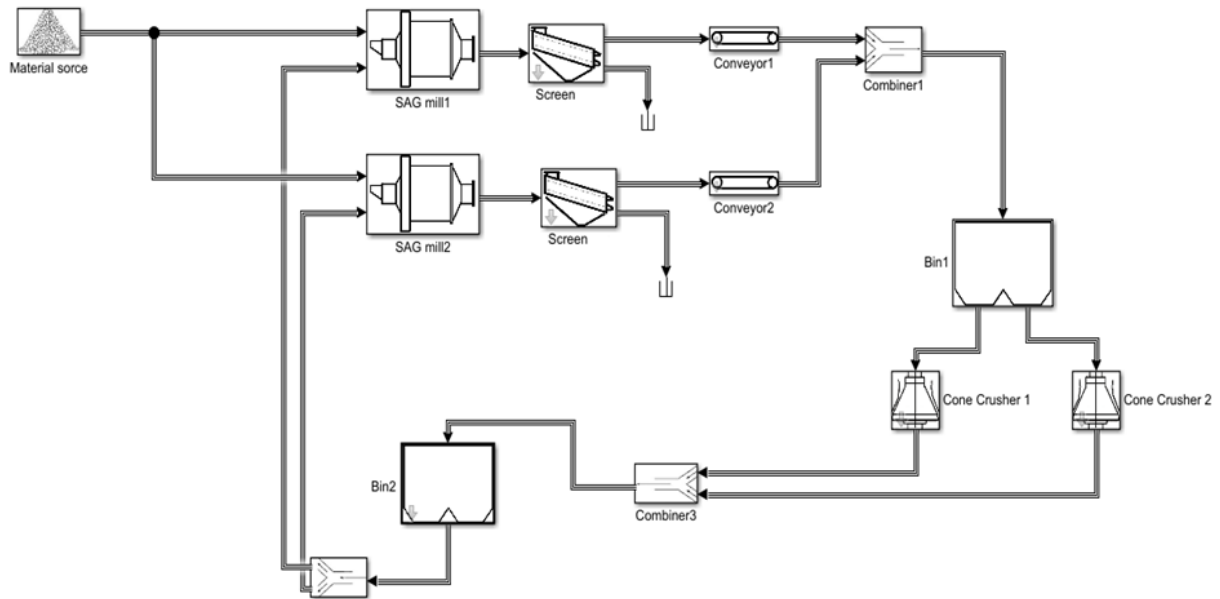


Figure 31. Flowsheet of the simulation with dual SAG mills, screenshot from Simulink (Paper B).

In this circuit, both SAG mills have the same throughput, feed rate, and recycling load. The following discussion focuses on the simulation results from SAG mill 1. The first plot in Figure 32 shows that the throughput of the SAG mills is affected by the pebble crusher settings. A cone crusher with settings such as CSS = 28 mm and eccentric speed = 280 rpm produces a coarser product than a cone crusher with a smaller CSS and higher eccentric speed. The crusher's capacity is higher with a larger CSS and lower speed compared to a small CSS and high speed. The second plot in Figure 32 shows the recycling load. The second cone crusher is switched on and off according to the mass level in Bin 1, as seen in the third plot. The last plot shows the material load in the chamber, which is directly related to the power draw of the SAG mill. The simulation results suggest that the total charge load in the mill could range from 454 tonnes to 510 tonnes, depending on the cone crusher settings. All these simulation results presented in Figure 32 demonstrate that the cone crusher settings can introduce changes in mass flow change within a SAG-cone circuit.

The results in Paper B show that significant dynamic fluctuations can be induced by the on/off behavior of the cone crushers, effectively acting as exciters of the circuit. Additionally, cone crusher operational parameters, such as the closed side setting and eccentric speed, have a notable impact on the recycling load and crusher utilization.

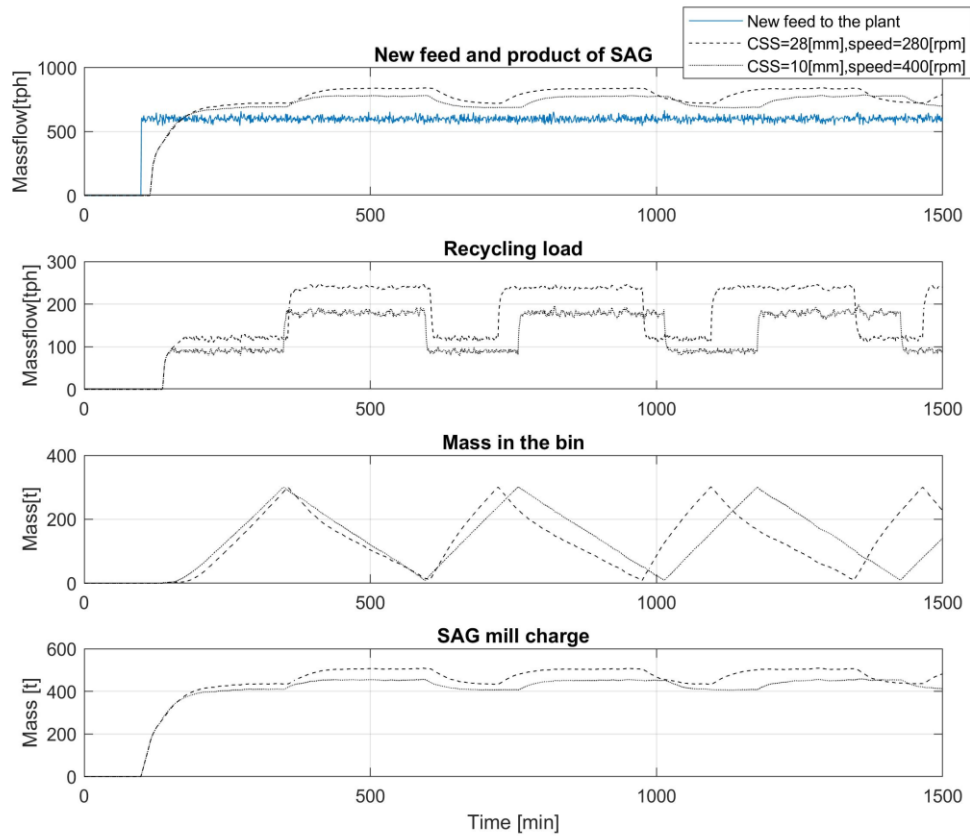


Figure 32. Simulation results from simulating with dual SAG mills (Paper B).

#### 4.4 Design of Experiment of SAG Mill Pebble Crushing circuit

Based on Paper B, a further step has been taken in Paper G using the Design of Experiments (DoE) approach. The application of DoE in evaluating crushing and screening performance, as discussed by Bhadani (Bhadani et al., 2024), provides a systematic method for optimizing the interaction between crushers and screens of a crushing plant. In this study, we investigate the effects of feed ore hardness, feed ore size (due to pre-crushing), pebble crusher settings, and the presence of a pebble stockpile on the overall performance of the SAG mill pebble circuit, see Figure 33. By incorporating these variables into dynamic simulations, this research aims to provide a more comprehensive understanding of the circuit's behavior under various conditions, leading to more robust and adaptable plant designs.

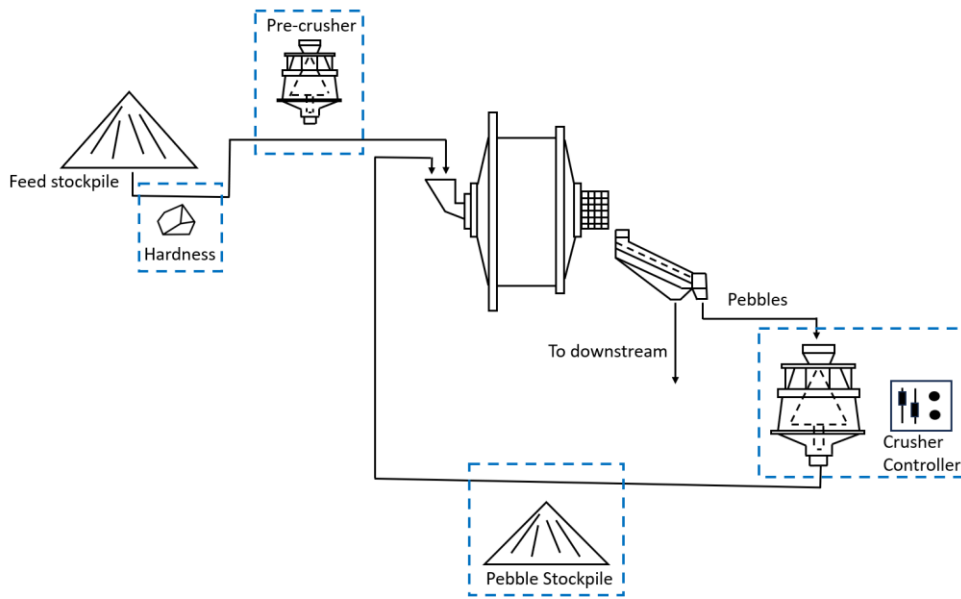


Figure 33. Flowsheet of a typical SAG mill-pebble crusher circuit with options adding pre-crushers, stockpiles and other circuit configurations. These different layouts will be simulated using a DoE approach (Paper G).

Two levels of the above-mentioned variables (ore hardness, feed size, crusher settings and pebble stockpile) are involved in the investigation, as shown in Figure 33. In total, 16 runs have been performed, with details listed in Table 1.

Figure 34 shows the dynamics of the studied dual SAG mills with double pebble crushers circuit. The four runs are conducted with fine crusher settings (smaller CSS, higher eccentric speed, but lower capacity) and an intermediate pebble stockpile for the crushed pebbles.

From Figure 34 (a), it can be seen that the average fresh feed rate is highest when the feed ore is soft and has been pre-crushed (Run 3). Due to the presence of the pebble stockpile, the recycling load back to the SAG mill can be managed by the stockpile control strategy. In this case, only an on/off controller is applied to the stockpile, resulting in a clear pattern between the fresh feed rate and the recycling rate.

Figure 34 (b) presents the crushers' capacity usage, showing that Crusher 1 is almost fully utilized, while Crusher 2 operates primarily when the bin level is high, as shown in Figure 34 (c). When the feed ore is soft and pre-crushed, the SAG mill generates significantly fewer pebbles, resulting in low utilization of Crusher 2. Conversely, when the feed is coarse and hard (Run 1 and Run 2), the pebble rate is relatively high, and Crusher 2's capacity is half occupied.

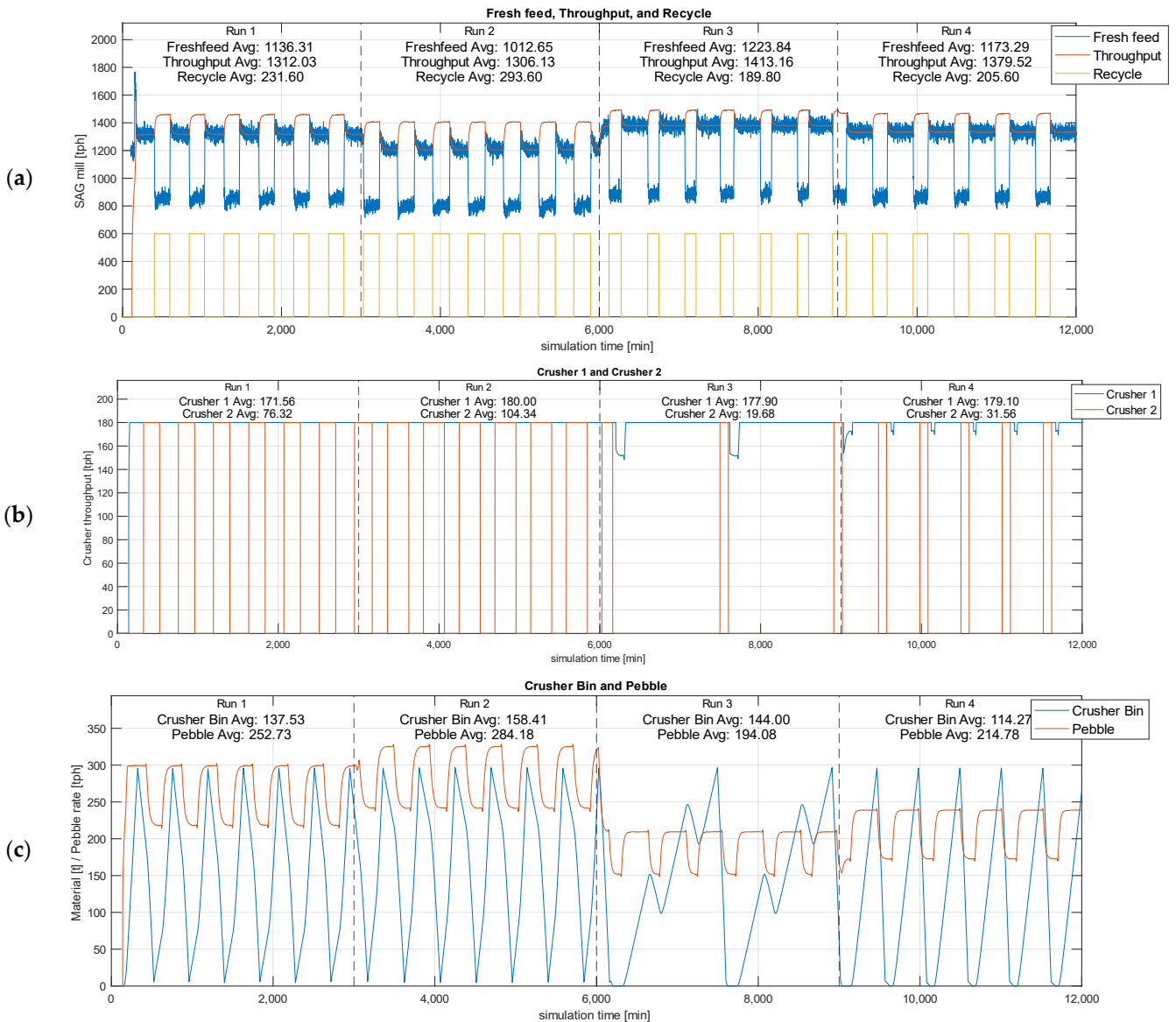


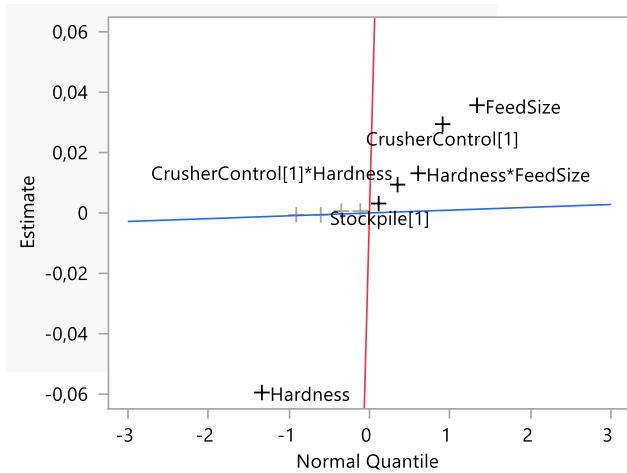
Figure 34. Simulation results from Run 1 to Run 4 include the circuit with stockpile and fine crusher settings. Figure (a) shows the throughput, fresh feed rate, and recycle rate of each SAG mill. Figure (b) shows the pebble crusher utilization rate. Figure (c) shows the pebble rate and crusher bin level (Paper G).

More simulation results can be found in the Paper G. The summary of all 16 simulations is presented in Table 1. The results are normalized based on their average values for each simulation run.

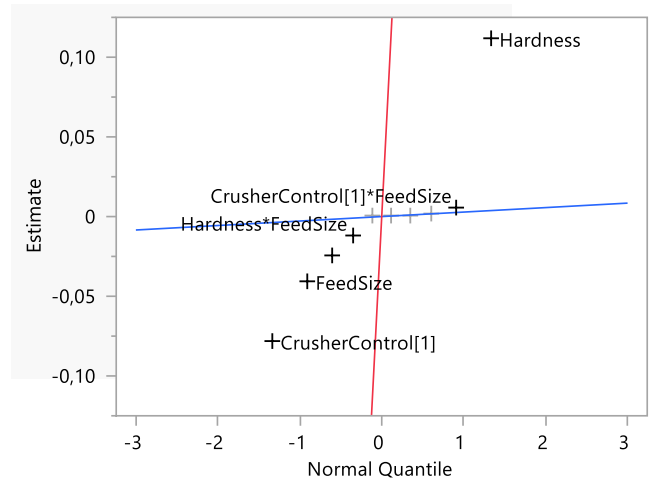
In Figure 35, the normal plots of DoE are presented. The blue lines represent the expected distribution of effects if they were all due to random noise. Points that deviate notably from the line are considered significant effects. These deviations suggest that the corresponding factors have a meaningful impact on the response variable.

Table 1. The simulation results of all DoE runs are normalized and highlight both the highest (orange) and lowest (blue) fresh feed rates (Paper G).

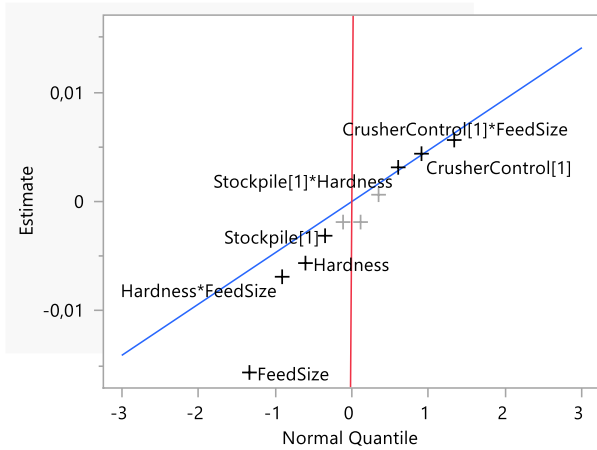
Run	Pebble Stockpile	Crusher Settings	Feed Size	Hardness	Fresh Feed Avg	Pebble Rate Avg	Pebble/Freshfeed	Crusher1 Usage	Crusher2 Usage	SAG T80 (mm)
1	Yes	Fine	Fine	Hard	0.93	0.69	0.22	0.96	0.42	2.2
2	Yes	Fine	Coarse	Hard	0.83	0.77	0.28	1	0.58	2.5
3	Yes	Fine	Fine	Soft	1	0.53	0.16	0.99	0.11	1.1
4	Yes	Fine	Coarse	Soft	0.96	0.58	0.18	0.99	0.18	1.3
5	Yes	Coarse	Fine	Hard	0.86	0.87	0.3	0.95	0.38	2.4
6	Yes	Coarse	Coarse	Hard	0.75	1	0.4	1	0.52	2.6
7	Yes	Coarse	Fine	Soft	0.96	0.63	0.2	0.95	0.02	1.3
8	Yes	Coarse	Coarse	Soft	0.92	0.69	0.22	1	0.06	1.4
9	No	Coarse	Fine	Hard	0.84	0.87	0.31	0.95	0.37	2.4
10	No	Coarse	Coarse	Hard	0.75	0.99	0.4	1	0.51	2.7
11	No	Coarse	Fine	Soft	0.96	0.63	0.2	0.98	0	1.2
12	No	Coarse	Coarse	Soft	0.91	0.69	0.23	1	0.05	1.4
13	No	Fine	Fine	Hard	0.92	0.68	0.22	0.96	0.42	2.3
14	No	Fine	Coarse	Hard	0.83	0.77	0.28	1	0.57	2.5
15	No	Fine	Fine	Soft	1	0.52	0.16	1	0.07	1.1
16	No	Fine	Coarse	Soft	0.95	0.58	0.18	1	0.19	1.3



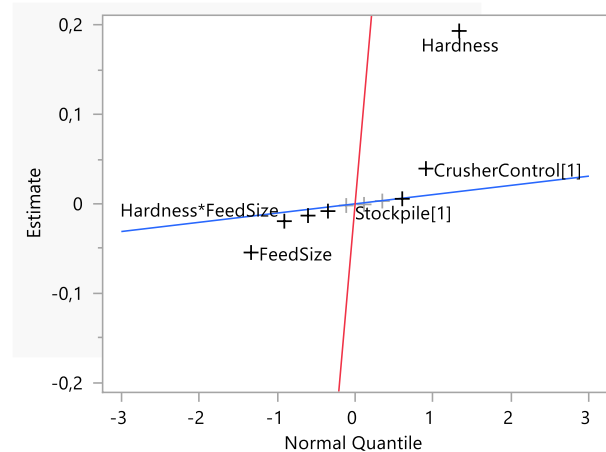
(a) Fresh feed rate, Lenth PSE 0.000937



(b) Pebble rate, Lenth PSE 0.0028125



(c) Crusher 1 capacity usage, Lenth PSE  
0.0046875



(d) Crusher 2 capacity usage, Lenth PSE  
0.0103125

Figure 35. Normal plots to assess the significance of effects in the DoE results. (a) is for fresh feed rate, (b) is for pebble rate, (c) and (d) are the crusher capacity utilization. Blue line has slope equal to Lenth's PSE, red line slope is 1 (Paper G).

Since Crusher 1 is almost fully utilized in all scenarios, all factors seem to have a minor impact, as shown in Figure 35 (c). However, the rest of the normal plots in Figure 35 (a), (b) and (d) highlight the substantial effect of ore hardness. A harder ore feed leads to a lower fresh feed rate and a higher pebble rate, resulting in increased usage of Crusher 2.

The second important factor is feed size. A finer feed size not only increases the fresh feed rate but also reduces the amount of pebbles generated by the SAG mill. The presence of the cone crusher controller (with a smaller CSS, higher eccentric speed, but lower capacity) appears to have a beneficial effect on both the feed rate and reducing the pebble rate.

Using the DoE approach, key findings show that implementing a crusher controller with smaller CSS and higher speed settings results in a finer product output. This finer product leads to a finer feed to the SAG mill, a reduction in the overall pebble rate, more efficient operation of both crushers, and, most importantly, a 5 to 10% increase in the overall fresh feed rate.

Softer feed materials lead to higher throughput and lower pebble rates. The highest fresh feed rates were observed with fine feed and soft ore conditions, highlighting the pronounced impact of ore hardness on mill circuit performance. Conversely, harder ore feed results in lower fresh feed rates and higher pebble rates, increasing the usage of Crusher 2. A finer feed size generated by a pre-crusher enhances the fresh feed rate and reduces pebble generation.

While the presence of a pebble stockpile does not directly improve the fresh feed rate or reduce the pebble rate, it enhances the manageability of the recycling rate. This manageability is crucial for stabilizing the circuit and preventing turbulence in the feed, thereby improving overall mill performance.

#### 4.5 SAG Mill Power Draw Prediction

In Paper C, the focus is primarily on the power model of SAG mills based on a data-driven approach. The original dataset consists of measurements from over 29,000 data points from the SAG mill-pebble crusher circuit at the Copper Mountain mine in British Columbia, Canada.

The collected operational data includes 24 variables, such as SAG power, SAG feed size, SAG main bearing pressure, fresh water added to the mill, crusher power, recycling load, and crusher product size, among others.

Two different approaches are presented. The first method employs a SAG mill power prediction model using artificial neural networks (ANN), K-nearest neighbors (KNN), random forests (RF), gradient boosting regression (GBR), and their weighted prediction errors to formulate an ensemble model. This model provides a soft measurement of mill power draw in relation to other variables.

The results for individual models and the ensemble model are shown in Figure 36. The mean squared errors (MSE) are calculated and listed in Table 2 to indicate the prediction accuracy. The RF and GBR, being inherently advanced ensemble algorithms, show fewer errors compared to ANN and KNN. Additionally, the combination of the four models, when weighted by their MSEs, demonstrates improved results. In Figure 36 from Paper C, all model results show some deviation from the actual values when the mill power drops dramatically at 600 minutes.

Table 2. Comparison of test errors (MSEs) for proposed individual methods (Paper C).

	ANN	KNN	Random Forest	Gradient Boosting	Ensemble
Test error (MSE)	0.0077	0.0058	0.0052	0.0046	0.0044

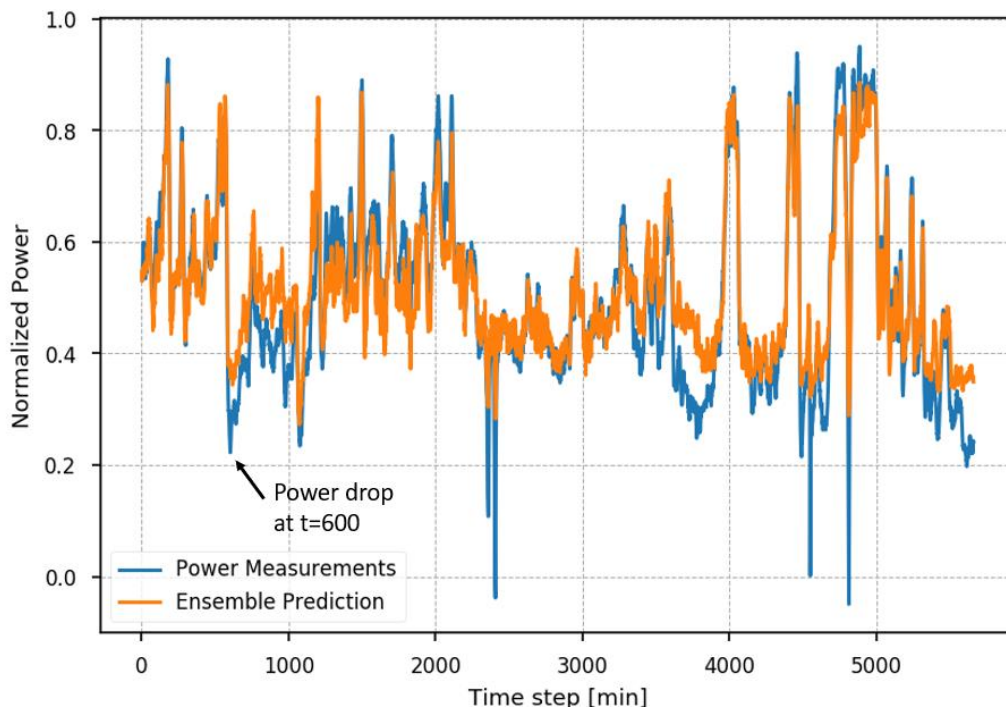


Figure 36. SAG mill power prediction with weighted results from individual predictors (Paper C).

The deviations can be attributed to some important features not being included in the training dataset. When these features change, the proposed models struggle to bridge the gap between predicted and actual power due to the missing information. Although some errors occur when the mill power drops dramatically, the overall trends still align well with the predictions. These

deviations are expected to be further reduced by introducing more diverse datasets, increasing training iterations, tuning the models, and applying proper data preprocessing.

The second approach treats the SAG mill power draw as a time-series problem. The original dataset is reformatted using a sliding window and trained with a Long Short-Term Memory (LSTM) algorithm. This LSTM prediction method uses 20 minutes of historical data to predict the mill power consumption for the subsequent 2 minutes.

This forecasting algorithm includes one Convolutional Neural Network (CNN) layer and two LSTM layers connected by a Fully Connected (FC) layer, as shown in Figure 37. The training data first passes through the CNN layer, which preliminarily analyzes the characteristics and trends of multiple consecutive time data points. Then, the LSTM layers are implemented to further extract patterns from different periods. The FC layer between the CNN and LSTM layers reframes the data structure to a specific format without changing any information. Additionally, dropout layers are introduced to randomly delete some information between two connected layers, thereby preventing model overfitting.

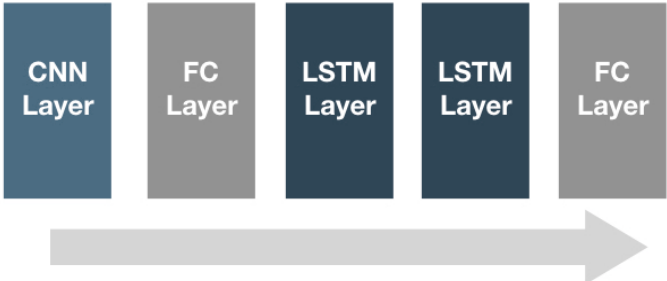


Figure 37. Sketch of the forecasting model structure with CNN layers and LSTM layers (Paper C).

The input data is reformatted using a sliding window technique. A larger window width captures more continuous-time information, though it increases computational effort. Conversely, a smaller window width may be too narrow to capture sufficient patterns. In this study, a window width of 20 minutes and a forecasting step size of 2 minutes are chosen, meaning the algorithm performs a 2-minute SAG mill power draw forecast using 20 minutes of historical data. Throughout the sliding window process, the input data contains both time dimension information and feature dimension information. As shown in Figure 38, the proposed method is capable of producing promising 2-minute forecasts of SAG mill power draw.

The data-driven methods presented in Paper C are flexible, easy to apply with suitable datasets, and demonstrate advantages in predicting SAG power draw under rapidly changing conditions. Furthermore, the forecasting method holds great potential for fault detection and predictive control in grinding processes.



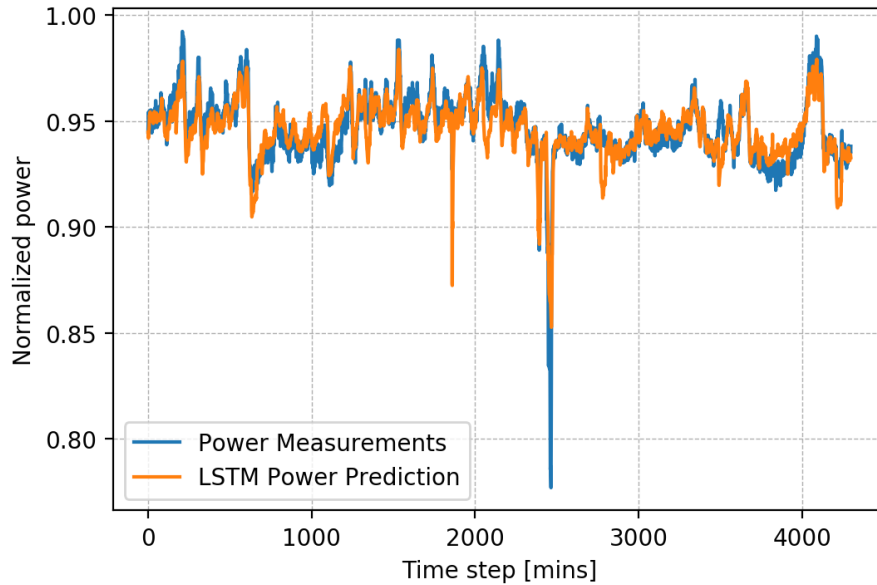


Figure 38. 2-minute forecasting model for SAG mill power with 20 minutes of historical data (Paper C).

#### 4.6 SAG Mill Pebble Rate Prediction

In Paper F, the main objective is to build a data-driven model to predict the rate of pebbles generated by a SAG mill and to interpret the importance of the input signals. In game theory, the Shapley value is often used to calculate the contribution of each player. In this work, the Shapley value is applied to determine which features contribute the most to this prediction model. The raw dataset consists of over 19,000 data points from the SAG mill circuit at KAZ Minerals in Kazakhstan. The collected operational data includes 14 variables with a 1-minute sampling frequency, such as SAG power, SAG main bearing pressure, fresh water added to the mill, SAG mill gearbox vibration, SAG sound signal, and SAG mill speed. During operations, the SAG mill liner was changed four times, and the results of this section will show each period separately.

In Figure 39, (a) the vibration measurement and (b) SAG mill power during period 1 are shown in a time-series format. In Figure 40, the vibration signal is plotted against the SAG mill power draw in scatter plots. The Gaussian mixture model is applied to cluster the vibration signals based on their distributions.

The results indicate that each set of vibration signals is divided into three clusters. In Figure 40 (d), the energy consumption and the vibration of the SAG mill show a negative correlation in the blue cluster, while the adjacent orange cluster has a different slope. In other words, the operating conditions of the SAG mill are classified into three categories based on the Gaussian classification of vibration signals, and the relationships between some variables in these three categories may differ.

In Figure 41, the time series of SAG mill power draw for four periods is presented. It shows that the SAG mill operating conditions with low/high power draw are clearly labeled by vibration clusters.

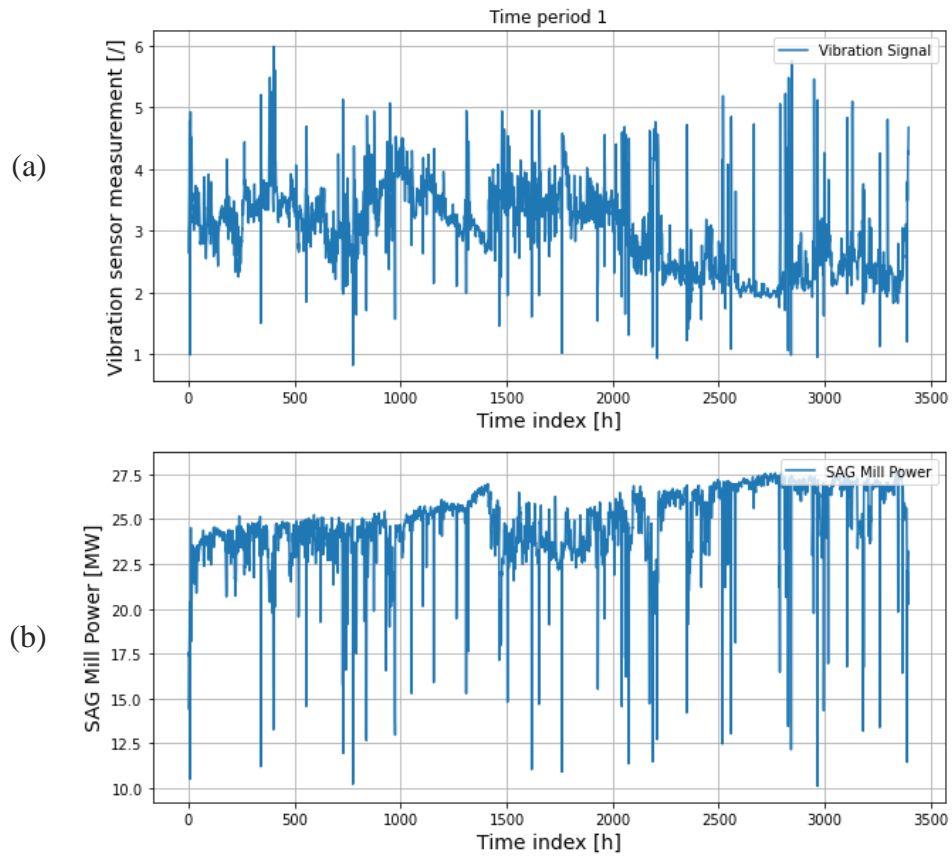
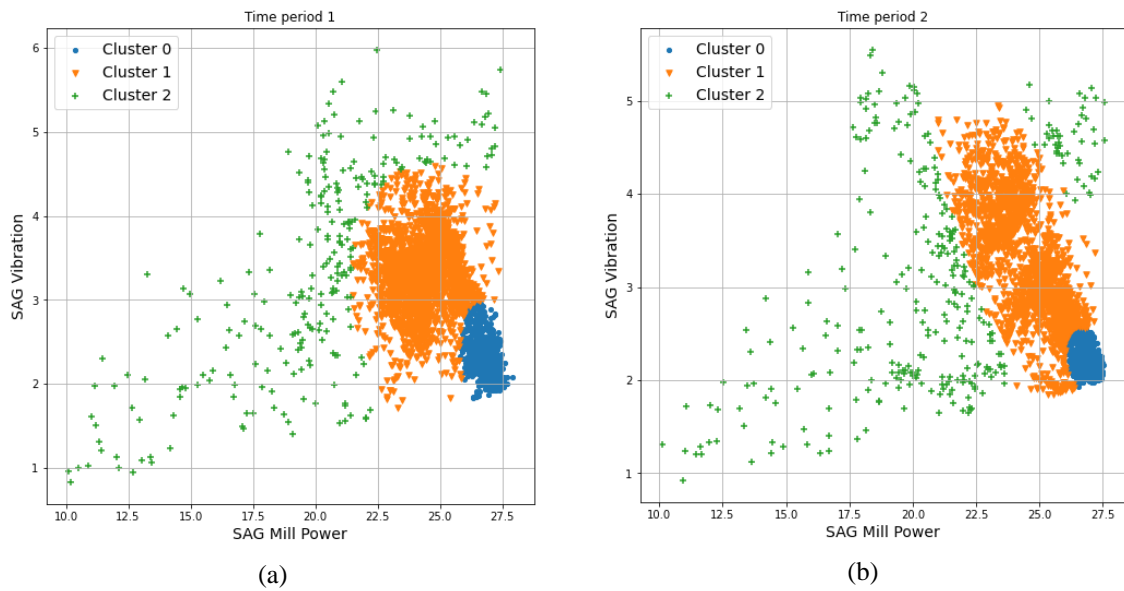
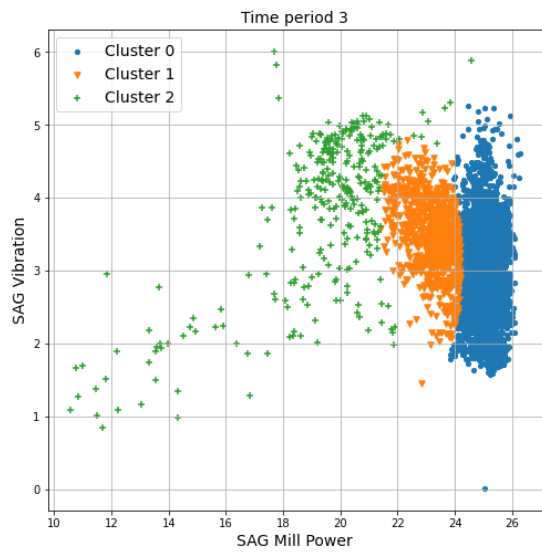
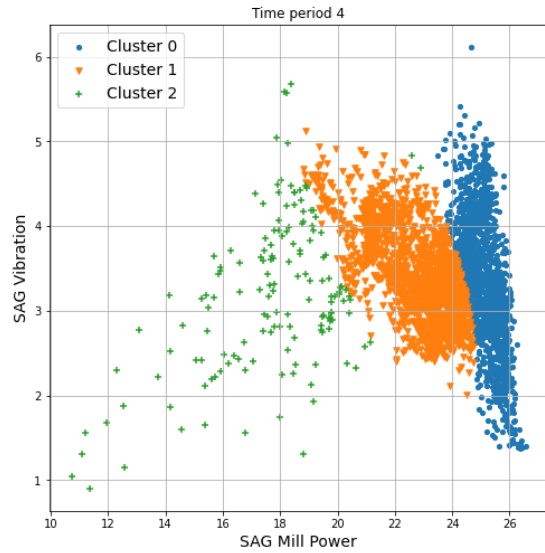


Figure 39. Vibration sensor measurement and SAG mill power from period 1 (Paper F).





(c)



(d)

Figure 40. Vibration signals plot with SAG mill power draw. The signals are clustered based on Gaussian mixture models (Paper F).

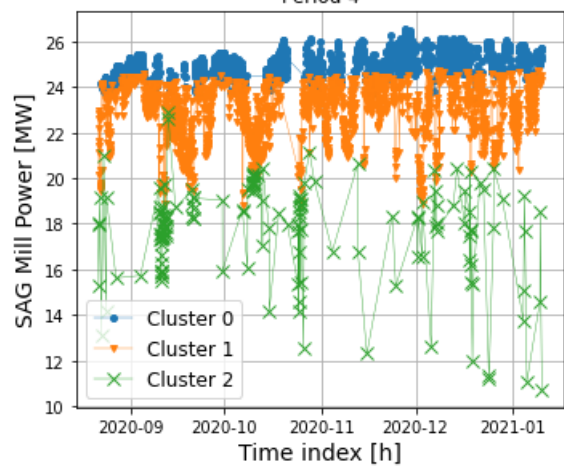
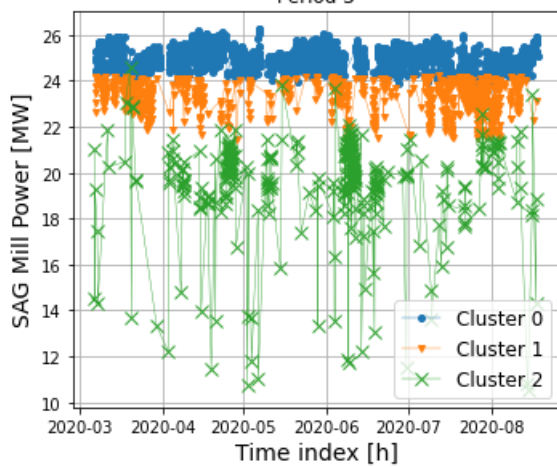
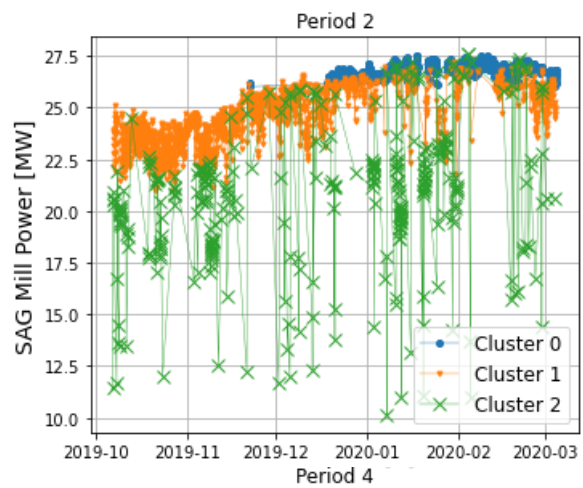
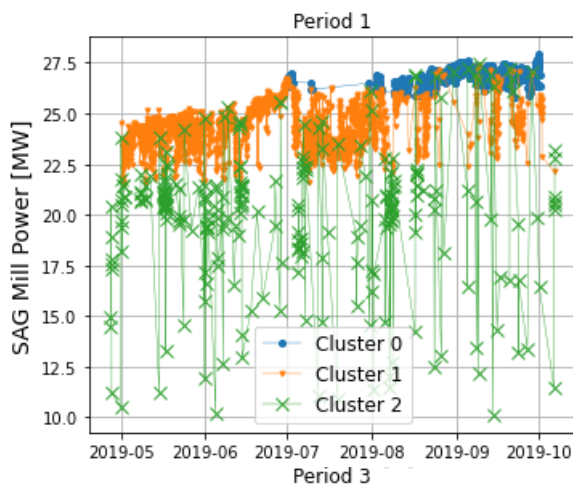


Figure 41. SAG mill power time-series plots. Data points are labeled based on vibration signal clusters (Paper F).

In most data-driven models of SAG mills, liner wear is not taken into account. However, SAG mill liners normally need to be replaced regularly (in this case every five months), and the weight of the SAG mill decreases as the liners wear during operation. To gain a better understanding of SAG grinding efficiency under different liner wear conditions, a soft measurement of the degree of liner wear was created using the pressure signal of the SAG mill's main bearing and the mill's power consumption, as shown in Figure 42.

The creation of soft measurements is intuitive, given the constant weight reduction of the SAG mill liner, and because of the increase in throughput and energy consumption. The liner wear soft sensor is expressed in Equation (4.1). The vibration clusters are then applied to remove the extreme values (as shown by the green cluster in Figure 41).

$$Liner = Pressure_s / Power_s \quad (4.1)$$

Where  $Pressure_s$  is the scaled pressure signal and  $Power_s$  is the scaled power draw.

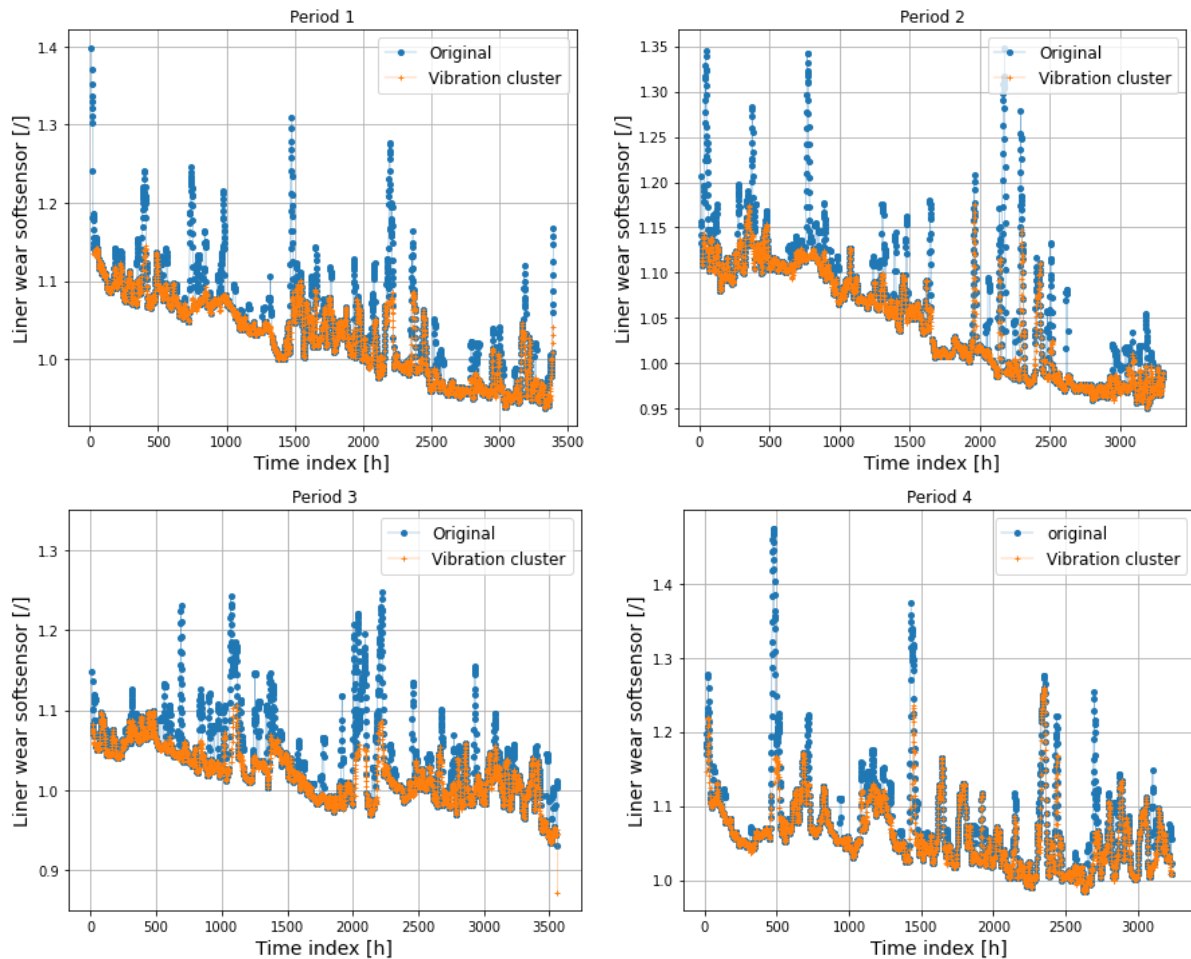


Figure 42. A soft sensor of the SAG mill liner wear. Vibration clusters are added to remove the outliers and to generate a smoother liner wear estimation. The scatters in orange color show data with cluster 0 and cluster 1, see Figure 41 (Paper F).

The prediction model of the pebble rate is built using XGBoost regression model (Chen & Guestrin, 2016) with the same hyperparameters. The main goal is to investigate the relationship between the pebble rate and SAG mill operating parameters, while also incorporating clusters

of vibration signals and the liner wear soft sensor into the training process. The final prediction results are shown in Figure 43. Prediction models that utilize more features produce better results.

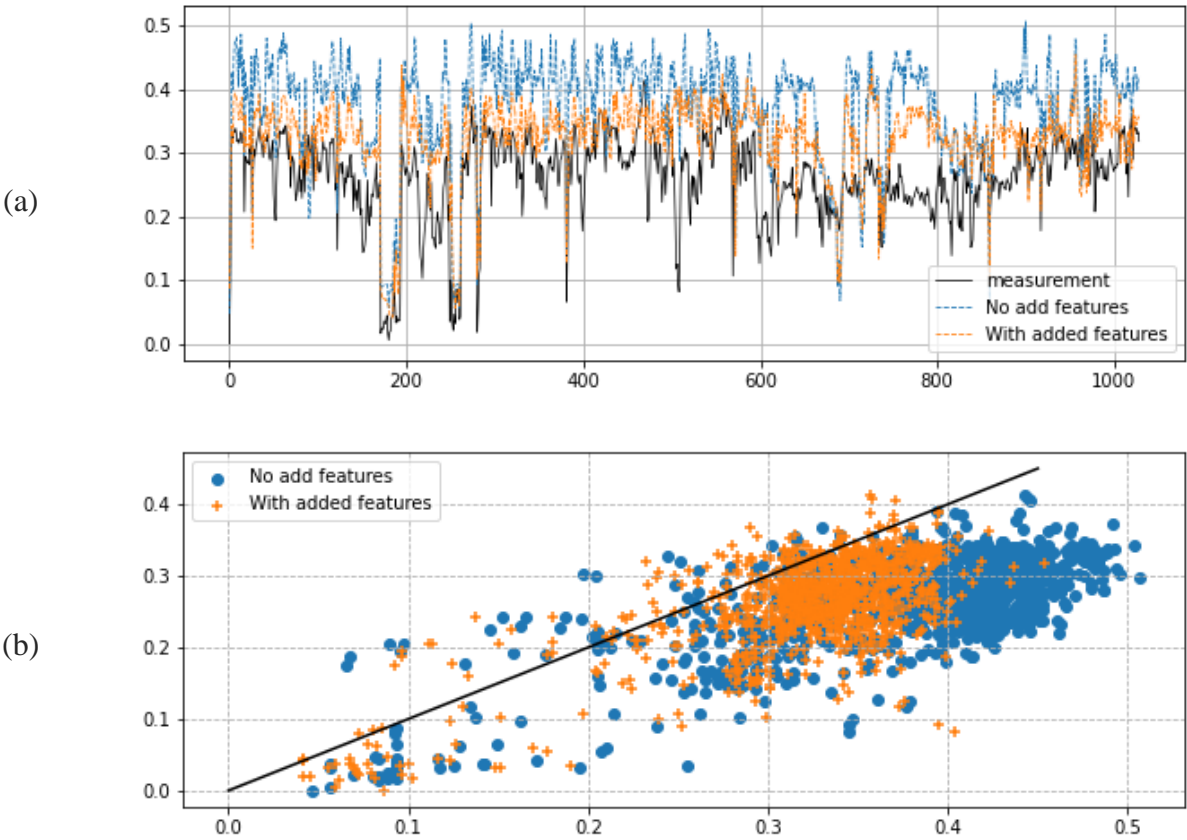


Figure 43. The pebble rate prediction: a) A time series plot of measured pebble rate and predicted pebble rate. b) Scatter plot of predictions against measured values. The blue dot is from the original features; the orange cross is with added features (vibration clusters and liner wear soft sensor) (Paper F).

More importantly, with Shapley value analysis shown in Figure 44, the contribution of each variable in this model can be quantified. Not surprisingly, the most relevant variables to the pebble production rate are the weight of the SAG mill, the bearing pressure, and the mill fresh feed rate. The vibration signals themselves do not provide much valid information and sometimes even introduce more noise. However, after Gaussian clustering, the SAG mill operating conditions represented by these vibration signals offer very useful features for the prediction model. Additionally, the soft measurements of the liners also provide a considerable contribution. The highlighted signals mentioned above are boxed in red in Figure 44.

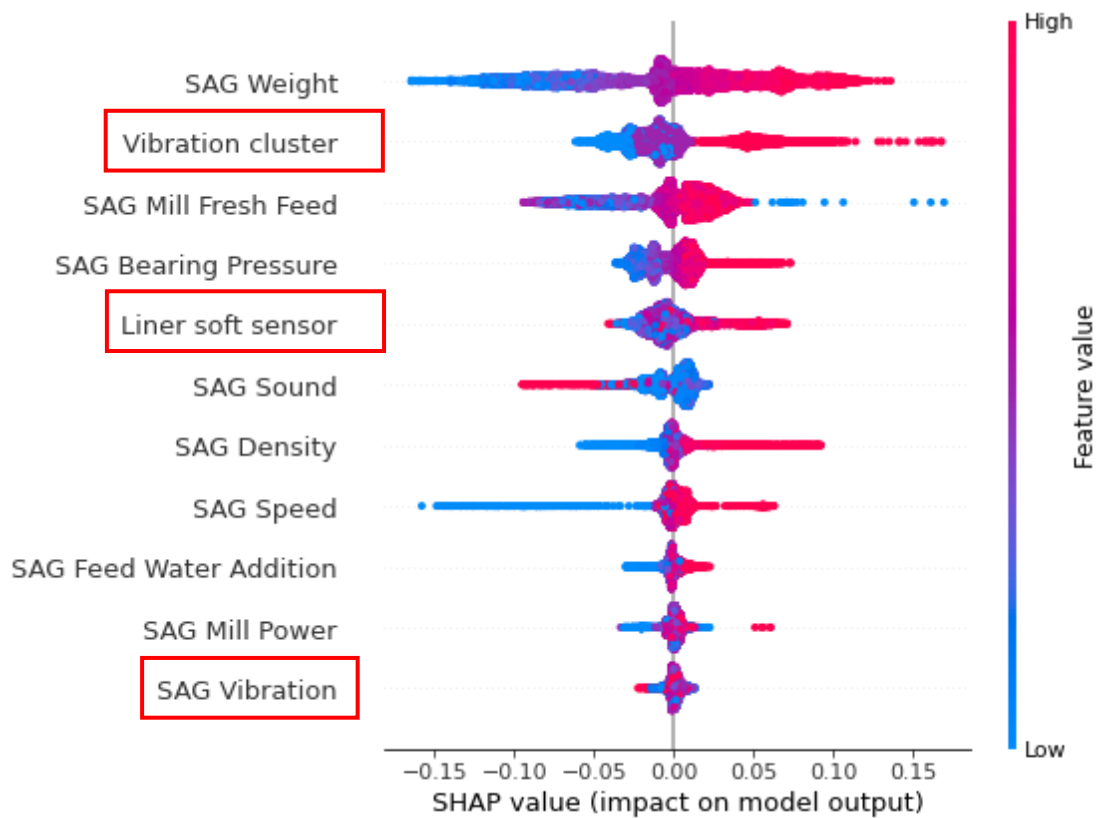


Figure 44. The Shapley Value of all features of the SAG mill pebble rate prediction (Paper F).

#### 4.7 The Impact of Recycling Load on a SAG Mill Circuit

In Paper D, the main purpose is to isolate and investigate the impact of the recycling load and pebble crusher operational settings on the total grinding circuit performance using historical plant operational data. The selected influencing variables are the crusher power and pebble specific power. The fresh feed rate is chosen as the circuit performance variable.

As shown in Figure 45 the pebble crusher power and pebble specific energy display certain distribution patterns. These variables indicate how much work the crusher has performed on the recycling load. The Gaussian mixture method is applied, with the number of clusters set to 4. Figure 48 illustrates that these 4 clusters correspond to zero crusher specific energy (SE zero), low crusher specific energy (SE L), middle crusher specific energy (SE M), and high crusher specific energy (SE H), respectively.

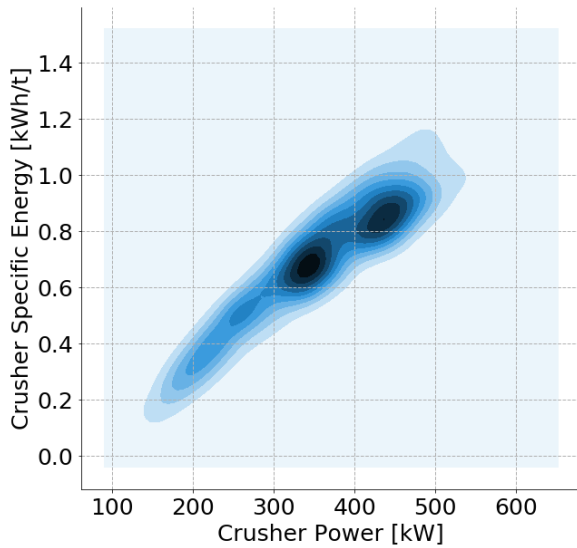


Figure 45. Kernel density estimation plot of the pebble crusher power and pebble specific energy (Paper D).

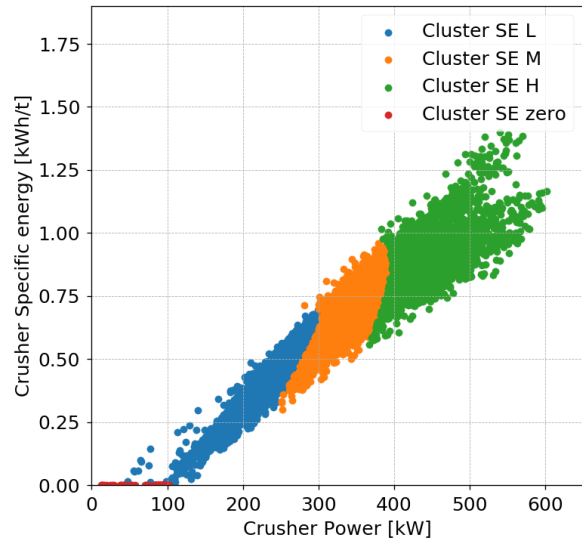


Figure 46. Clusters of recycling load based on crusher power and pebble specific energy (Paper D).

The SAG mill fresh feed rate is set as the key performance variable. Change point analysis (CPA) is implemented to identify patterns in the time-series dataset. CPA is a powerful tool for determining whether a change has actually occurred (Taylor, 2000). This analysis is conducted using the Ruptures package in Python (Truong et al, 2018), identified 66 changes in the entire dataset, as shown in Figure 47. These periods are then categorized based on their average feed rates, which are 1619 tph, 1720 tph, and 1821 tph, respectively. The corresponding data are labeled according to the fresh feed rate. It should be noted that a data point with a low SAG mill feed rate (such as 1600 tph) can still be labeled as ‘high feed rate’ if the period to which it belongs has a high average value, and vice versa.

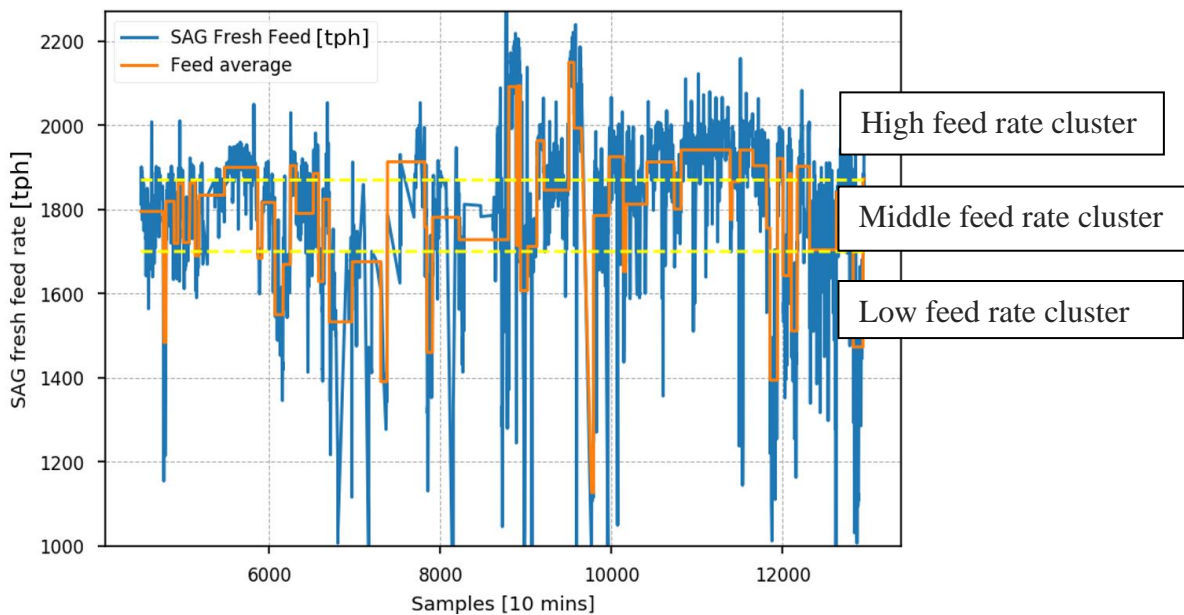


Figure 47. Change points of fresh feed rate. It is categorized into three classes based on their average value in each period (Paper D).

In the final step, the impact of the key variables on circuit performance was investigated. In Figure 48, circuit performance variables such as SAG power, SAG feed rate, and SAG specific energy are compared against their crusher cluster labels.

The SAG mill specific energy is calculated from SAG power draw and fresh feed rate, as shown in Figure 48 (a). Data points with SE H have an average SAG specific energy of 6.9 kWh/t compared to 7.5 kWh/t for SE L, representing an 8% decrease in specific energy.

Figure 48 (b) and Figure 48 (f) show the SAG fresh feed rate and SAG pebble rate, respectively. The results indicate clear trend: data points with SE H have higher fresh feed rates compared to those with SE L. The average fresh feed rate with low crusher utilization is 1715 tph, while it increases to 1850 tph with high crusher utilization.

The plots in Figure 49 present variables with different SAG mill throughput labels. Plot (e) shows the feed size F80, and plot (f) shows the pebble rate. Neither plot shows a significant difference, suggesting that this site has a uniform feed due to the presence of a pre-crusher. Additionally, higher mill throughput does not necessarily result in increased pebble production.

In conclusion, the visualized results with crusher power/specific energy clusters show strong correlations between pebble crusher operational settings and circuit performance variables.

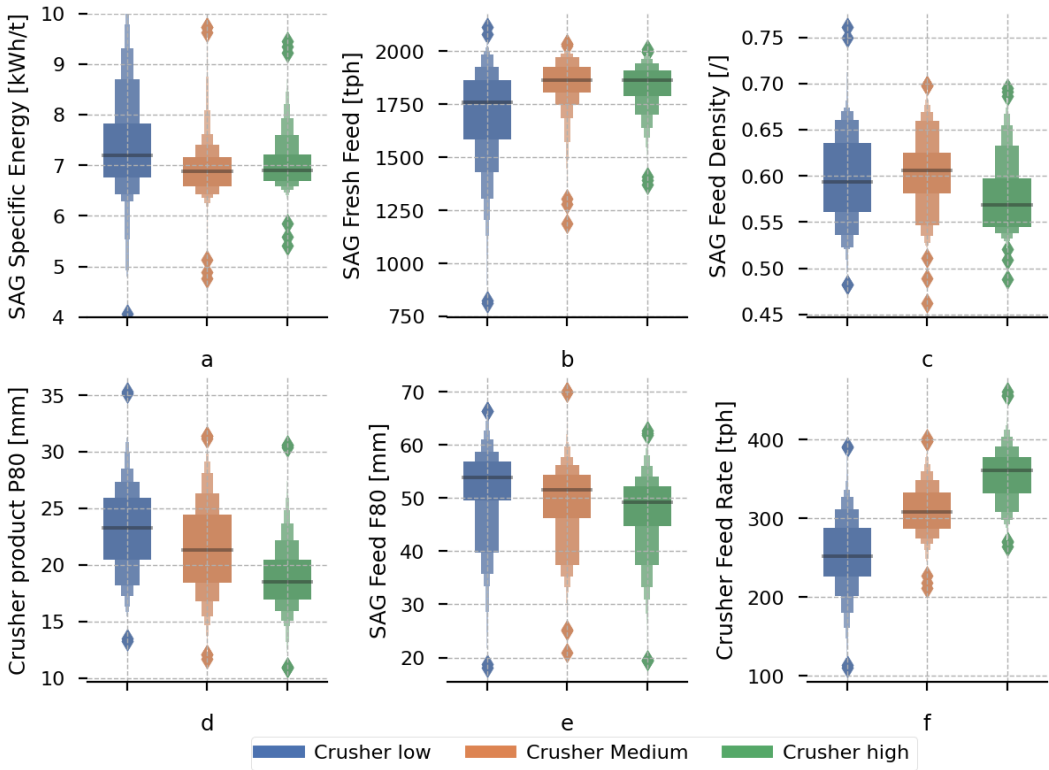


Figure 48. Comparison of SAG mill parameters under different cone crusher clusters (Paper D).



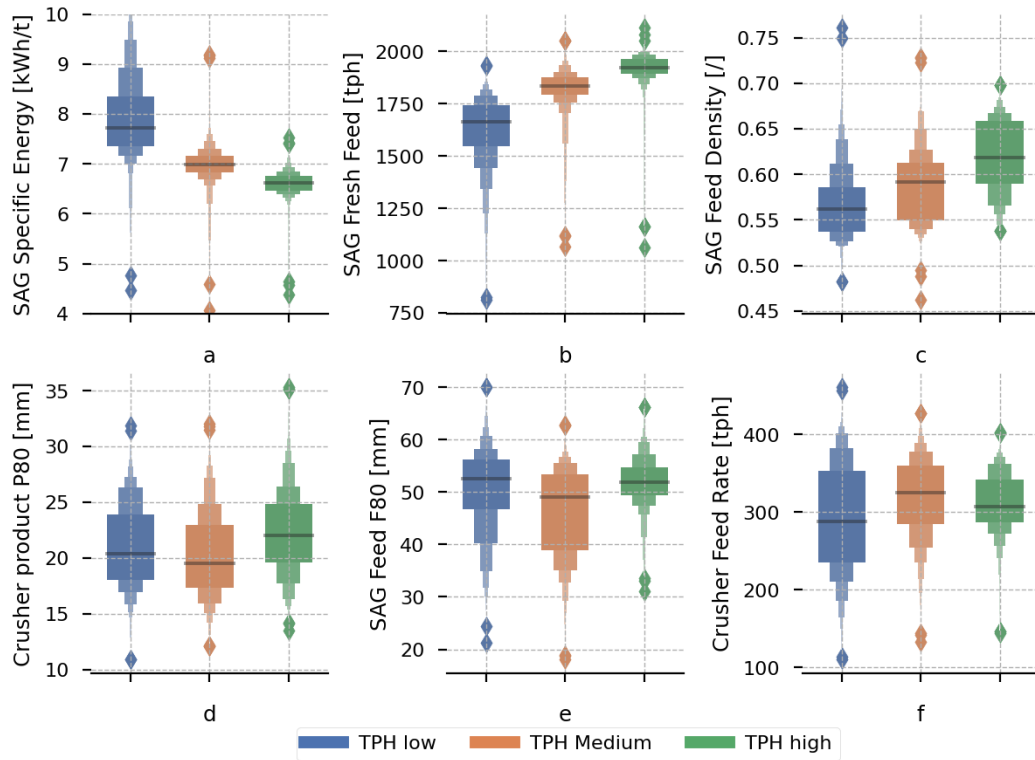


Figure 49. Comparison of operational data under different SAG mill feed rate clusters (Paper D).

Data points with feed rate labels are presented in Table 3 and Figure 50. The mean values of recycling pebble flow rate and pebble size in Table 3 show that the recycling load is very similar in all cases, and the fresh rock feed size to the SAG mill shows no significant difference either.

The results show that when the pebble crusher maximized its power utilization to break critical-size rocks into finer particles, as indicated by the pebble specific energy in Table 3, the circuit throughput boosted.

Table 3. Comparison of circuit variable average values based on feed rate labels (Paper D).

Variables	Feed rate low	Feed rate mid	Feed rate high
SAG fresh feed size [mm]	51.2	50.4	50.6
Pebble size [mm]	38.2	37.1	37.3
Pebble flow rate [tph]	292	310	307
Pebble specific energy [kWh/t]	0.55	0.66	0.78

A summary of the identified categories is shown in Figure 50. During the low feed rate period (mean value 1619 tph), 794 data points fall into the ‘low utilization of crusher’ category, while the high feed rate period (mean value 1821 tph) contains 1054 data points labeled as ‘high utilization of crusher’. Since each crusher cluster has a similar rock feed size, the distribution difference is likely due to variations in crusher operational settings. Therefore, it is reasonable to conclude that higher utilization of the pebble crusher leads to higher circuit throughput.

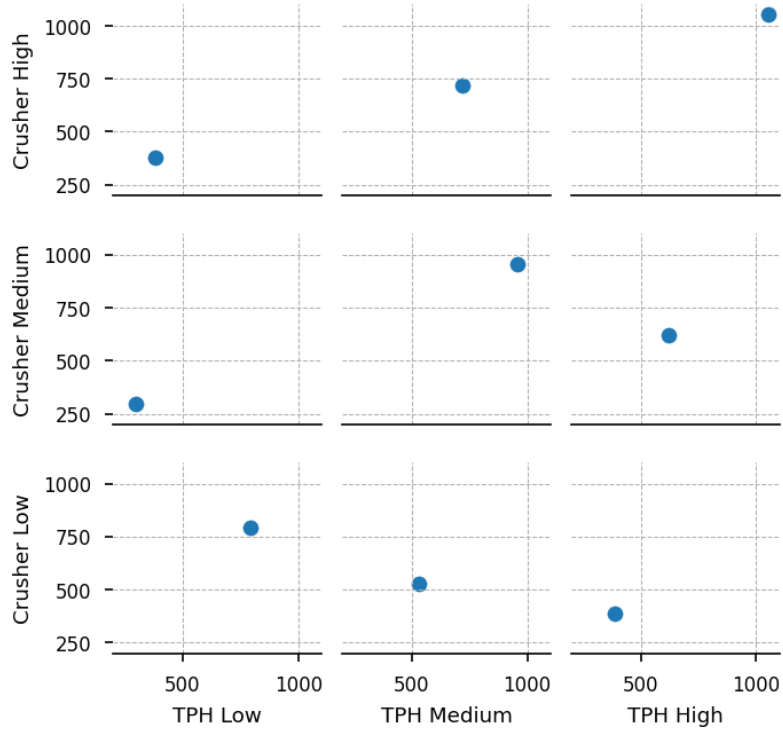


Figure 50. The correlations between crusher clusters and SAG mill fresh feed rate clusters (Paper D).

#### 4.8 Particle Size Distribution Estimation for Crushed Products

In Paper F, a framework for estimating the particle size distribution of crushed products is presented. This approach aims to track the real-time rock size fed to a grinding circuit. As discussed in previous sections, feed/product size distribution is not only a crucial parameter for modeling, but it also allows for evaluation of circuit performance. However, measuring of rock particle size remains very labor-intensive and time-consuming.

To identify a rock from an image, it is first necessary to draw a clear and sharp edge around all the particles in that image. The edge detection algorithm DexiNed network is used in Paper F. The DexiNed network is a general algorithm for edge detection, allowing the proposed method to be implemented without a pre-trained dataset.

In Figure 51, an example of a raw image and its processed results are presented. Once the edge map is created, a binary filter with a size of 3x3 pixels is applied. The binary image is shown in Figure 51 (b). Next, the OpenCV ‘ContourArea’ function is used to calculate the pixel area of an enclosed region. The convex area for each contour is determined using the ‘ConvexHull’ function. The ratio between the convex hull area and the contour area is then used to filter single rocks from fine particles and neighboring rocks. Figure 51 (c) illustrates all the contours identified by the OpenCV built-in function ‘findContours’. The ratio between the convex hull area and the contour area is obtained:

$$R_{ci} = A_{ci}/A_{hi} \quad (4.2)$$

where  $R_{ci}$  is the area ratio for the  $i$ th contour,  $A_{ci}$  is the contour area, and  $A_{hi}$  is the convex hull area.  $R_{ci} = 1.2$  is the threshold to determine if this contour belongs to one single rock or

several connected rocks. In this step, we set an upper limit for the pixel area where a region larger than the upper limit is least likely a single rock.

After the previous filtering processes, the remaining contours are categorized into three classes: the fine region in Figure 51 (d); the connected rocks in Figure 51 (e); and the single rock in Figure 51 (f). As illustrated in Figure 52, the connected rocks are further examined to identify and generate more single rocks.

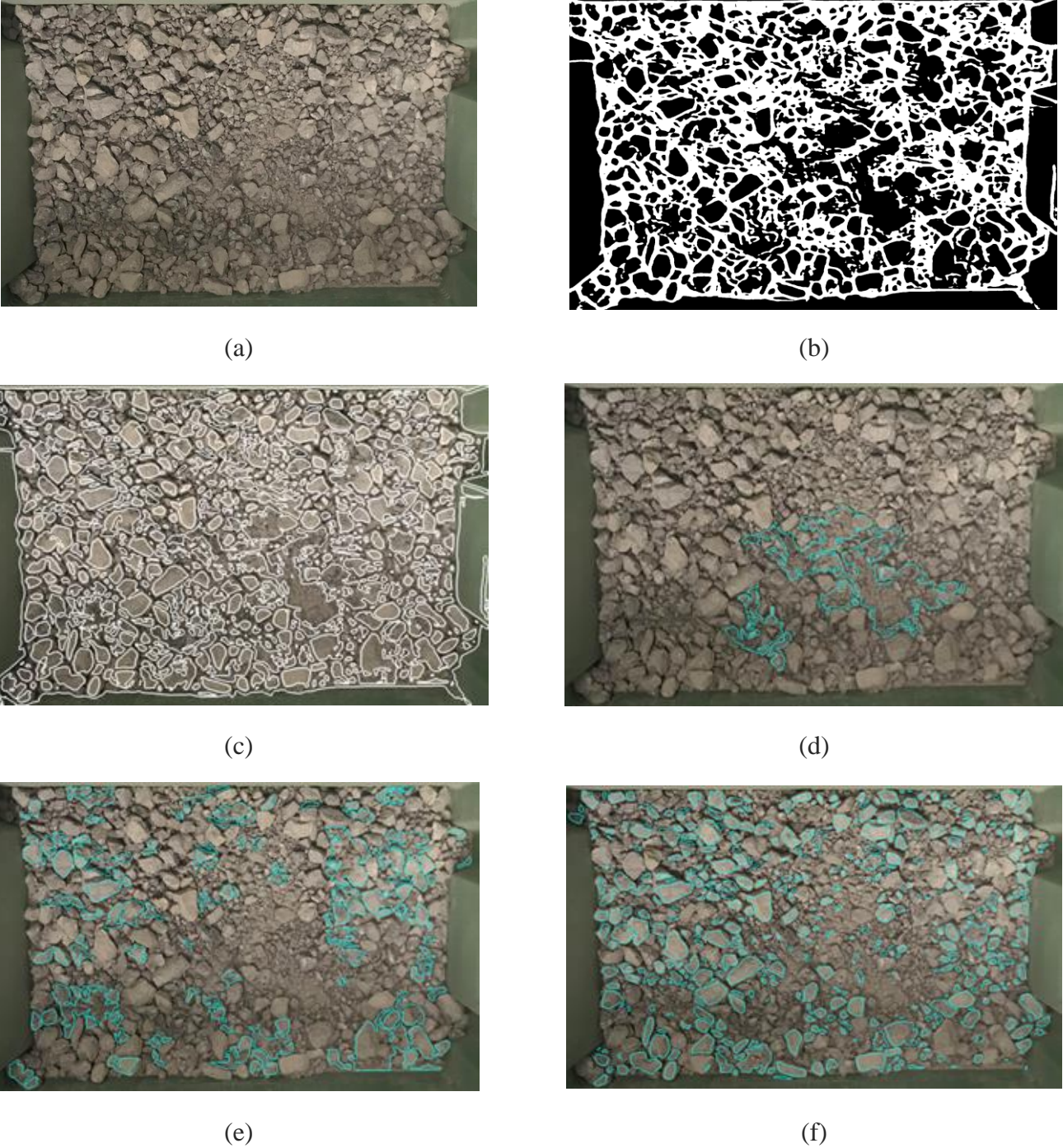


Figure 51. An example of raw image and processed results: (a) the raw image; (b) the binary image of detected edge; (c) all contours found; (d) fine region; (e) connected rock region; (f) single rock region (Paper E).

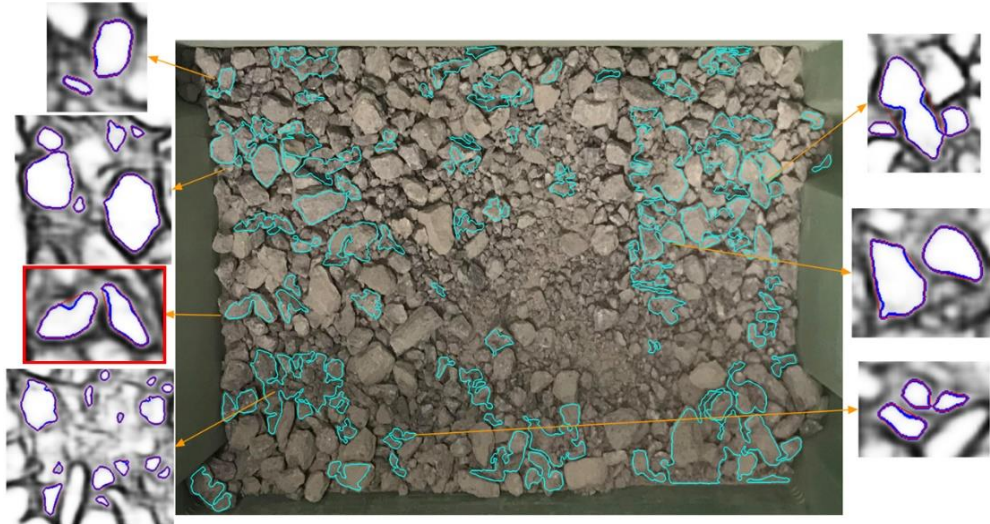
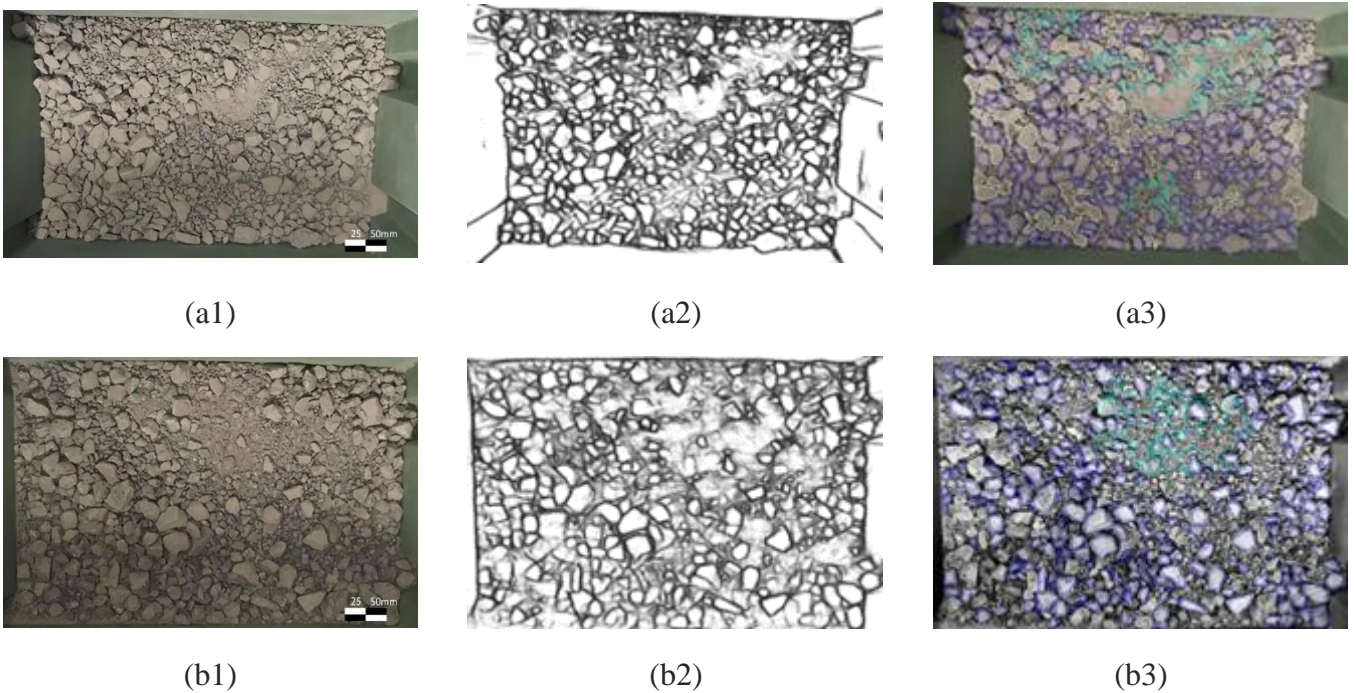


Figure 52. An example of the connected neighboring rocks and the contour map of the extracted images with the new threshold value (Paper E).

This study was performed on Google Colab Pro using Python 3.7.10 and OpenCV version 4.1.2.30. The image acquisition device was the rear camera of an Apple iPhone X. The original image resolution was 4032 by 3024 pixels. Images were cropped to fit the boundaries of the samples, with a box size of 345 mm by 490 mm. Five images were selected after completely reshuffling the samples. The average execution time per image was 30 ms for DexiNed edge mapping, 200 ms for contour segmentation, and 50 ms for mass distribution estimation.

Images from Figure 53 show the fused-edge maps and filtered results of the fine region, the connected rock region, and the single rock region, respectively. The connected rock regions are processed again with adjusted threshold values.



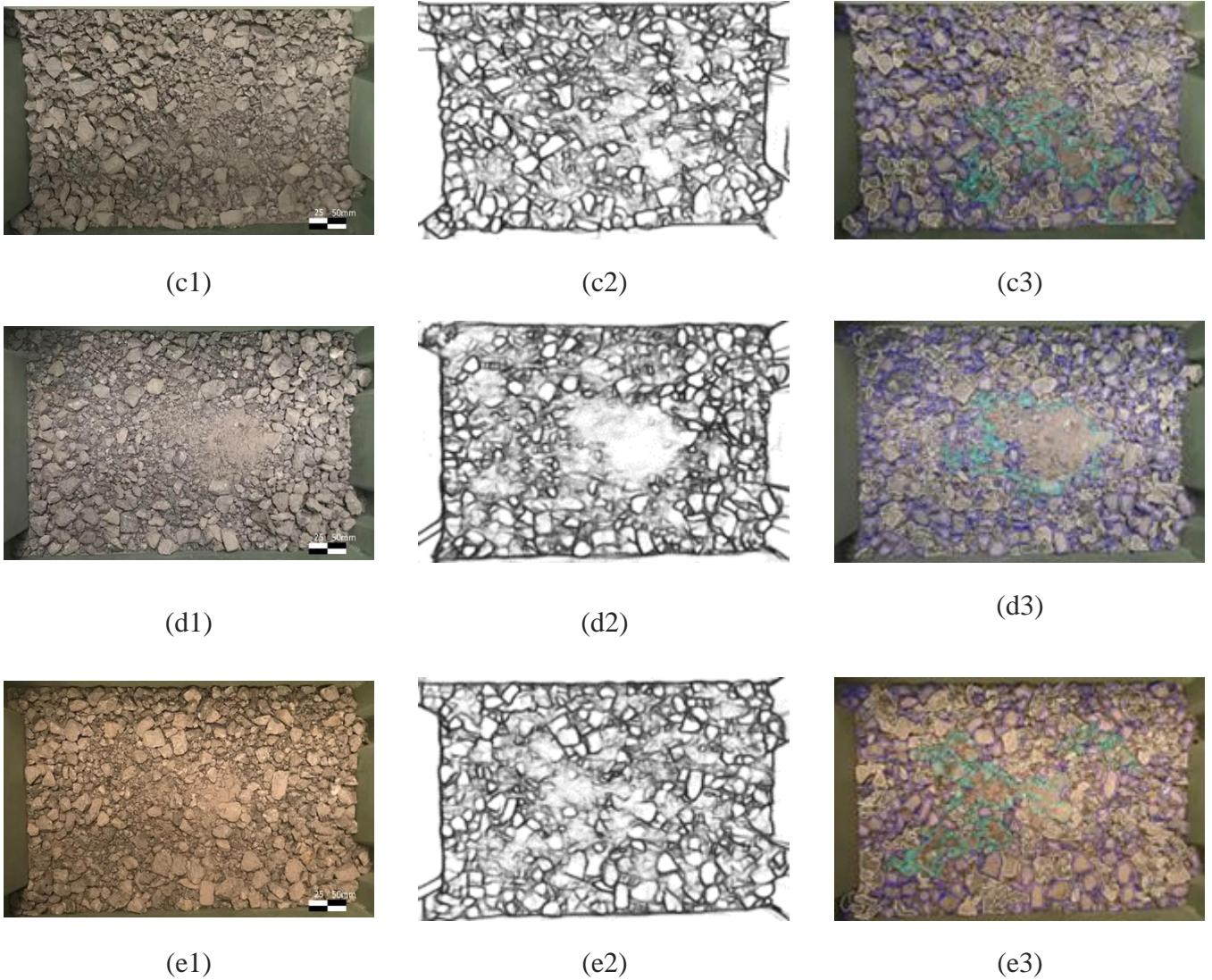


Figure 53. The processed results: (a1,b1,c1,d1,e1) raw images of lab samples; (a2,b2,c2,d2,e2) edge maps of input images; (a3,b3,c3,d3,e3) contour maps with three filters results, where the light green contour is the fine region, the white contour is the connected rock region and the blue is single rock region (Paper E).

In Table 4 and Table 5, the estimated mass distributions from tested images are listed. The laboratory sample was manually screened twice, and its particle size distribution is shown in Table 6. Due to shape irregularity, the weight estimation from the pixel area can be biased. In Figure 54 (a, b), the results of size distributions are presented, and the  $R^2$  values are illustrated in Figure 54 (c). These results show that  $R^2$  values greater than 0.9 were obtained for all five images, with their average mass estimation yielding an  $R^2$  of 0.975. This indicates that there is no significant difference between the averaged estimated value and the actual value. Additionally, the averaged cumulative distribution shows even higher accuracy with an  $R^2$  of 0.985.

The total deviation of the screened samples from the calculated estimation could originate from the following factors: (1) incorrect edge and contour drawing; (2) area calibration for fine

particles; (3) area calibration for erosion loss; (4) pixel area to rock mass conversion; and (5) overlapped particles not identified or treated as smaller particles.

The proposed method calculates mass fractions from non-overlapped rocks. In the experiment, the same sample was reshuffled five times, and similar threshold values were applied for each test. Therefore, the result deviation from factors (1), (2), (3), and (4) remains consistent. The differences between these five trials are mainly due to the presence of overlapped particles. In Table 4, the frequency of coarse particles varies from 3.1% to 7.0% (-22.4 mm) and from 2.4% to 8.7% (-19 mm). These variances demonstrate that overlapped particles can introduce considerable bias into the particle size distribution from rock segmentation. However, the averaged results indicate that this deviation can be mitigated by using multiple images of the same sample. A potential industrial solution to the issue of overlapped rocks is the installation of several cameras at different conveyor positions with varying view angles.

Table 4. The frequency of rock mass distribution of images 1 to 5 (Paper E).

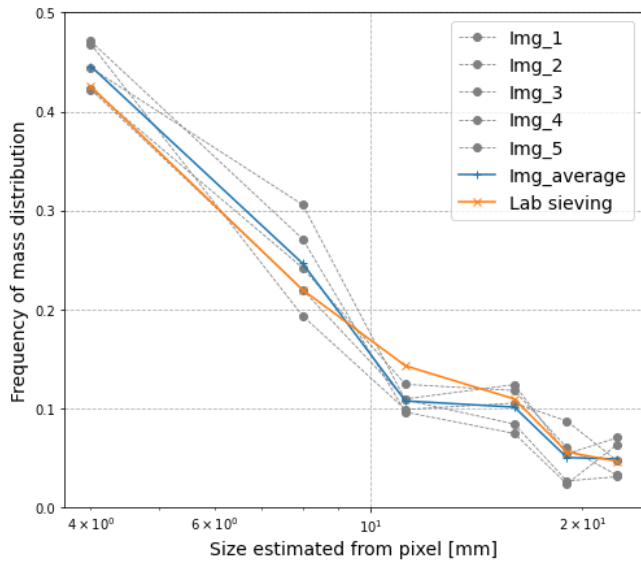
Image no.	Frequency of Mass Distribution (%)					
	4	8	11.2	16	19	22.4
Image 1	47.1	27.1	9.6	7.5	2.4	6.3
Image 2	42.3	24.2	12.4	11.8	6.0	3.2
Image 3	42.2	22.0	10.9	12.4	5.4	7.0
Image 4	44.4	30.6	10.8	8.4	2.7	3.1
Image 5	46.8	19.3	9.9	10.5	8.7	4.7
Average	44.5	24.6	10.7	10.1	5.0	4.8

Table 5. The cumulative rock mass distribution of images 1 to 5 (Paper E).

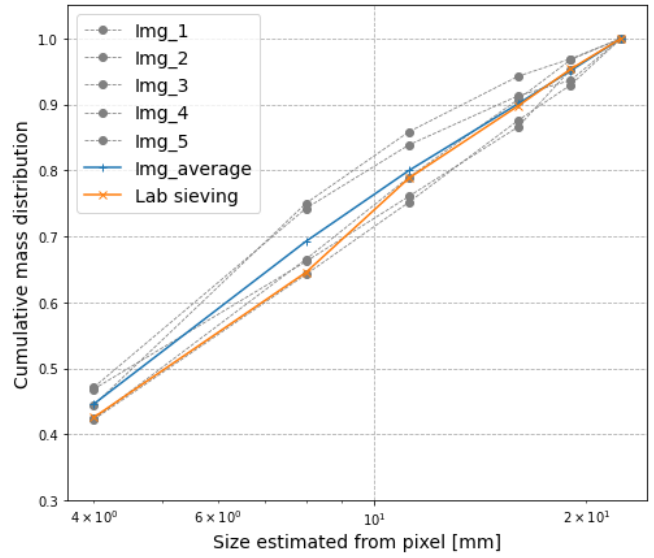
Image no.	Cumulative Mass Distribution (%)					
	4	8	11.2	16	19	22.4
Image 1	47.1	74.2	83.9	91.3	93.7	100
Image 2	42.3	66.5	79.0	90.8	96.8	100
Image 3	42.2	64.2	75.1	87.6	93.0	100
Image 4	44.4	75.0	85.9	94.3	96.9	100
Image 5	46.8	66.2	76.1	86.6	95.3	100
Average	44.5	69.2	79.9	90.0	95.1	100

Table 6. The results of lab sieving (Paper E).

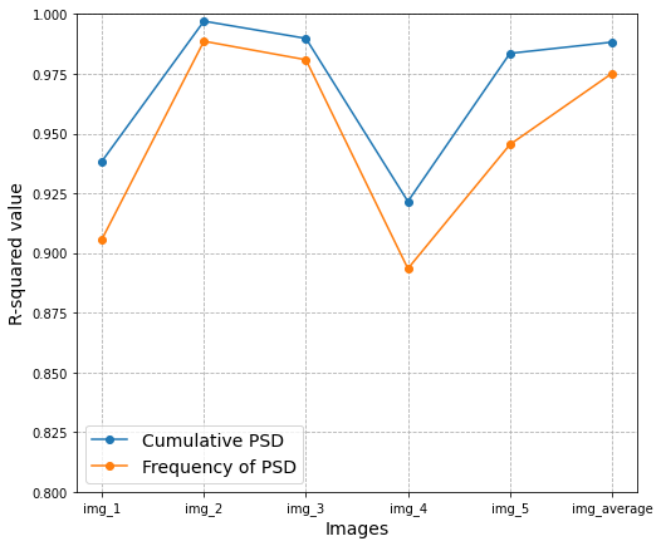
Columns	Size (mm)					
	4	8	11.2	16	19	22.4
Weight 1 (g)	1622.1	797	521.7	400.0	234.6	194.3
Weight 2 (g)	1483.0	807.1	521.6	398.5	172.6	144.7
Frequency of Mass Distribution (%)	42.6	22.0	14.3	10.9	5.6	4.6
Cumulative Mass Distribution (%)	42.6	64.5	78.8	89.8	95.4	100



(a)



(b)



(c)

Figure 54. The results of the estimated mass distribution compared with lab sampling: (a) frequency of the size distribution; (b) cumulative size distribution; (c)  $R^2$  of the estimated results (Paper E).





# 5 DISCUSSION

The aim of this *chapter is to:*

- *Discuss the highlights and important conclusions drawn in this thesis.*
- *Answer the research questions raised in the introduction chapter.*
- *Discuss the future work concerning deeper analysis and new proposals that have been raised during this research work.*

## 5.1 General Conclusions

The research presented in this thesis aims to understand the dynamic interactions between a SAG mill and its pebble crushers. The motivation behind this work was to develop a flexible, powerful, and efficient framework to predict and optimize the SAG mill grinding process, with an emphasis on different pebble crusher operational settings. The methodologies presented in this thesis were developed to address the stated research questions at various levels to achieve the overall objective

Papers A and B presented a generic tumbling mill model based on a population balance framework, integrating sub-processes such as particle breakage, particle transportation, breakage appearance, and particle discharge. Meanwhile, models of cone crushers, conveyors, and screens were implemented for dynamic simulation of the plant circuit. The results in Paper B demonstrated that dynamic fluctuations in the entire grinding circuit could be induced by pebble crusher operating parameters, such as CSS and eccentric speed. Furthermore, the hypothesis that increasing pebble crusher efficiency boosts overall circuit performance was validated with industrial data in Paper D.

In Paper G, a systematic investigation of the effects of feed ore hardness, feed size, pebble crusher settings, and the pebble stockpile on SAG mill circuit performance was conducted using the DoE approach and the simulation platform based on Paper B. The results show that softer feed materials result in higher throughput and lower pebble rates, while harder feed materials decrease fresh feed rates and increase pebble rates. A pre-crusher reduces pebble generation and enhances feed rates. Although a pebble stockpile doesn't directly improve feed rates, it offers better manageability of the circuit.

Papers C and F incorporated several data-driven methods for estimating SAG mill power draw and SAG mill pebble rate. In Paper C, both the prediction model and the time-series forecasting model demonstrated promising accuracy for SAG mill power draw estimation. In Paper F, by adding a liner wear soft sensor and vibration clustering signals, the SAG mill pebble rate estimation showed improved accuracy compared to results using only the original features. The Shapley analysis also highlighted the importance of expertise in related fields when applying data-driven methods.

Paper D presented a general framework for a data analysis method. The main purpose of this paper is to develop an approach that can step-by-step isolate the influence of any arbitrary machinery or rock characteristic on plant performance from raw data. This method aids in extracting key information that can potentially be used for future optimization and new machine

design. In the case study in Paper D, the impact of pebble crushing on grinding circuit performance was investigated. Circuit performance variables and crusher operating settings were clustered, and the original dataset was then split into different categories according to the clustering labels. The labeled data distributions revealed clear correlations between high crusher utilization and high mill throughput.

As new issues and challenges emerge in the process of addressing each research question, the information on particle size distribution becomes crucial not only for calibrating the proposed model but also for evaluating machine performance. In Paper E, an image processing framework for estimating rock particle size distribution is proposed. This method effectively identifies edge maps of crushed rocks, accurately segments coarse material from connected fine regions, and provides relatively precise estimates of particle size distribution based on pixel regions. Furthermore, this algorithmic framework can be extended to process images of rocks on conveyor belts and accommodate a wider range of rock sizes.

### 5.2 Answering Research Questions

In Figure 55, a mapping shows how the research questions are answered in the appended papers. The size of the marker indicates the contribution of the corresponding paper to the research questions.

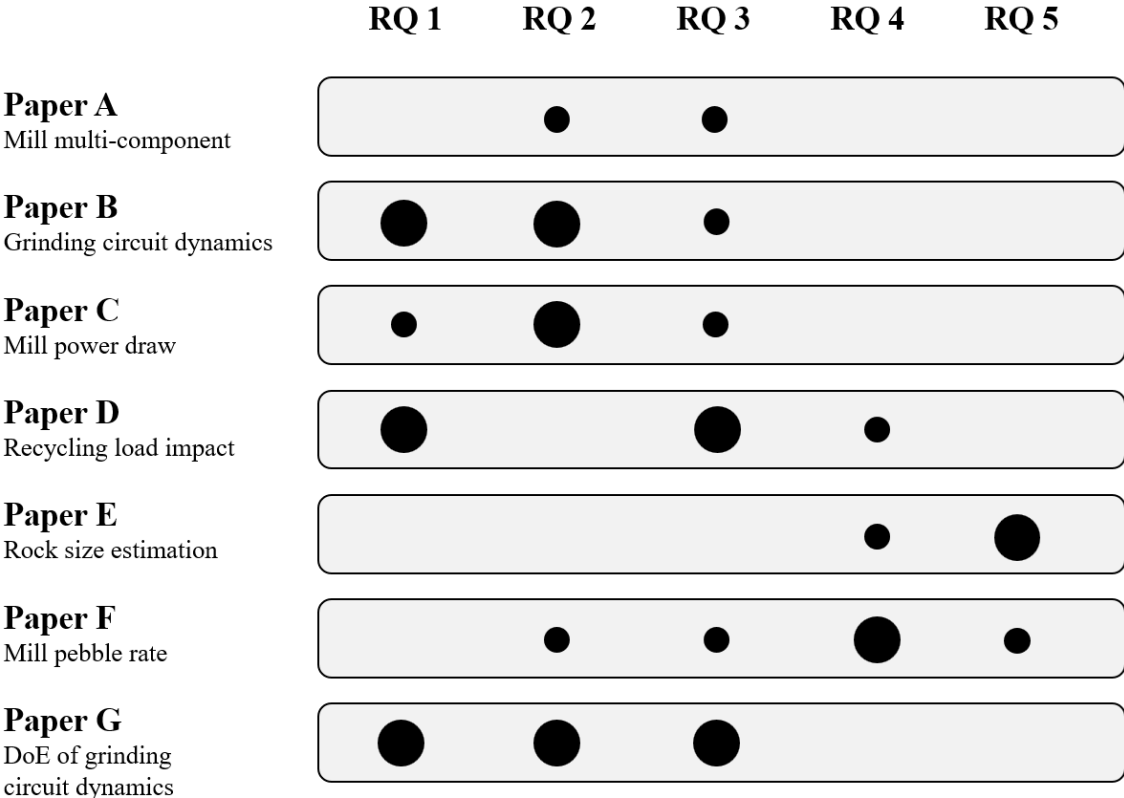


Figure 55. Illustration of the relationships between the appended papers and research questions. The size of the markers indicates the strength of the relationships.

RQ 1: What are the dynamic interactions between the SAG mill and the pebble crusher in a grinding process?

Answer: In Paper B, the dynamics of a SAG mill and its pebble crushers are studied using simulation tools built on individual models for each machine. It is demonstrated in Paper B that even with a constant feed rate to the circuit, the recycling load flow rate can be changed by altering the cone crusher settings. Simulation results indicate that if the recycling material is crushed down to a certain size class where particles have a higher breakage rate, this leads to a higher SAG mill efficiency. In more complex circuits, where multiple pebble crushers are integrated, dynamic fluctuations can occur due to the pebble crushers switching on and off during operations.

Furthermore, in Paper G, a systematic study of the dynamic effects of ore hardness, feed size, pebble crusher settings, and pebble stockpile is conducted. The DoE results show that the implementation of a crusher controller with smaller CSS and higher eccentric speed, along with the use of a pebble stockpile, improves the throughput of the SAG mill circuit by up to 10%. Similar dynamic behaviors are observed and reported by Erwin (Erwin et al., 2023) in several SAG mill circuit case studies involving two pebble crushers with active CSS and speed control developed based on Hulthén's research (Hulthén, 2010).

In Paper D, statistical analysis of the industrial data is performed. The quantitative results show that the SAG mill specific energy decreases from 7.5 kWh/t to 6.9 kWh/t with higher utilization of pebble crushing. Clear correlations between circuit performance and pebble crusher utilization levels are observed.

RQ 2: What approach can be used to model these interactions and other internal dynamics for SAG mills and pebble crushers?

Answer: Two modeling techniques are presented in this thesis. The first approach, detailed in Paper A, Paper B and Paper G, proposes fundamental models based on physical principles. A population balance framework is implemented for a tumbling mill with sub-models that consider breakage and transportation. Fundamental models for cone crushers, conveyors, bins, and screens are also developed considering mass balance, material tracking, and size reduction. The data structures within these modeling units are standardized, allowing for flexible adaptation to any circuit.

One of the advantages of this fundamental modeling approach is its broad applicability to a wide variety of plants. Models based on the underlying physics can provide adequate accuracy for new comminution circuits and offer valuable insights for future machinery design and optimization.

The approaches introduced in Paper C and Paper F utilize several types of data-driven methods. The strengths and weaknesses of these methods are the opposite of those of fundamental models. While data-driven models can provide accurate predictions, they cannot represent the mechanistic understandings of the physical processes. The flexibility of this approach allows for the discovery of complex nonlinear relationships between input variables and certain target outputs. However, the accuracy of the method mainly depends on the quality of the training dataset. This dataset needs to be high-quality with minimal missing or outlier data points. A

real-time online monitoring system that continuously updates and trains models is recommended.

RQ 3: How can the approaches proposed in the thesis be adapted and implemented in industrial applications?

Answer: Minerals processing operations collect large amounts of data from multiple sources. However, this data is often neither systematically analyzed nor effectively used to gain a better understanding of the process or for process optimization (Suriadi et al., 2018). In Paper D, a data analysis framework is presented, and a case study isolating the impact of a pebble crusher operating setting in a comminution circuit is conducted. The proposed approach provides standardized steps to extract key information from data and allows for narrowing down operating conditions to a specific plant to identify optimization potential.

The fundamental dynamic modeling methods introduced in Papers A, B, and G can be applied to various aspects of the comminution process, including control system development, plant pre-design evaluation, maintenance planning, and operation optimization.

The data-driven modeling and analysis methods introduced in Papers C and F can be used for soft sensing of complex conditions that are difficult to measure directly. These methods also offer great potential for high-accuracy modeling and advanced control. However, expertise in mineral processing and a deep understanding of data analysis are essential for mineral engineers to effectively analyze data and adapt to the dynamic environment of the industry.

RQ 4: How can operational signals be used to identify different units' working conditions to improve the modeling accuracy?

Answer: With the development and application of sensor technology, obtaining high-frequency real-time data has become easier, resulting in a larger volume of data available for use in data-driven models. While this vast amount of data can improve the accuracy of these models, it also presents challenges. Not all data is valid, and blindly applying all data can sometimes be counterproductive. This is where the importance of mineral processing knowledge becomes evident. Careful screening of selected features is crucial to remove confounding information and enhance the model's accuracy.

In both Paper D and Paper F, the Gaussian mixture model is applied to perform cluster analysis and generate a new feature. This new feature is created to describe the operational state of the machine. For example, in Paper F, vibration data and mill energy consumption were used to classify the data into three categories: low, medium, and high working states.

After clustering, nearly every group showed a linear correlation between vibration signals and mill power draw. The added clustering feature also improved the accuracy of the pebble rate estimation model. Notably, the importance analysis using Shapley values revealed that this added vibration clustering feature was the second most important of all features. In contrast, the raw vibration signal itself had the lowest contribution value in the pebble rate estimation.

In Paper C, several data-driven models are proposed for predicting SAG mill power. However, these models showed some deviations when the power dropped significantly. By identifying the operating conditions and creating new features, a more accurate power draw model can be developed.

RQ 5: What additional information needs to be collected on top of the current sensing system to help enhance the process modeling and controlling?

Answer: The particle size distribution is not only used to measure the accuracy of the proposed models in this thesis but is also an important indicator of machine performance in the minerals processing and aggregate industries. However, obtaining the particle size distribution is difficult and generally labor-intensive and time-consuming. Despite the rapid advancement of image processing technology and significant research investment in this area, a mature industrial solution has not yet been achieved (Mukherjee et al., 2009; Yang et al., 2020).

In Paper E, a general image processing procedure for measuring rock particle size distribution is presented. A common challenge with many similar algorithms is the need for a large amount of training data to effectively segment the rocks in an image. To make the proposed method easy to implement, we use a general edge detection algorithm, DexiNed, which does not require an additional rock image training dataset (Poma et al., 2020). The proposed method is capable of identifying edge maps of crushed rocks, correctly segmenting coarse material from connected fine regions, and providing relatively accurate estimates of particle size distribution from pixel regions. Furthermore, this algorithmic framework can be extended to conveyor belt rock image processing and a larger range of rock sizes.

Furthermore, Paper F highlights the importance of creating new features based on known signals. Developing these features requires a deep understanding of the process and expertise in data analytics. Consequently, the added features contribute to the development of more accurate models.

### 5.3 Future Work

Grinding is a complex process involving many machine and process parameters. The performance of a grinding circuit is influenced not only by the individual machines but also by the interactions between various factors. This thesis presents a variety of modeling and data analysis methods that can be implemented at different levels of a grinding/crushing plant. Topics that can be developed to bring further insights into the modeling and optimization of grinding processes are:

- Further develop the fundamental models with high fidelity to implement the proposed simulation tools in a wider range of applications.
- Develop an online framework using data-driven methods where the models can be continuously updated based on the collection of real-time data. This can provide additional insights into process fault detection and wear monitoring.
- Formalize a modeling framework that combines data-driven methods and physics-based methods. Combining fundamental models with complex nonlinear machine learning algorithms has the potential for improved process modeling and optimization.

- Build a real-time particle size estimation system and create an industrial case study. Integrate the real-time particle size distribution into the simulation process.

The approaches presented in this thesis were developed for the mineral grinding process industry. The modeling and methods for tumbling mills, crushers, and screens can be extended to a wider range of application scenarios.

# References

- Aldrich, C. (2020). *Process variable importance analysis by use of random forests in a shapley regression framework*. Minerals, 10(5), 420.
- Asbjörnsson, G. (2015). *Crushing plant dynamics*. (PhD Thesis), Chalmers University of Technology, Gothenburg, Sweden.
- Austin, L. G., & Cho, H. (2002). *An alternative method for programming mill models*. Powder technology, 122(2-3), 96-100.
- Bhadani, K. (2022). *Optimization Capabilities for Crushing Plants*. (PhD Thesis), Chalmers University of Technology, Gothenburg, Sweden.
- Bhadani, K., Asbjörnsson, G., Hofling, K., Hulthén, E., & Evertsson, M. (2024). *Application of design of experiments (DoE) in evaluating crushing-screening performance for aggregates production*. Minerals Engineering, 209, 108616.
- Bishop, Christopher M., and Nasser M. Nasrabadi. *Pattern recognition and machine learning*. Vol. 4. No. 4. New York: springer, 2006.
- Bourgeois, F. S. (1993). *Single-particle fracture as a basis for microscale modeling of comminution processes*. The University of Utah, 1993.
- Breiman, L. (2001). *Random forests*. Machine learning, 45(1), 5-32.
- Bueno, M., Shi, F., Kojovic, T., & Powell, M. (2010). Investigation on multicomponent semi-autogenous grinding. In *XXV International Mineral Processing Congress*. Australasian Institute of Mining and Metallurgy, Brisbane, Australia.
- Chen, T., & Guestrin, C. (2016). Xgboost: A scalable tree boosting system. In *Proceedings of the 22nd acm sigkdd international conference on knowledge discovery and data mining* (pp. 785-794).
- Choi, S. W., Morris, J., & Lee, I.-B. (2008). *Dynamic model-based batch process monitoring*. Chemical Engineering Science, 63(3), 622-636.
- Collins, S. E., Holberk, P., & Strickland, D. (2018). NI 43-101 *Technical Report for the Copper Mountain Mine*.
- Carvalho, M. (2013). *Mechanistic modelling of semi-autogenous grinding*. (ph.D. thesis) UFRJ/COPPE. University of Rio de Janeiro.

- Delaney, G., Morrison, R., Sinnott, M., Cummins, S., & Cleary, P. (2015). *DEM modelling of non-spherical particle breakage and flow in an industrial scale cone crusher*. *Minerals Engineering*, 74, 112-122.
- Ding, J., Yang, C., & Chai, T. (2017). *Recent progress on data-based optimization for mineral processing plants*. *Engineering*, 3(2), 183-187.
- Erwin, K., Meinke, C., Chandramohan, R., Lane, G., & Foggatto, B. (2023). *Pebble Crushing Circuits: A SAG Mill's Unappreciated Saviour*. In *SAG Conference*, Vancouver, 2023.
- Evertsson, C. M. (2000). *Cone crusher performance*. (PhD Thesis), Chalmers University of Technology, Gothenburg, Sweden.
- Fuerstenau, M. C., & Han, K. N. (2003). *Principles of mineral processing*. SME, 2003.
- Ge, Z. (2017). *Review on data-driven modeling and monitoring for plant-wide industrial processes*. *Chemometrics and Intelligent Laboratory Systems*, 171, 16-25.
- Ge, Z., Song, Z., Ding, S. X., & Huang, B. (2017). *Data mining and analytics in the process industry: The role of machine learning*. *IEEE Access*, 5, 20590-20616.
- Ge, Z., Song, Z., & Gao, F. (2013). *Review of recent research on data-based process monitoring*. *Industrial & Engineering Chemistry Research*, 52(10), 3543-3562.
- Gers, F. A., Schmidhuber, J., & Cummins, F. (1999). *Learning to forget: Continual prediction with LSTM*. *Neural computation*, 12(10), 2451-2471.
- Graves, A., Jaitly, N., & Mohamed, A. R. (2013). *Hybrid speech recognition with deep bidirectional LSTM*. In *the 2013 IEEE workshop on automatic speech recognition and understanding* (pp. 273-278).
- Haque, K. E. (1999). *Microwave energy for mineral treatment processes—a brief review*. *International journal of mineral processing*, 57(1), 1-24.
- Hastie, T., Tibshirani, R., Friedman, J., & Franklin, J. (2005). *The elements of statistical learning: data mining, inference and prediction*. *The Mathematical Intelligencer*, 27(2), 83-85.
- Hochreiter, S., & Schmidhuber, J. (1997). *Long short-term memory*. *Neural computation*, 9(8), 1735-1780.
- Horn, Z., Auret, L., McCoy, J., Aldrich, C., & Herbst, B. (2017). *Performance of convolutional neural networks for feature extraction in froth flotation sensing*. *IFAC-PapersOnLine*, 50(2), 13-18.



- Hoseinian, F. S., Faradonbeh, R. S., Abdollahzadeh, A., Rezai, B., & Soltani-Mohammadi, S. (2017). *Semi-autogenous mill power model development using gene expression programming*. Powder technology, 308, 61-69.
- Hulthén, E. (2010). *Real-time optimization of cone crushers*. (PhD Thesis), Chalmers University of Technology, Gothenburg, Sweden.
- Jia, R., Dao, D., Wang, B., Hubis, F. A., Hynes, N., Gürel, N. M., Spanos, C. J. (2019). Towards efficient data valuation based on the shapley value. In *The 22nd International Conference on Artificial Intelligence and Statistics* (pp. 1167-1176). PMLR.
- Jia, X., Willard, J., Karpatne, A., Read, J., Zwart, J., Steinbach, M., & Kumar, V. (2019). Physics guided RNNs for modeling dynamical systems: A case study in simulating lake temperature profiles. In *Proceedings of the 2019 SIAM International Conference on Data Mining* (pp. 558-566).
- Valery, W., Morrell, S. (1995). *The development of a dynamic model for autogenous and semi-autogenous grinding*. Minerals Engineering, 8(11), 1285-1297.
- Johnson, G., Hunter, I., & Holle, H. (1994). *Quantifying and improving the power efficiency of SAG milling circuits*. Minerals Engineering, 7(2-3), 141-152.
- Kapur, P., & Fuerstenau, D. (1989). *Simulation of locked-cycle grinding tests using multicomponent feeds*. Powder technology, 58(1), 39-48.
- Karpatne, A., et al. (2017). *Theory-guided data science: A new paradigm for scientific discovery from data*. IEEE Transactions on Knowledge and Data Engineering, 29(10), 2318-2331.
- Karpatne, A., et al. (2022). *Physics-guided neural networks (pgnn): An application in lake temperature modeling*. Knowledge Guided Machine Learning. Chapman and Hall/CRC, 2022. 353-372
- King, R. P. (2001). *Modeling and simulation of mineral processing systems*. Elsevier, 2001.
- Kojovic, T., Hilden, M., Powell, M., & Bailey, C. (2012). Updated Julius Kruttschnitt semi-autogenous grinding mill model. In *11th AusIMM Mill Operators' Conference 2012 ed.* Hills, P. AusIMM: Australasian Institute of Mining and Metallurgy Hobart, Victoria pp. 71-79.
- Lindqvist, M. (2008). *Energy considerations in compressive and impact crushing of rock*. Minerals Engineering, 21(9), 631-641.

- Lindqvist, M., & Evertsson, C. M. (2004). *Improved flow-and pressure model for cone crushers*. Minerals Engineering, 17(11-12), 1217-1225.
- Lindqvist, M., & Evertsson, C. M. (2006). *Development of wear model for cone crushers*. Wear, 261(3-4), 435-442.
- Lippmann, R. P. (1987). *An introduction to computing with neural nets*. ACM SIGARCH Computer Architecture News, 16(1), 7-25.
- Long, Y., She, X., & Mukhopadhyay, S. (2018). HybridNet: integrating model-based and data-driven learning to predict evolution of dynamical systems. In *Conference on robot learning* (pp. 551-560). PMLR
- Marino, D. L., Amarasinghe, K., & Manic, M. (2016). Building energy load forecasting using deep neural networks. In *IECON 2016-42nd Annual Conference of the IEEE Industrial Electronics Society* (pp. 7046-7051).
- Maugis, C., Celeux, G., & Martin-Magniette, M. L. (2009). *Variable selection for clustering with Gaussian mixture models*. Biometrics, 65(3), 701-709.
- McCoy, J., & Auret, L. (2019). *Machine learning applications in minerals processing: A review*. Minerals Engineering, 132, 95-109.
- Morrell, S. (1992). *The simulation of autogenous and semi-autogenous milling circuits*. Comminution: Theory and Practice, 369-380.
- Morrell, S. (1996a). *Power draw of wet tumbling mills and its relationship to charge dynamics. 2. An empirical approach to modelling of mill power draw*. Transactions of the Institution of Mining and Metallurgy. Section C. Mineral Processing and Extractive Metallurgy, Section C, 105.
- Morrell, S. (1996b). *Power draw of wet tumbling mills and its relationship to charge dynamics. Pt. 1: a continuum approach to mathematical modelling of mill power draw*. Transactions of the Institution of Mining and Metallurgy. Section C. Mineral Processing and Extractive Metallurgy, Section C, 105.
- Morrison, R., & Cleary, P. W. (2004). *Using DEM to model ore breakage within a pilot scale SAG mill*. Minerals Engineering, 17(11-12), 1117-1124.
- Mukherjee, D. P., Potapovich, Y., Levner, I., & Zhang, H. (2009). *Ore image segmentation by learning image and shape features*. Pattern Recognition Letters, 30(6), 615-622.
- Napier-Munn, T. J., Morrell, S., Morrison, R. D., & Kojovic, T. (1996). *Mineral comminution circuits: their operation and optimisation*. JKMRRC, Queensland, Australia, 1996.

- Narayanan, S. (1987). *Modelling the performance of industrial ball mills using single particle breakage data*. International journal of mineral processing, 20(3-4), 211-228.
- Narayanan, S. S., & Whiten, W. (1983). *Breakage characteristics for ores for ball mill modelling*. Proc. Australas. Instn Min. Metall, 31–39.
- O’Bryan, K. (2014). *On trend*. Mining Magazine, July/August, pp. 27.
- Ouchterlony, F. (2005). *The Swebrec© function: linking fragmentation by blasting and crushing*. Mining Technology, 114(1), 29-44.
- Pauw, O. G., & Maré, M. S. (1988). *The determination of optimum impact-breakage routes for an ore*. Powder Technology, 54(1), 3-13.
- Poma, X. S., Riba, E., & Sappa, A. (2020). Dense extreme inception network: Towards a robust cnn model for edge detection. In *Proceedings of the IEEE/CVF winter conference on applications of computer vision*, (pp. 1923-1932).
- Powell, M., Evertsson, C. M., & Mainza, A. (2019). Redesigning SAG Mill Recycle Crusher Operation. In *SAG Conference, 2019 Vancouver*.
- Quist, J., & Evertsson, C. M. (2016). *Cone crusher modelling and simulation using DEM*. Minerals Engineering, 85, 92-105.
- Rose, D., Meadows, D. G., & Westendorf, M. (2015). Increasing SAG mill capacity at the Copper Mountain mine through the addition of a pre-crushing circuit. In *SME Annual Conference, Denver, USA*.
- Sun, Q., & Ge, Z. (2021). *A survey on deep learning for data-driven soft sensors*. IEEE Transactions on Industrial Informatics, 17(9), 5853-5866.
- Suriadi, S., Leemans, S. J., Carrasco, C., Keeney, L., Walters, P., Burrage, K., Wynn, M. T. (2018). *Isolating the impact of rock properties and operational settings on minerals processing performance: A data-driven approach*. Minerals Engineering, 122, 53-66.
- Tang, J., Chai, T., Zhao, L., Yu, W., & Yue, H. (2012). *Soft sensor for parameters of mill load based on multi-spectral segments PLS sub-models and on-line adaptive weighted fusion algorithm*. Neurocomputing, 78(1), 38-47.
- Tang, J., Zhao, L., Yu, W., Yue, H., & Chai, T. (2010). *Soft sensor modeling of ball mill load via principal component analysis and support vector machines*. Advances in Neural Network Research and Applications (pp. 803-810).
- Taylor, W. A. (2000). *Change-point analysis: a powerful new tool for detecting changes*. 2000.

- Tozlu, F., & Fresko, M. (2015). Auto-Genous and Semi-Auto-Genous Mills—2015 Update. *SAG Conference 2015*.
- Truong, C., Oudre, L., & Vayatis, N. (2018). ruptures: change point detection in Python. *arXiv preprint arXiv:1801.00826* (2018).
- Weinberger, K. Q., Blitzer, J., & Saul, L. K. (2006). *Distance metric learning for large margin nearest neighbor classification*. The Advances in neural information processing systems, 18.
- Whiten, W. (1974). *A matrix theory of comminution machines*. Chemical Engineering Science, 29(2), 589-599.
- Witten, I. H., & Frank, E. (2002). *Data mining: practical machine learning tools and techniques with Java implementations*. Acm Sigmod Record, 31(1), 76-77.
- Xing-yu, Q., Peng, Z., Chengcheng, X., & Dong-dong, F. (2017). RNN-based Method for Fault Diagnosis of Grinding System. In *2017 IEEE 7th Annual International Conference on CYBER Technology in Automation, Control, and Intelligent Systems (CYBER)*.
- Yang, H., Huang, C., Wang, L., & Luo, X. (2020). *An improved encoder–decoder network for ore image segmentation*. IEEE Sensors Journal, 21(10), 11469-11475.
- Yu, P. (2016). *A generic dynamic model structure for tumbling mills*. (PhD Thesis), University of Queensland, Australia.
- Yu, P., Xie, W., Liu, L., & Powell, M. (2014). Development of a dynamic mill model structure for tumbling mills. In *XXVII International Mineral Processing Congress-IMPC 2014 Conference Proceedings*.
- Zhang, L., Wang, G., & Giannakis, G. B. (2018). Real-time power system state estimation via deep unrolled neural networks. In *2018 IEEE Global Conference on Signal and Information Processing (GlobalSIP)*.
- Zhang, Y., & Haghani, A. (2015). *A gradient boosting method to improve travel time prediction*. Transportation Research Part C: Emerging Technologies, 58, 308-324.